UiT
THE ARCTIC UNIVERSITY OF NORWAY

Faculty of Science and Technology

Department of geoscience

Atmospheric circulation patterns associated with avalanche cycles in the Troms region

Marius Jenssen

GEO-3900 Master thesis in geology

May 2018

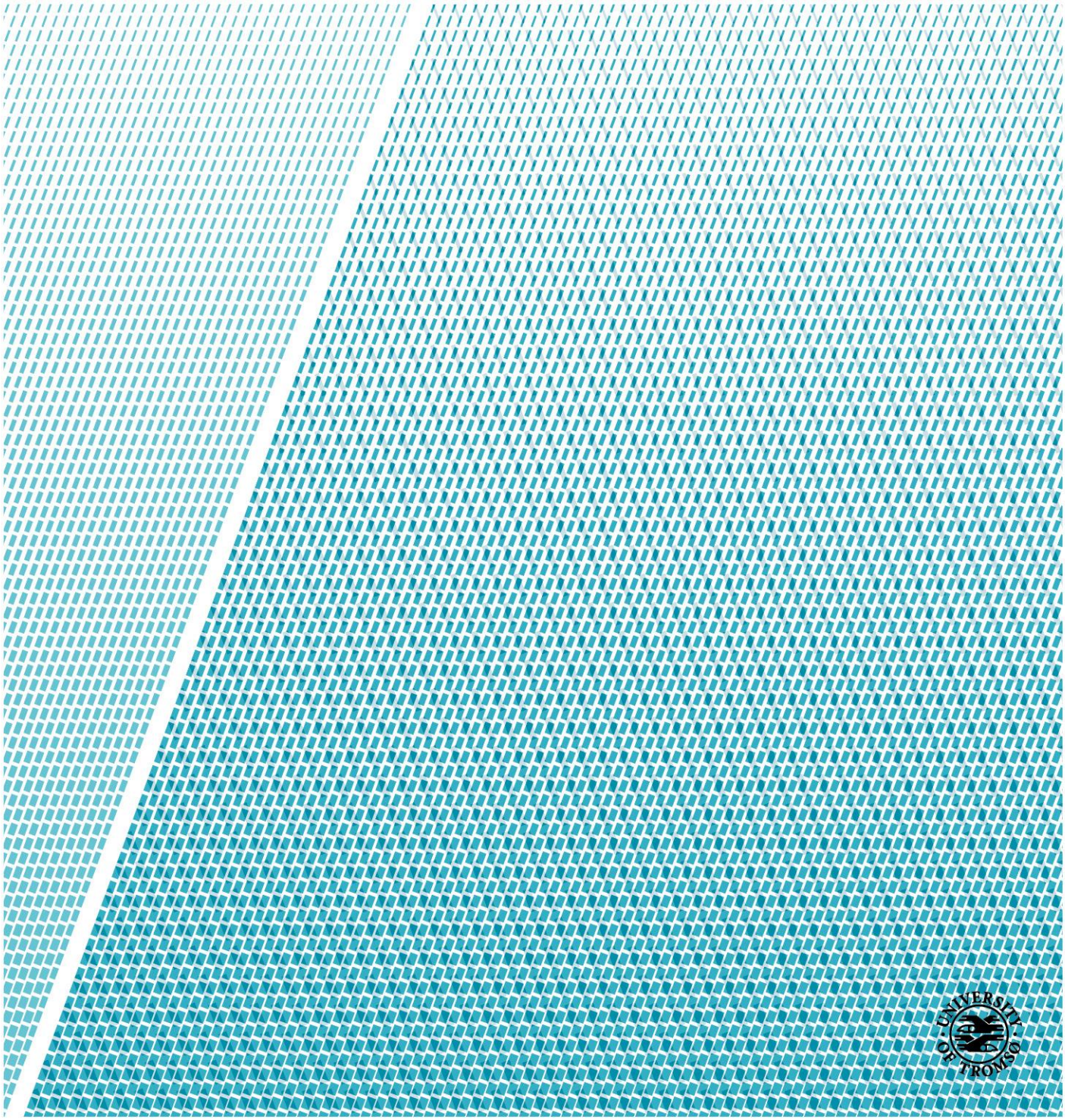

Abstract

Snow avalanches endangers human lives and infrastructure situated in alpine environments during the winter season. Occurrence of avalanche activity is a product of processes taking place in the snow cover situated in steep terrain, which are governed by meteorological conditions induced by synoptic weather patterns. Avalanche forecasting can therefore better forecast avalanche activity if they understand the causal relationship between atmospheric circulation patterns and the boundary layer conditions responsible for the triggering of avalanches. Such an analysis has never previously been done for the studied region. This study assesses the occurrence of periods with high avalanche activity in Troms, Northern Norway with respect to the governing atmospheric circulation patterns and the meteorological conditions they induce. An avalanche activity dataset for the 16/17 winter season was used to distinguish nine avalanche cycles and meteorological observations for these cycles from local weather stations were used to describe the conditions leading to avalanche activity. Then, 500mb geopotential height maps, 850mb geopotential height maps and mean sea level pressure plots over the North Atlantic region were downloaded from NCEP/NCAR reanalysis project for avalanche cycle periods, and were used to categorize five synoptic situations responsible for these avalanche cycles. Avalanche cycle days are characterized by higher wind speeds and lower temperatures relative to the rest of the winter, causing wind transport of snow and delayed stabilization of the snowpack. The different synoptic types induces a range of meteorological settings causing avalanches, and the most prominent for avalanching are the induction of snow precipitation and wind, causing storm and wind slab avalanches during winter, and conditions favorable for warming events and subsequent wet snow avalanche activity in the end of the snow season.

Acknowledgements

I would most of all like to thank my supervisor Markus Eckerstorfer from Norut for the avalanche activity dataset used in this thesis, allowing for the unique opportunity to study snow avalanches in Troms. Also, thank for all the guidance, comments, meetings and for allowing me to do my own project. Without you, this thesis would not have been what it is at all.

The Center for Avalanche Research and Education (CARE) at the University of Tromsø is thanked for the scholarship making it possible for me to attend at the Nordic Conference of Snow Avalanches and Mountain Recreation. Also thanks to Nord-Troms Regionråd for the scholarship, allowing me to focus on the thesis and also spend my free time doing what I love, which is being in the outdoors.

Thanks are given to Lis, Finn Kristoffer, Paul, Sam, Kristin and Andreas for proofreading of my thesis and improving the writing. Thanks a lot to the lunch-crew Lars, Christine, Andreas, Håvard, Martin, Christian, Paul and all other who were partaking. Thanks to Ragnhild for being an awesome office mate and for accepting me to keep all my smelly training clothes and dirty skiing gear in the office. Thanks to everyone who took me on trips and included be in social events while I was in "the bubble". You are all awesome!

Snow avalanches are, despite their brutal and sometimes lethal nature, some of the most delicate natural phenomena occurring. The conditions causing them are controlled to the change in characteristics of countless individual snow crystals occurring over timespans from hours to months, which may eventually lead to the collapse of carrying structures in the snow pack and ultimately the release of enormous snow masses subjugating to gravity. When considering the chaos in nature, it is a very unlikely process that takes place when a continuous layer of facets develops in the same stratigraphic position in the snow cover, across miles of snow-covered terrain. I appreciate the opportunity this master thesis has given me to study snow avalanches, and I hope to be able to work with this subject in the future.

Marius Jenssen

Tromsø, May 2018

Table of Contents

List of Tables

List of Figures

1 Introduction

1.1 Motivation

Norway is a country with large mountainous areas with steep topography and long snow seasons. The inherent hazard of avalanches in snow-cowered pose a risk to people who travel and perform recreational activities in the mountains. Furthermore, it does present a threat to infrastructure such as housing and roads, which needs protection. Every winter several people are involved in and sometimes killed in snow avalanche (from heron referred to as avalanche) accidents in Norway. The Norwegian Geotechnical Institute (NGI) has registered avalanche accidents with fatal outcome since 1975 and found that on average 5.7 persons a year have been killed by avalanches in the period 1975 to 2015(NGI, 2017). Eighty-two of these were during work or recreational activities, while the residual 18% involved people driving on roads or staying inside their houses. A significant amount of the avalanche accidents with fatal outcome in Norway during the recent years has occurred in Troms county (NVE, 2017c) since the early 2000s.

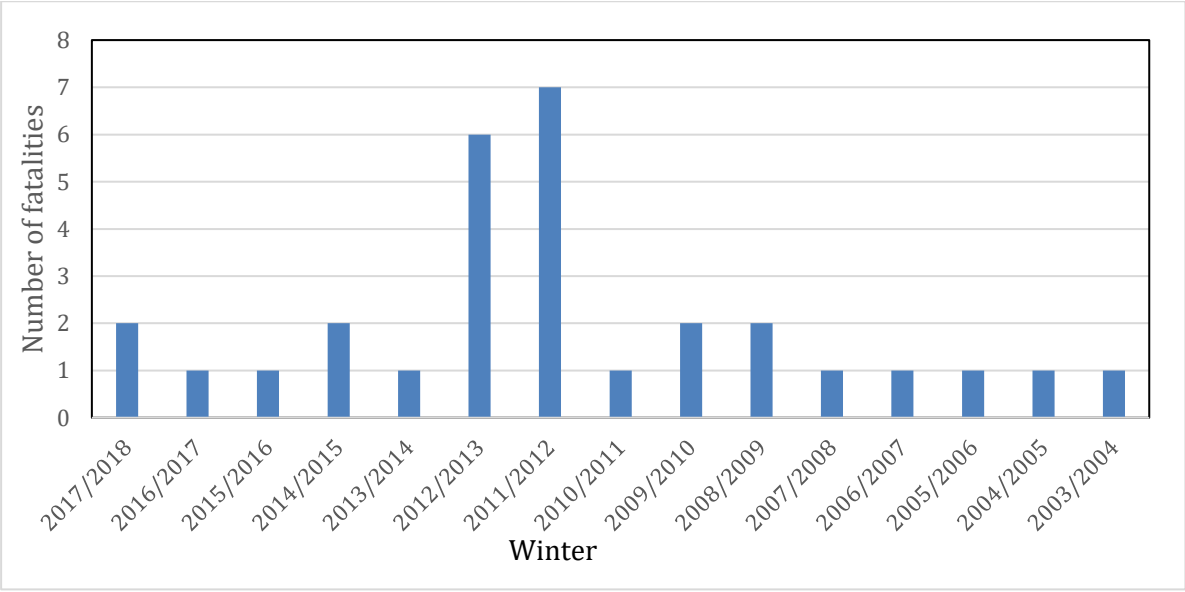

Figure 1. Number of people killed in avalanches in Troms from 2003 to present day. Data from (NGI, 2017). Note. Fatalities related to cornice fall are also included.

All of the fatalities that this statistic represents are recreational skiers and snowmobilers, but accidents with fatalities that are connected to traffic on roads being hit has also occurred (NGI, 2017; VG, 2000). Winter tourism in Tromsø has become more popular during the recent decade (Aronsen, 2016), and specifically ski-tourism makes out a large portion of this (Hansen, 2015). This is also seen in the fatalities, as 9 out of 21 of the victims that died from 2010 until present day were travelling from abroad

(NGI, 2017). Avalanche hazards leads to road closures, evacuation of inhabitants in avalanche prone areas and the need for mitigative measures, and does therefore constitutes a significant financial expense for the local authorities and the Norwegian Public Roads Administration (NPRA)(SVV, 2015). Avalanche forecasting attempts to predict the spatial and temporal occurrence of snow instability relative to a given level of triggering that may cause the release of avalanches. Avalanche forecasters aim to minimize the uncertainty about snow instability that is induced by four main factors; temporal and spatial variability of the snow cover and influence from the terrain, critical changes in snow and weather conditions and the presence of humans and their behavior(McClung, 2006). Since synoptic weather conditions acts as a background for the prevailing local mountain weather conditions and consequently the development of the snow cover (Mock et al., 2017), knowledge about atmospheric circulation patterns that produce periods of increased avalanche activity are of importance for the regional snow and avalanche regime classification. Such new knowledge can be used as an additional information layer in avalanche forecasting in order to prevent avalanche accidents (Hendrikx et al., 2005). This thesis aims to provide the avalanche forecasting in Troms with new knowledge about controlling synoptic meteorological conditions leading to periods of increased avalanche activity in space and time.

1.2 Objectives

Regional avalanche forecasting requires daily updated snowpack and avalanche observations and direct manual weather observations. It also rely heavily on weather forecasts, which is particularly important in areas where the field observations are sparse. Information about weather conditions correlated to avalanche activity in the past can be used to improve future avalanche forecasting (Birkeland et al., 2001). One approach in understanding this causal relationship has been the study of synoptic atmospheric circulation patterns and their correlation to recorded occurrences of increased avalanche activity. Studies of atmospheric conditions leading to prominent avalanching have been carried out in mountainous regions worldwide e.g. in Western U.S (Birkeland et al., 2001), in Iceland (Bjornsson, 1980) and in the Swiss Alps (Hächler, 1987). A common feature of these studies is that they use historical avalanche records from cases where avalanches in a monitored area reached a certain size or periods where avalanches has taken lives because of avalanche activity with abnormal magnitude. A new method for detecting avalanche debris using satellite-born synthetic aperture radar (SAR) imaging has been applied by Vickers et al. (2016). This method allows for detection of avalanche debris on a daily basis for large areas, in this case Troms County, which represents a unique opportunity for an more precise approach of defining avalanche cycles and their properties. Furthermore, a complete spatiotemporal avalanche activity record allows for a more detailed comparison between avalanche release and the meteorological factors responsible for the release.

This study aims to explore the causal relationship between different synoptic weather conditions and periods of high avalanche activity in Troms, based on a one-year dataset of daily avalanche observations from satellite-born SAR monitoring. Based on this initial analysis, I aim to correlate spatial release patterns with local weather conditions induced by the synoptic weather conditions. This is done in order to improve the understanding of the causal link between certain meteorological conditions release and specific types of avalanches where and when the avalanches occur. The work will overall contribute to a better understanding of the snow climate and avalanche regime in Troms. The outcome can be implemented by the regional avalanche forecasting service in order to improve early recognition of avalanche producing weather patterns.

1.3 History of avalanches in Troms

Troms County has a long history of recorded fatal and non-fatal avalanche accidents, some dating back more than 100 years (NVE, 2017a). Much of these early records concerns avalanches that destroyed houses and killed the people in them. Some major accidents where several lives were lost have occurred (NGI, 2017). Accidents worth mentioning are for example is the tragic accident in Vassdalen on Senja in 1986 where 32 soldiers were hit by an avalanche during a military exercise and 16 of them died (Nygaard, 1986). Another tragic accident is the skier-triggered avalanche at Sorbmegaisa in Kåfjord in 2012 where 6 skiers where taken by an avalanche and 5 of them died (Brattlien, 2012). NGI has produced reports about avalanche incidents with fatal outcome from 2002 until 2014 (NGI, 2017). The reports includes detailed analysis of snowpack and weather data from the accidents. Since then, some of the fatal accidents have been added to the regObs database (NVE, 2017c) as accident observations, with snowpack and weather data included. Data from the reports concerning fatalities, activities and avalanche problem are shown in Table 1. According to Table 1, in 78% of the accidents, persistent slabs was the main avalanche problem if this information was given. This means that since the remaining accidents were due to cornice falls, all of the slab-avalanches in the data occurred due to persistent slab. In three of the accidents that occurred in 2013 (Tromdalen, Kroken and Langfjellaksla) the avalanches were examined and thought to be released due to similar weak layers with the same stratigraphic position and temporal origin within the snow cover.

Table 1. Showing avalanche accidents with fatal outcome in Troms from 2004 until present Note: Main avalanche problem classification is according to (varsom.no, 2017). Data from (NGI, 2017; NVE, 2017c).

Date/year	***Deaths***	***Location***	***Activity***	***Main avalanche problem***
12.04.2018	1	Russelvfjellet, Lyngen	Ski/Snowboard	NA
29.03.2018	1	Kildalen, Nordreisa	Ski/Snowboard	NA
16.03.2017	1	Kavringtinden, Lyngen	Ski/Snowboard	Persistent slab
27.03.2016	1	Russelvfjellet, Lyngen	Ski/Snowboard	Cornice fall
10.02.2015	1	Reisadalen, Nordreisa	Snowmobile	NA
17.02.2015	1	Fastdalstinden, Lyngen	Ski/Snowboard	Persistent slab
16.03.2014	1	Brennmotinden, Balsfjord	Snowmobile	Persistent slab
17.03.2013	1	Langfjellaksla, Tromsø	Ski/Snowboard	Persistent slab
24.03.2013	1	Kroken, Tromsø	Ski/Snowboard	Persistent slab
26.03.2013	3	Tromdalen, Berg	Snowmobile	Persistent slab
21.04.2013	1	Storhaugen, Kåfjord	Ski/Snowboard	Cornice fall
18.02.2012	2	Middagstinden, Tromsø	Ski/Snowboard	Persistent slab
19.03.2013	5	Sorbmegaisa, Kåfjord	Ski/Snowboard	Persistent slab
18.12.2010	1	Fagerfjellet, Tromsø	Ski/Snowboard	Persistent slab
01.04.2010	2	Durmålstinden, Tromsø	Ski/Snowboard	Persistent slab
26.02.2009	1	Kroken, Tromsø	Ski/Snowboard	Persistent slab
17.05.2009	1	Tromsdaltinden, Tromsø	On foot	Cornice fall
21.04.2008	1	Uløya, Skjervøy	Ski/Snowboard	Persistent slab
23.03.2007	1	Kvalvikfjellet, Lyngen	Snowmobile	Persistent slab
08.04.2006	1	Hamneidet, Nordreisa	Ski/Snowboard	NA
03.04.2005	1	Tromsdalstind, Tromsø	On foot	Cornice fall
15.02.2004	1	Mauken, Målselv	Hunting/ski	Persistent slab

1.4 Literature study

1.4.1 Avalanche forecasting

Avalanche forecasting aims to evaluate current avalanche conditions in order to predict future avalanche conditions based on analysis of snow cover instability (LaChapelle, 1966; McClung, 2006). Snow instability is deduced by directly assessing snow pack structure and its propensity to produce avalanches with causing meteorological parameters as indirect evidence (Lachapelle, 1980). It thus follows that there is a ranking of data used in avalanche forecasting that is based on how direct evidence of snow instability the data indicates and how easy it is to interpret (McClung, 2002) as shown in Figure 2.

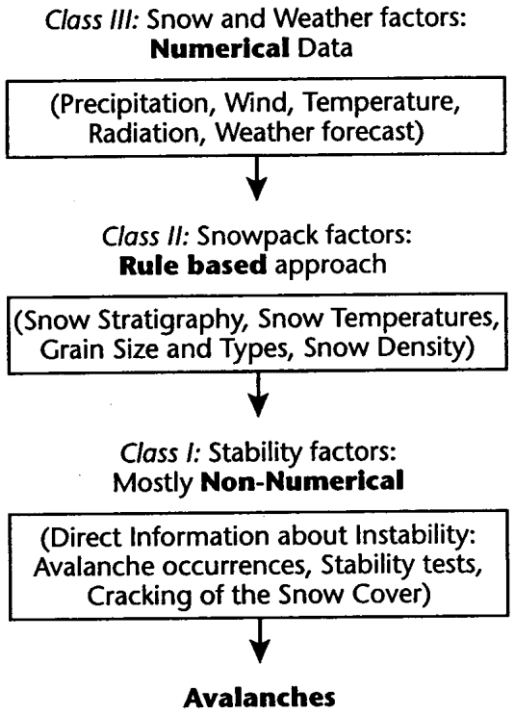

Figure 2. The three classes of data types used for interpreting instability in the snowpack (McClung, 2006)

The classes involve *class III* weather data measured near the surface of the snow, *class II* snowpack structure data assessing instability and *class I* observation that directly indicates snowpack instability. These classes are weighted according to informational entropy defined as their relevance and ease of interpretation with, *class III* having the highest entropy and *class I* having the lowest entropy. Ultimately this weighting indicates what the classes may reveal about instability (McClung, 2002). The process of forecasting avalanche conditions requires the integration of these observation data in different spatial and temporal scales and in order to be precise, the information used should match the scale of the problem (Hägeli and McClung, 2000). Three different operational spatial scales are given by Lachapelle (1980) and McClung (2006): Synoptic-scale (e.g. forecasting for a mountain range $>10^4$ km^2), meso-

scale (e.g. ski area $>10^2$ km^2) and micro-scale (e.g. avalanche path $<1km^2$). As the spatial scale decreases, the avalanche problem normally becomes more difficult to forecast and the need for accurate information increases, which best solved by acquiring low entropy data at the micro scale as Figure 3. illustrates (McClung, 2002).

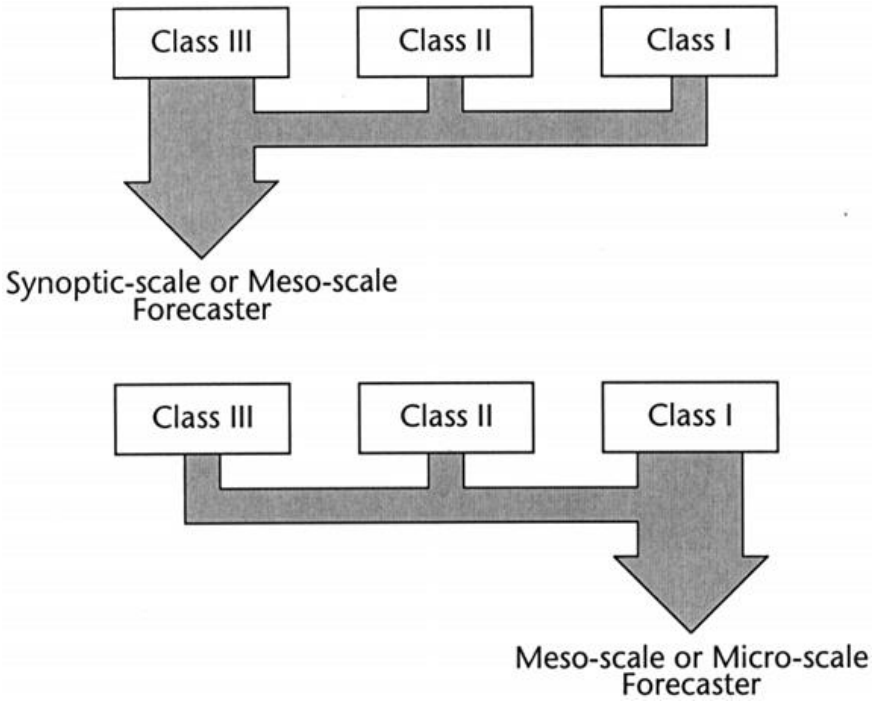

Figure 3. Spatial scales for avalanche forecasting with data flow of different entropy classes. Forecasters often use data from all data types for all scales(McClung, 2002).

Since the temporal occurrence of an avalanche release is dependent on conditions in the snowpack that may have developed over months and days (Fitzharris, 1987), addressing the timing of instability on a temporal scale requires avalanche forecasters to understand the weather and snowpack data on different temporal scales. Ultimately, avalanche forecasting and weather forecasting share the same problem since the first is dependent of the latter, where forecasts have progressively increasing uncertainty the further ahead they try to predict future conditions (McClung, 2002). For forecasting regions where low entropy data is less available due to the combination of few snowpack observations and large area, high entropy data such as weather forecast and meteorological observations often become more important to predict and determine avalanche danger (Bellaire et al., 2011). For the case of the Troms region with its vast areas and large geographical differences, forecasting is complex and class III data is particularly important (Barfod et al., 2013).

1.4.2 Snow climate classification

The first snow climate classification was presented by Roch (1949) for Western USA and further developed by LaChapelle (1966), Mock and Birkeland (2000), McClung (2006) and Haegeli and McClung (2007) resulting in three snow climate zones; maritime, continental and transitional. The analysis of a snow climate is based on the combination of meteorological and snowpack data in a given region during the winter months (Haegeli and McClung, 2007). Since maritime, continental or transitional snow climates characteristics differ from each other, the concept of a snow climate classification gives a general sense of the different characteristics of snow avalanching in a given mountain range or region (McClung, 2006). Armstrong and Armstrong (1987) compiled data from five high elevation sites with continuous snow and weather data for at least 15 years to describe the average conditions for each site in order to evaluate variability within the climate zones. Typical meteorological factors are synthesized in Table 2, which characterize the spatial variability of snow climates from maritime to continental.

Table 2. Climate characteristics for maritime, transitional and continental snow climates. By McClung (2006) after Armstrong and Armstrong (1987)

Type	***Total precipitation (mm)***	***Air temperature (°C)***	***Snow depth (cm)***	***New snow density (kg/m^3)***
Maritime	1280	-1.3	190	120
Transitional	850	-4.7	170	90
Continental	550	-7.3	110	70

The maritime snow climate is characterized by abundant precipitation as both snow and rain, producing a high-density snowpack with low temperature gradients. Further characteristics are prevalence of mild air temperatures causing fast stabilization and avalanches often occurring during or directly after a storm in near-surface layers of the snowpack (LaChapelle, 1966; McClung, 2006). The continental snow climate is characterized by less abundant snowfall producing a thinner snowpack with less density and high temperature gradients. The continental snowpack is also known for inhabiting more faceted crystals that act as persistent weak layers, and avalanches releasing from these layers are a distinct feature of this snow climate. The transitional snow climate displays features from both the previous snow climates, and may also occur in a region that normally exhibits a maritime or continental snow climate (Mock and Birkeland, 2000).

Other studies have been performed in various avalanche prone regions in the world e.g. in the Japanese alps (Ikeda et al., 2009) and in Spitsbergen on Svalbard (Eckerstorfer and Christiansen, 2011), where a more complex approach to the snow climate classification was required. According to Ikeda et al. (2009), the Japanese alps exhibits a combination of snow climate characteristics from both maritime and continental snow climates, where snow depth and structure displayed characteristics of continental snow climate, and a mean snow season rainfall close to the threshold of maritime climate. Thus, the classification "rainy continental snow climate" was introduced to describe this region.
In the case of Spitsbergen, Eckerstorfer and Christiansen (2011) found that the snow climate in the region produces a relatively thin and cold snow cover with persistent structural weaknesses due to depth hoar, and significant amounts of ice layers produced by maritime climatic influence. Therefore, the authors suggested "High Arctic maritime snow climate" as snow climate classification for this region.

1.4.3 Avalanche climatology and synoptic avalanche forecasting

Avalanche climatology is a study that investigates the relationship between snow avalanches and climate based on historical avalanche records and climate and weather data on a range of time scales from daily to decadal. Avalanche climatology represents an idea of the avalanche problems that often occur in a certain area (Mock et al., 2017). As availability of consistent mountain weather data and avalanche records became more common in the 1970s, avalanche climatology researchers applied statistical quantification analysis in order to identify which weather variables could be associated with avalanches at certain locations. E.g. are (Perla, 1970), who correlated wind speed and heavy precipitation with avalanche occurrences in Alta, Utah and (Föhn et al., 1977) who evaluated multivariate and nonparametric techniques for avalanche forecasting. The introduction of detailed synoptic weather maps in the mid-20th century allowed operational avalanche forecasting to link daily synoptic-scale circulation patterns to periods of high avalanche activity (Mock et al., 2017). Studies where this approach has been used are Bjornsson (1980) for Iceland, Fitzharris and Bakkehoi (1986) for Norway, Birkeland and Mock (1996) for Bridger Bowl in the US, Esteban et al. (2005) for the Pyrenees and Farukh and Yamada (2014) for Sapporo, Japan. Although a common feature of these studies is the application of composite and/or anomaly weather maps to identify synoptic circulation patterns, it is important to emphasize that the datasets may differ from one study to another concerning identifications of periods of high avalanche activity, and the temporal and spatial scale of avalanche activity that is investigated. Fitzharris and Bakkehoi (1986) analyzed the synoptic climatologies for 12 major avalanche winters from 1867-1979 using Grosswetterlagen. This analysis included the whole country, and winters were chosen if 20 or more people had died in avalanches. They recognized three synoptic situations, often occurring in combination; westward extension of the Siberian High, making winters cold and a higher likelihood of less stable snowpack, west to north-west air streams due to anticyclonic blocking near Britain producing massive direct-action avalanching. The third involved rapid switch in circulation patterns and

normalization from the previous two, producing south-west or south flow, overloading a weak snowpack.

Birkeland and Mock (1996) assumed a connection between heavy snowfall and avalanche activity, and investigated 53 days in one winter season classified as abnormally high snowfall events with the criterion of 32,8 cm of snowfall accumulation during one day in Bridger Bowl Ski Area in Montana, USA and correlated these periods with 500mb composite and anomaly weather maps. They found that during and prior to a heavy snowfall event, Bridger Bowl was beneath the backside of an upper lever trough, with storms coming predominantly from northwest. Similar approaches where snow precipitation thresholds was used for determining periods to investigate, include (Esteban et al., 2005) for the Andorran Pyrenees and (Farukh and Yamada, 2014) for Hokkaido, Japan. Birkeland et al. (2001) combined data from West-wide Avalanche Network (WAN), a database for high-elevation climate and avalanche records in the US with 2-3 day new snowfall to investigate four sites in the US with a spatial distribution that represented the three snow climate zones. Occurrences of reported size-5 avalanches during nine storm events was studied by Hansen and Underwood (2012) on Mt. Shasta, California to find synoptic weather types responsible for extreme avalanching. Recently Hancock et al. (2016) used a record of road closures due to snow drift on a mountain road in close vicinity of Longyearbyen in the Svalbard archipelago, to investigate periods of high avalanche activity. As the dominant avalanche activity in this snow climate is connected to snow being transported by winds and accumulated as cornices on the top of steep slopes that eventually falls and trigger slab avalanches (Eckerstorfer and Christiansen, 2011), a relation between snowdrift occurrences and avalanche activity was suggested.

1.4.3.1 Avalanche cycles

The term avalanche cycles may be considered as periods of increased avalanche activity induced by specific weather condition, and is in practical applications often used based on different criteria (Holler, 2009). The term has been used in studies for periods where avalanches led to fatalities e.g. (Bjornsson, 1980) or in cases of widespread avalanche activity e.g. (Birkeland and Mock, 2001) , but no study has set a universal definition for the term. Previous definitions of avalanche cycles were made by Scweizer. Jürg (1998), involving the application of an avalanche activity index (AAI), where all observed avalanches were assigned a weight for the size based on the destructive size scale by Greene (2010). The weights given were 0.01, 0.1, 1 and 10 for the sizes 1-4, since the mass increases tenfold for very avalanche size. The sum of these avalanches represented the magnitude of the avalanche cycle. When investigating the North Atlantic Oscillations relation to avalanching on Iceland, Keylock (2003) defined an avalanche cycle as a seven-day period within which one or more avalanches were observed. Hageli and McClung (2003) used an AAI where the sizes of observed avalanches is rated by the size of the avalanche relative to their path on a scale from 1-5 according to the U.S avalanche size classification (Greene et al., 2010).

1.4.3.2 **Remote sensing of avalanches**

Remote sensing of avalanches provides safe and continuous data acquisition for avalanche research and operational avalanche forecasting compared to field based approaches, and does also reduce observational biases towards more easily observable objects (Eckerstorfer et al., 2016). The first application of satellite born Synthetic Aperture Radar (from heron referred to as SAR) in Troms was conducted by Malnes et al. (2013), who detected three large avalanches in Troms county, using very high resolution Radarsat-2 satellites data. This technique proved useful since SAR obtains images in any light and cloud cover conditions. Eckerstorfer et al. (2014) and Eckerstorfer and Malnes (2015) used Landsat-8 and Radarsat-2 images with several different resolutions for manual detection of avalanches in Troms. Later, Malnes et al. (2015) showed that Sentinel-1A satellite (from heron referred to as S1A) images mode with resampled 20 x 20m spatial resolution could be used for detection of avalanche debris by utilizing the increase in backscatter from avalanche debris with increased snow depth, snow water equivalent (SWE) and surface roughness. In this study, 489 avalanches were detected in a 250x250 km^2 large ground swath S1A image from a cycle of wet snow avalanches that occurred in the beginning of January 2015. Since S1A provides too large data quantities for manual detection of avalanche debris, an automatic avalanche detection algorithm is imperative for operational uses (Eckerstorfer et al., 2016). Such an algorithm was developed by Vickers et al. (2016) by basing the algorithm on both radar backscatter change detection and unsupervised object classification approaches. This algorithm proved to have a probability of correctly detecting avalanche debris of >70% when compared to manual detection, but had needs for refinement if the result where to be used without additional human input.

2 Methods

2.1 Data sources and processing

2.1.1 Avalanche activity dataset

A snow avalanche activity dataset kindly provided by (Eckerstorfer, 2017) formed the basis of the analyses in order to define avalanche cycles. This dataset was compiled using Sentinel-1A radar images with resampled 20x20m spatial resolution to detect avalanche debris by utilizing the increase in backscatter from avalanche debris with increased snow depth, snow water equivalent and surface roughness (Malnes et al., 2015). An automatic avalanche detection algorithm developed by Vickers et al. (2016) based on both radar backscatter change detection and unsupervised object classification approaches was applied to detect avalanche debris. The dataset consisted of 1254 registered avalanches from the period 23.11.2016 to 31.05.2017 and contained several parameters for each avalanche (Table 4).

Table 3. Description for data properties in avalanche activity dataset

Parameter	***Unit***	***Example***	***Description***
FID	Number	1	Identifier for each detected avalanche debris
Area	Square meters	2000	Area detected debris
Date	yyyymmdd	20161123	Date of debris detections
Coordinates	xxxxxx East, xxxxxx North	E699740, N7748820	UTM 33N, WGS 84 coordinate system
Min DEM	Meters above sea level	514	Lowest point of avalanche debris
Max DEM	Meters above sea level	603	Highest point of avalanche debris
Mean DEM	Meters above sea level	550	Mean height of avalanche debris
Mean Slope	Degrees	26°	Mean slope of detected avalanche debris

Mean aspect	Degrees	55°	Aspect of debris
Length	Meters	160	Horizontal length of debris from highest to lowest point
Width	Meters	160	Length from one side to the other on the avalanche debris

2.1.2 Avalanche cycles

Definitions of avalanche cycles in previous studies are based on various criteria, e.g. avalanche activity indexes (Hageli and McClung, 2003; Scweizer. Jürg, 1998) or thresholds for number of fatalities (Holler, 2009), which are not applicable for this dataset Therefore, the following criteria was established to define avalanche cycles.

1. Avalanche cycles are periods where the number of avalanches detected per day and area (m^2) of avalanche debris detected per day exceeded 3 times the average per day for the whole dataset period for each respective parameter.

2. Each avalanche cycle begins the day before the day when the amount of avalanches exceeds the average per day for the season since the satellite detects avalanches that has occurred since the previous orbiting, and ends when the amount of avalanches per day is less than the average per day for the whole dataset period.

2.1.3 Avalanche forecast

I used the public avalanche forecasting service varsom.no to assess the triggering factor of avalanches during cycles that offers daily bulletins for specific regions in the country. Varsom.no is a joint service made by The Norwegian Meteorological Institute, The Norwegian waters and Energy Directorate, Norwegian Public Road authorities and The Norwegian Rail Administration (NVE, 2018b)

2.1.4 Weather maps

I used NCEP/NCAR Reanalysis Project dataset (Kalnay et al., 1996) and the plotting tool available from the NOAA/ESRL Physical Science Division's website to produce daily 500 mb and 850 mb geopotential height maps and sea surface pressure maps over the North Atlantic region for each day in periods

classified as an avalanche cycle. This dataset allows user to produce historical plots at several atmospheric layers and different meteorological parameters, and has globe-spanning data coverage. In order to recognize synoptic scale weather systems and categorize them, these weather maps were described according to their properties of high and low pressure over the north Atlantic region and Scandinavia. They were then manually grouped into categories of similar synoptic types based on their general pattern of 500 mb and/or 850 mb geopotential heights on the individual daily plots. Synoptic circulation classification based on subjective a priori definition of synoptic patterns are called subjective or manual classifications (Huth et al., 2008) and has been successfully employed in the past through the use of Grosswetterlagen synoptic types e.g. (Fitzharris and Bakkehoi, 1986).

2.1.5 Meteorological data

Meteorological values obtained using the mapping tool xgeo.no from four weather stations in the region for the specific avalanche cycles were downloaded to analyze the spatial properties of the synoptic situations concerning wind speed, direction, precipitation and air temperature in order to characterize the boundary layer conditions that trigged avalanches. Xgeo.no is a freely available tool for emergency preparedness, monitoring and warning for floods, snow avalanches and landslides in Norway, and allows for extraction of weather data from specific weather stations. The service is a joint responsibility of The Norwegian Public Roads Administration, The Norwegian Meteorological Institute NVE, The Norwegian Mapping Authority and The Norwegian Rail Administration (NVE, 2017b). This service offers the possibility to download hourly meteorological data. Eklima.no is a web portal for The Norwegian Institute of Meteorology's climate database, which contains data from all weather stations that is currently and previously operational, and data from other partners (MET, 2018). Two automatic weather stations (from heron referred to as AWS) and one manually operated weather station was selected based on their spatial distribution in the study area, temporal data availability, type of parameters measured and data accessibility.

The Tromsø Vervarslinga weather station is located on the Tromsø Island at 100 m.a.s.l and has been operated since 1895. It is manually operated and records precipitation, air temperature, snow depth and wind. The Nordnesfjellet AWS is situated at 700 m.a.s.l close to the summit of Nordnesfjellet in Kåfjord and has been operated since 2010. It measures wind, snow depth, precipitation and air temperature. Bardufoss weather station is situated at 76 m.a.s.l in Målselv municipality and has been operated since 1940. It measures precipitation, air temperature, snow depth, wind speed and wind direction. It is situated south of the study area. The period of interest was decided to be 23.11.2016 – 31.05.2017 and only weather data from this time frame will be assessed in relation the dataset.

Table 4. Data sources used in this thesis and their characteristics.

Data	***Source***	***Parameters***	***Temporal Resolution***	***Temporal Coverage***
Avalanche activity dataset	Eckerstorfer, M (2017)	Avalanche debris with time of detection, area, length, width, height, coordinates, slope, aspect	Daily	23.11.2016 – 31.05.2017
NCEP/NCAR Reanalysis 1	NOAA/ESRL Physical Science Division	500 and 850 mb geopotential height maps, sea level pressure maps	Daily	1948 - present
Gjerdvassbu AWS, Lyngen	Met.no	Air temperature, snow depth	Hourly, daily	2011 - present
Nordnesfjellet AWS, Kåfjord	Met.no	Air temperature, precipitation, snow depth, wind speed and wind direction	Hourly, daily	2010 - present
Tromsø Vervarslinga WS, Tromsø	Met.no	Air temperature, precipitation, snow depth, wind speed and wind direction	Hourly, daily	1895 - present
Bardufoss weather station, Målselv	Met.no	Precipitation, air temperature, snow depth, wind speed and wind direction	Hourly, Daily	1040 - present

3 Study area

3.1.1 Physical setting

Figure 4. Study area.

The study area lies within the Troms County, which is situated in Northern Norway at between 68.2° – 70° degrees north and 15.4° – 22° degrees east. It covers an area of 25.877 km^2 and has mountains reaching up to 1800m.a.s.l (Thorsnæs, 2016). The study area is defined by the coverage of the Sentinel-1 satellite images used for avalanche-debris detection.

The bedrock in the county consists mainly of four elements: (I) Precambrian basement rocks in West Troms Basement Complex in the island's north and west of Tromsø and (II) Caledonian nappes in the mainland to the south and east of Tromsø with (III) Post-Caledonian and (IV) Post-Cenozoic elements. The two latter involves faults and fractures in the bedrock that constitutes weakness zones that influences erosion and dictates the orientation of the valleys and fjords. The region was elevated to its current level during Paleogene and Neogene (Ramberg et al., 2007). The geography in the County is defined by alpine topography with alpine peaks, fjords and cirques created by glacial erosion and sediment transport during the Quaternary period, and glaciers that nearly reaches sea-level are also present today (Andersen, 2000). The mountains in the west have an alpine character, and the most prominent alpine region is the Lyngen Alps, which inhabits the highest peaks and the largest glaciers. Towards the east the topography becomes less alpine, featuring mainly mountain plateaus (Thorsnæs, 2016). The study area is sparely populated, with exception of Tromsø in West Troms, the largest city in Northern Norway with 75 000 inhabitants (SSB, 2018). The main mode of transportation is along public

roads, most of which that are located in alpine terrain and are thus prone to avalanches during the winter season (Helgaas et al., 2012).

3.1.2 Climatic and meteorological setting

Northern Norway is on average ten times warmer than other locations at the same latitude during winter. This can be attributed to The North Atlantic current bringing warm water from southwest, and low pressure systems bringing warm air from across the Atlantic Sea (I. Hanssen-Bauer, 2015). Cyclones in the Northern Atlantic Ocean moves along preferred tracks either in a northeasterly direction over the Norwegian Sea, bringing precipitation to northwestern Europe and mild weather for surrounding areas, or a more southerly track, producing precipitation in southern Europe and cold periods in northern Europe (Van Loon and Rogers, 1978). There is a positive correlation between mean precipitation and number of cyclones in Scandinavia, indicating that cyclonic activity from The North Atlantic Storm Track causes a significant amount of precipitation and warmer air than average along the Norwegian coastline during wintertime. However, these cyclones may be blocked by high pressure systems over the Scandinavian region, causing cold dry periods in the winter (Parding, 2016). These fluctuations are related to variations in the large-scale atmospheric circulation patterns e.g. the North Atlantic Oscillation (Rogers, 1997) and Arctic Oscillation (Thompson and Wallace, 1998). Pohjola and Rogers (1997) found that winter precipitation and snow accumulation in northern Scandinavia was low during years where the Siberian high-pressure cell was unusually strong and the Icelandic low as well as the low-pressure trough over the Norwegian Sea was weaker. In the opposite case, a weak Siberian high allows for westerly maritime influence, and more precipitation both summer and winter. This is consistent with Uvo (2003), who found that a strong year for the NAO gives stronger westerly winds in mid latitudes and an intensification and shift in the North Atlantic Storm Track.

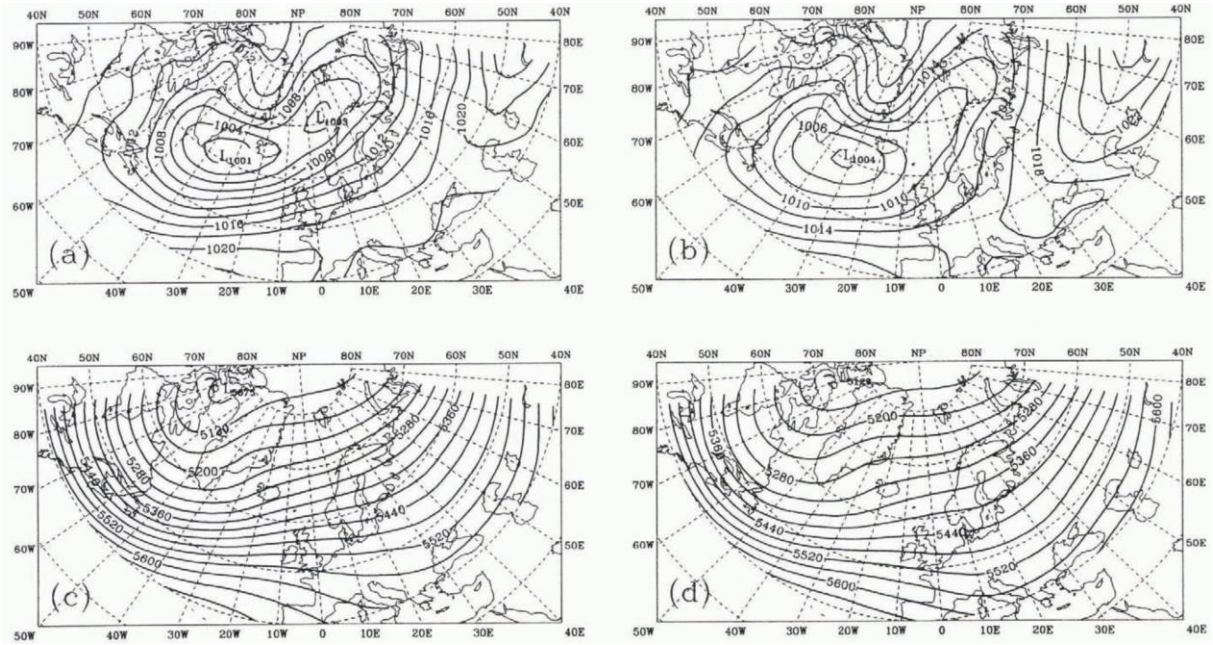

Figure 5. (a) SLP and (c) 500mb geopotential height plot for winters with high snow accumulation and strong Icelandic low, and (b) SLP and (d) 500mb geopotential height plot for winters with low snow accumulation and strong Siberian high .Edited from (Pohjola and Rogers, 1997).

Another important source of intense periods of wind and snow precipitation is the occurrence of polar low-pressure systems originating from the arctic sea that reach the coast of Northern Norway during wintertime, mainly between December - March (Rabbe, 1975). Because of the short lifetime and the mesoscale spatial extent of polar lows, they are difficult to predict and the impact is often local (Wilhelmsen, 1985). The conditions leading to the occurrence of polar lows are described by Kolstad et al. (2009) who correlated polar lows to marine cold-air outbreaks that happen when high pressure anomalies in the western Nordic seas occur in addition to the movement of synoptic lows entering the region. Mallet et al. (2013) also suggested that cold air outbreaks and stratospheric intrusions are favorable conditions for the creation of polar lows, and that within the specific regions, polar lows develop with northerly flow in the Norwegian Sea and northeasterly flow in the Barents Sea.

The weather in Troms is influenced by the rough topography that generates differences in precipitation and air temperature (Dannevig, 2009), a tendency that is seen in Figure 6 and Figure 7. This is due to orographic lifting of warm, moist weather systems that are reaching the mountainous coast and precipitate there, and then become progressively less moist towards the leeside of the Scandes mountains (Uvo, 2003). Troms has a mild coastal zone with large amounts of precipitation as snow during wintertime, while the inland has a cooler climate and less snow precipitation (Klimaservicesenter, 2016). This is shown in Figure 6 and Figure 7 that show measured snow depth and air temperature respectively, using average values for each month in every winter season (October – May) for the last recent 30

years. The measurements were recorded at two locations: Tromsø, which is close to the coast (30 km from open sea); and Bardufoss, which is further inland (70 km from open sea,). Figure 6 shows that snow depth in Tromsø was thicker every winter, and in some cases twice the depth than in Bardufoss, although both locations had the same snow rich or poor winters. While nine out of thirty winters in Tromsø had a snowpack exceeding one meter depth, and only one winter with less than a half a meter of snow depth, only ten of the winters in Bardufoss had a snowpack deeper than a half meter. The deepest snow measurement in Tromsø is 202cm in April 1997, and for Bardufoss this is 116 cm in March 2002. The lowest air temperature measured in Tromsø and Bardufoss is -7.1°C and -15.8°C respectively.

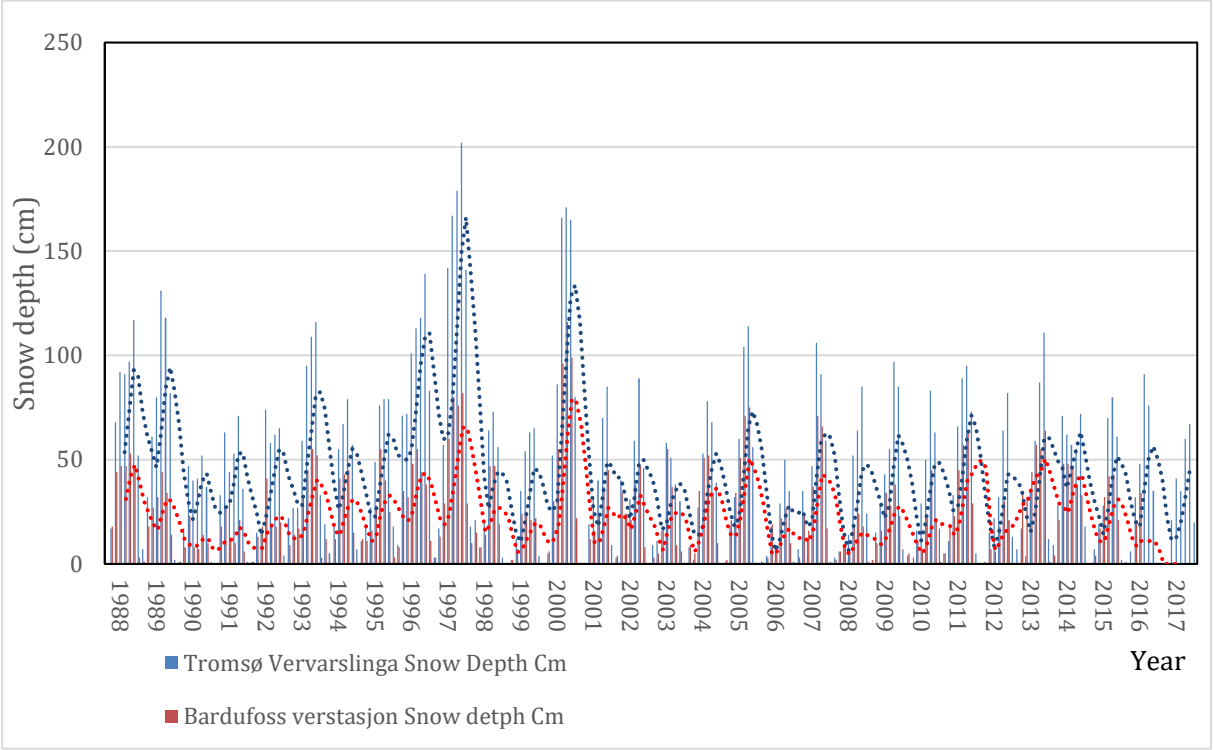

Figure 6. Measured snow depth average for each month (Oct-May) in the winter seasons 1988-2017 at weather stations in Tromsø and Bardufoss. (Data source eklima.no)

In Figure 7 the winter air temperature in Tromsø and Bardufoss are compared, showing that Bardufoss had lower air temperatures during mid-winter with several winters that are twice as cold as in Tromsø, with monthly average air temperatures falling to between -10°C and -15°C in about half the winters compared to Tromsø, which rarely has monthly averages below -5°C. However, at the beginning and end of every winter, the air temperatures are almost the same.

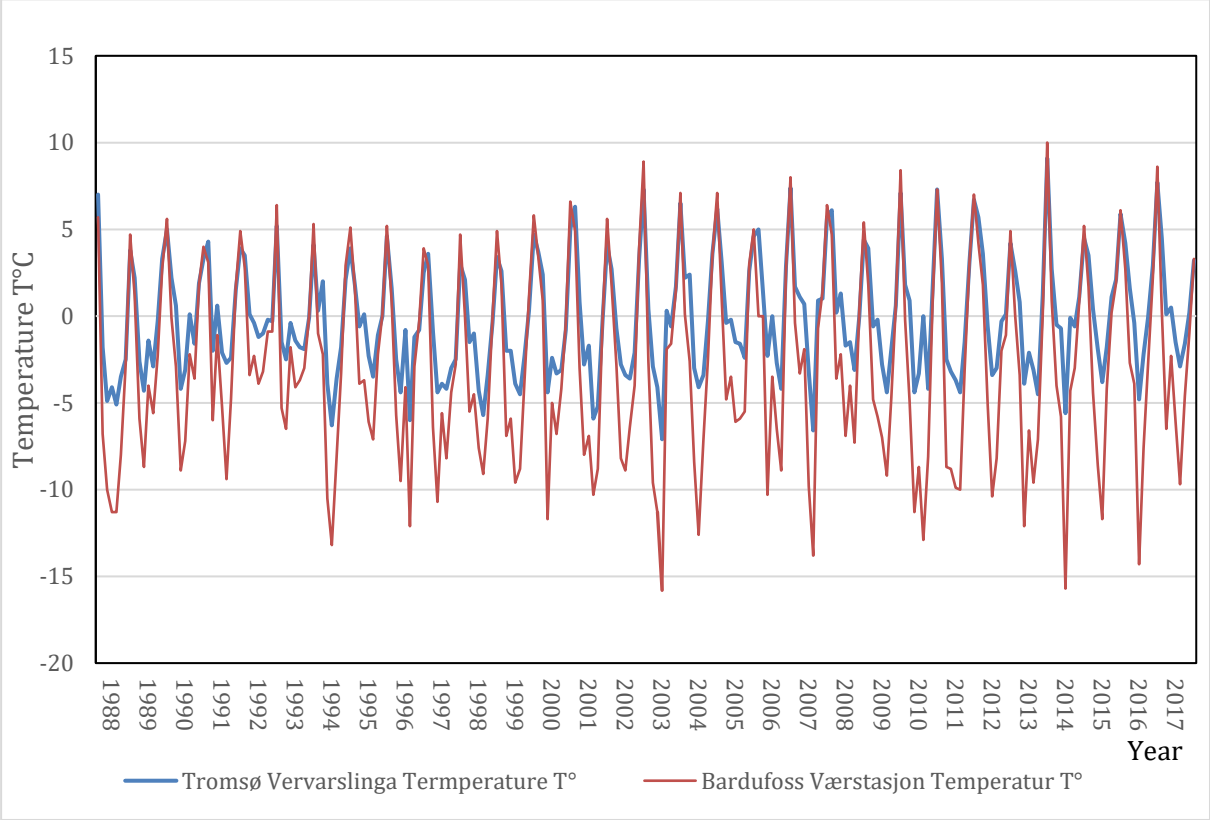

Figure 7. Average air temperature for each month (Oct-May) in the winter seasons 1988-2017 at weather stations in Tromsø and Bardufoss. (Data source eklima.no)

The average snow depth for winter moths (Oct-May) in Tromsø is 44.8 cm with the deepest snow pack measuring 202cm in April 1997. For Bardufoss, the average is 22cm and the deepest snow pack measuring 116 cm in March 2002. Furtherly the difference in climatic conditions are indicated by lower average and median air temperatures in Bardufoss when compared to Tromsø as seen in Table 5.

Table 5. Key meteorological features for Bardufoss weather station and Tromsø weather station for each month (Oct-May) in the winter seasons 1988-2017. (Data source eklima.no)

Weather station	***Average T°C***	***Average Snow depth cm***	***Median T°C***	***Median Snow depth cm***	***Max T °C***	***Min T °C***
Bardufoss	-2.86	22	-3.3	19	10	-15.8
Tromsø	-1.2	44.8	-0.4	35	9.1	-7.1

3.1.3 Snow climate

The snow climate in Troms was investigated by Velsand (2017) with respect to the development of the snow cover in terms of snow depth, stratigraphy, snow temperatures and stability at two different study sites representing maritime and continental sites. In addition, modelled meteorological data from 1957 to 2017 for these sites was analyzed, assisting in classifying both sites into one of the three snow climate classes. This study discovered the occurrence of rain induced ice layers in the snowpack during warmer years and depth hoar formation in colder years, and increasing occurrence of constructive metamorphism of snow crystals further inland. This combination of snow climate features are not consistent with existing classifications of snow climates, where rain crusts are common in maritime snow climates and depth hoar is a typical feature for continental climate (Mock and Birkeland, 2000). Thus, the term Arctic Transitional Snow climate was suggested for the region.

4 Results

4.1 Temporal analysis of avalanche cycles

The avalanche cycles in the 16/17 winter occurred from after Christmas and until the end of the snow season (Table 6). Five cycles took place from December to February, which was shorter than those during April and May were. The avalanches with highest intensity occurred in February and April. May had 21 days defined as avalanche cycles, which is the highest for any month in the dataset. Cycle 8 was the longest cycle for this season, lasting for 12 days and had 1554 avalanches, which was also the highest number for avalanches in one cycle.

Table 6. Avalanche cycles with key data.

Cycle	***Date***	***Days***	***Average avalanches pr. day***
1	25.12 – 30.12.2016	6	189
2	13.01 – 15.01.2017	3	166
3	22.01 – 23.01.2017	2	116
4	30.01 – 04.02.2017	6	214
5	17.02 – 20.02.2017	4	219
6	19.03 – 22.03.2017	4	126
7	06.04 – 13.04.2017	8	178
8	05.05 – 16.05.2017	12	141
9	22. 05 – 31.05.2017	10	79

The temporal occurrence of avalanche cycles in this dataset is displayed together with key meteorological parameters for Nordnesfjellet AWS (from heron referred to as NF) in Figure 8 and Tromsø Vervarslinga (from heron referred to as TV) in Appendix figure 13 and described in the next section.

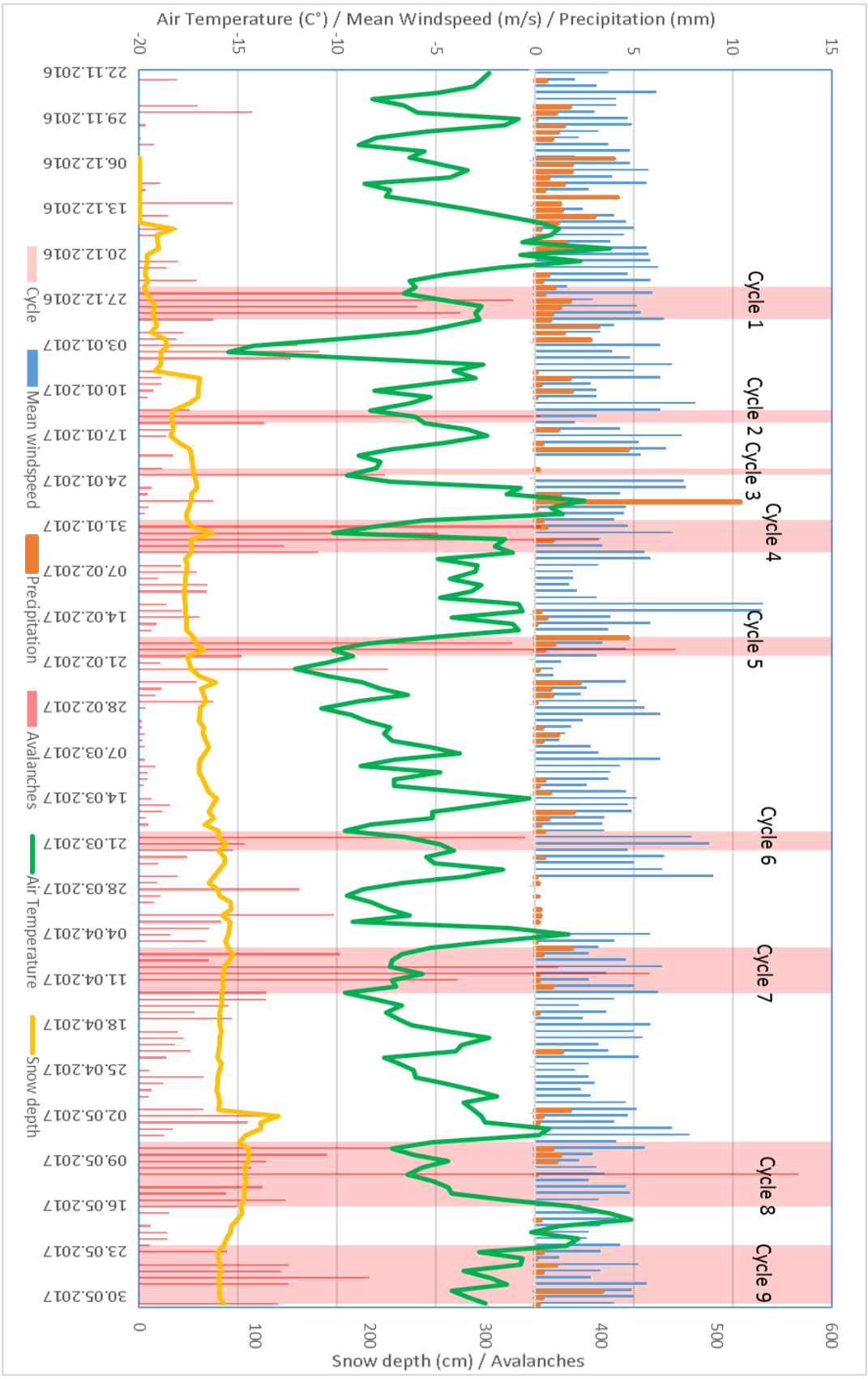

Figure 8. Avalanche activity with meteorological data of daily averages from Nordnesfjellet (Data source: eklima.no)

Note: wind speed measurements during the 21.03-23.03.2017 are missing.

4.1.1 Avalanche cycle 1. 25.12-30.12 2017

During 20th December, the snowpack at the weather stations at NF and in TV had shrunk due to air temperatures above 0° degrees in the previous week. At TV, the snow cover increased from 0 cm to 19 cm from the 22nd – 24th of December, and as the first avalanche cycle started on the 25th, the snowpack increased furtherly until the 28th when it reached 26 cm. Less precipitation and snow cover increase occurred at NF, however higher wind speeds were recorded here, with up to 11 m/s from the western sector as hourly average during the 26th. The air temperature rose to zero °C in TV and -2.8 °C at NF weather stations during the 28th and remained high during the rest of the cycle.

4.1.2 Avalanche cycle 2. 13.01-15.01 2017

The first avalanche cycle in 2017 occurred after 3 days with low air temperatures and no precipitation, however increased wind speeds were measured from southwest at NF. During the cycle, air temperature increased to about -2 degrees C, but wind speeds were low, coming from southern sector at NF, and some precipitation was measured at TV.

4.1.3 Cycle 3. 22.01-23.01 2017

The second cycle that occurred in 2017, and the shortest cycle in this winter season occurred after a weeklong period of snowfall and the snow cover at TV increased from 29 cm at the 17th to 85 at the 23rd, with wind speeds up to 10 m/s measured at NF from the eastern sector. During the cycle, the air temperatures were low, dropping to almost -10 °C at NF.

4.1.4 Cycle 4 30.01-04.01 2017

Intense precipitation occurred on the 26th and 27th with the highest daily measurement of this winter season were measured at the 27th of January in TV with wind coming from the western sector. The temperatures were above 0 °C during this precipitation event at TV and NF. As the cycle commenced, the air temperature dropped to just below -10 °C at NF. Wind speeds were moderate during the first days of the cycle, coming from east. At them 1st of February, wind speeds reached up to 9m/s from south – southwest. For the remaining days of the cycle, wind were low, coming from southwest. Some precipitation occurred at TV where air temperatures was just below zero °C.

4.1.5 Cycle 5 17.02-20.02 2017

In the days prior to cycle five, TV measured air temperatures well above 0 °C and precipitation came as rain. The snow cover became thinner until the 16th. On the 17th, the air temperature started to drop, reaching well below 0 °C on both weather stations. The snow thickness increased by 20 cm from the 16th to the 18th at TV and NF recorded moderate wind speed from the north and later from south during the 17th. Wind direction remained in the southern sector for the rest of the cycle, with wind speeds up to 7.5 m/s as hourly average.

4.1.6 Cycle 6 19.03-22.03 2017

Cycle 6 occurred after a 4-day period with moderate precipitation and air temperatures below zero °C, and an increase of 10cm snow thickness at TV. NF recorded wind from northwest at the 18th, and during the cycle, winds were coming from the southern sector with hourly wind speeds up to 12.5 m/s as hourly average. Air temperatures increased to during the 20th to above freezing at sea level, and NF recorded heightened wind speeds during the cycle days. As the cycle ended, air temperatures dropped to below freezing.

4.1.7 Cycle 7 06.04-16.04 2017

During the 72 hours prior to cycle seven a total of 30.8mm of precipitation were measured at TV, with air temperatures between 2 and 4 °C. Air temperatures at NF also reached above freezing temperatures at the 4th, but fell to between -5 and -7 °C during the cycle. 2-4mm of precipitation per day was measured during the cycle at TV, with air temperatures below freezing, but the snow cover did not gain significant thickness. Winds at NF came from north and east during the 6th, and changed to a southerly on the 7th and 8th with hourly wind speeds up to 5m/s. Air temperatures at NF remained low for the rest of the cycle, and moderate westerly winds prevailed.

4.1.8 Cycle 8 05.05-16.05 2017

The longest avalanche cycle in the dataset occurred after a warm period from the 4th to the 5th of May were air temperatures rose above 0 °C degrees at both weather stations. No significant amount of precipitation were measured, but winds at NF reached 10 m/s as hourly average at the fourth and fifth coming from east and southeast. As the cycle commenced, air temperatures dropped below 0 °C and 7-8 cm of new snow were measured on both stations from the sixth to the seventh. Hourly wind speeds at NF reached 10 m/s as hourly average coming from north during the seventh, but no wind speeds above 6 m/s were recorded for the rest of the cycle. Daily air temperature rose above freezing at TV on the 12th and remained warm throughout the cycle. On NF, the air temperatures were below freezing until the 16th, when air temperature rose to 1.8 °C.

4.1.9 Cycle 9 22.05-31.05 2017

The last cycle of the dataset occurred after a period with air temperatures above freezing at NF and TV. Some precipitation occurred during the cycle, but no significant increase in snow cover was recorded. Hourly wind speeds rarely exceeded 7 m/s during the cycle. Wind directions varied a lot throughout the cycle but was mainly from the northeastern sector during the 22nd to the 25th, and northwestern sector for the rest of the period.

4.2 Meteorological conditions for avalanche winter 16/17

Meteorological values for the 16/17 winter season from the weather station at Nordnesfjellet is represented in Table 7 with respect to differentiation between days defined as avalanche cycle and days not defined as avalanche cycle. Mean values for each parameter was found using hourly measurements in the period 01.10.2016 to 31.05.2017. Days defined as avalanche cycle days show higher mean wind speed and mean air temperature than non-cycle days and the average for the whole period, but lower mean precipitation. Key meteorological data from October 2016 to May 2017 is displayed in Figure 8 for Nordnesfjellet AWS and Appendix figure 13 for Tromsø Vervarslinga. Periods of high precipitation are correlated to increase in air temperature. The snowpack was growing thicker in periods with air temperatures increasing, but not passing zero degrees, and the snowpack became thinner in periods with air temperatures above zero degrees °C. However, it gradually grew thicker throughout the winter season until it reached peak thickness in the beginning of May.

Table 7. Means of hourly meteorological values for 01.10.2016 - 31.05.2017 at Nordnesfjellet weather station (Data source NVE (2018a))

Type	***Days***	***Hourly mean air temperature °C***	***Hourly mean Precipitation (mm)***	***Hourly mean wind speed (m/s scalar average)***
All days	243	-3.44	0.025	4
Non cycle days	188	-3.13	0.026	3.9
Avalanche cycle days	55	-4.55	0.021	4.25

Wind direction and speed for the entire winter and days defined as avalanche cycles are shown in Figure 9 using hourly measurements from Nordnesfjellet AWS. The main wind component for both wind roses are from the south west, however the cycle days displays higher occurrence of wind speed above 11 m/s. Wind directions in cycle days has a slightly more prominent northern component and less in southeastern sector.

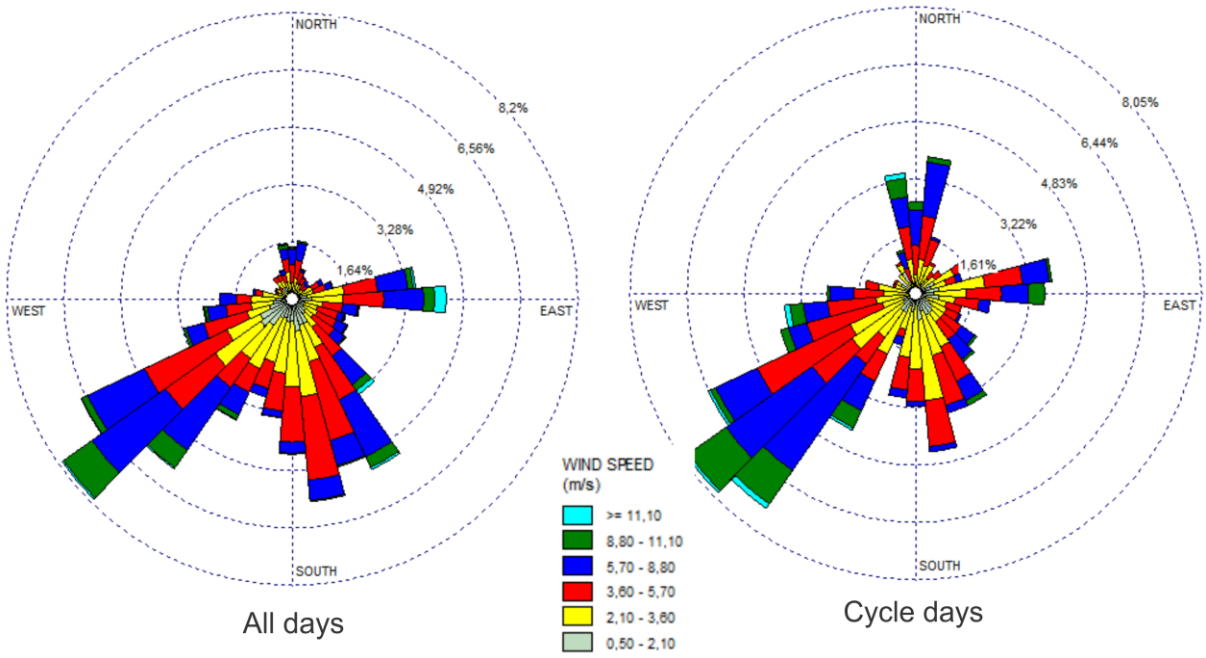

Figure 9. Wind rose for all winter days and days defined as avalanche cycle days at Nordnesfjellet AWS. Data source: (NVE, 2018a)

Wind speed comparison with hourly measurements in between all winter days and cycle days in Figure 10 shows that cycle days has slightly lower wind speeds in the third quartile and considerably lower air temperature in the upper quartile.

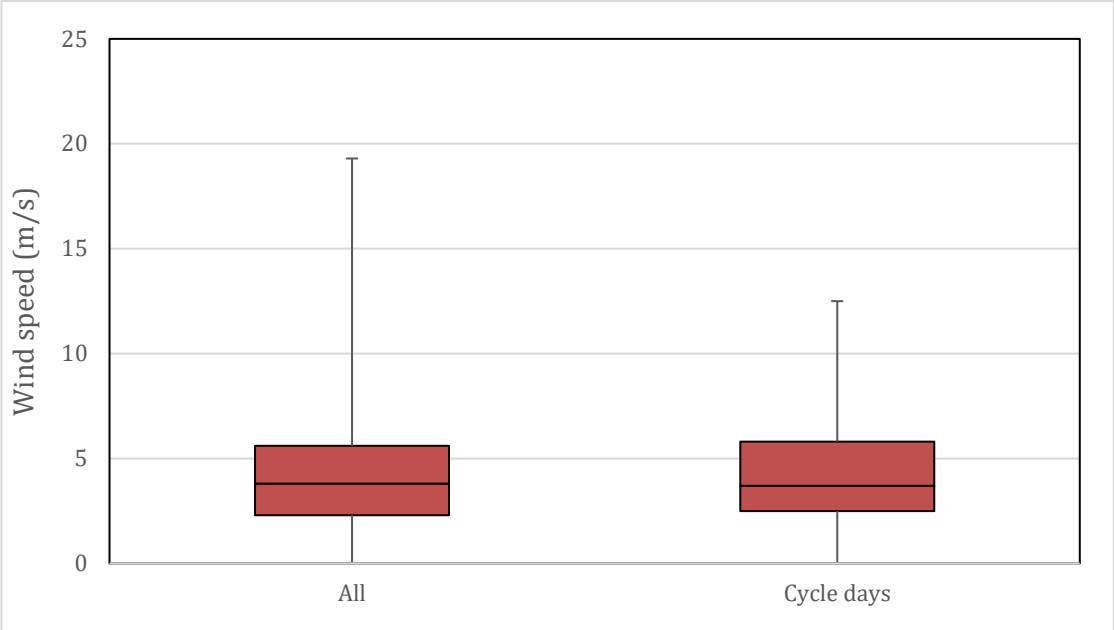

Figure 10. Box plot for wind speed from hourly measurements at Nordnesfjellet AWS for all winter days and cycle days. Data source: (NVE, 2018a)

Air temperatures for cycle days has lower values for second, median and third quartile when compared to all winter days when hourly measurements from Nordnesfjellet AWS are considered. The air temperature minimum however, is considerably lower for all winter days.

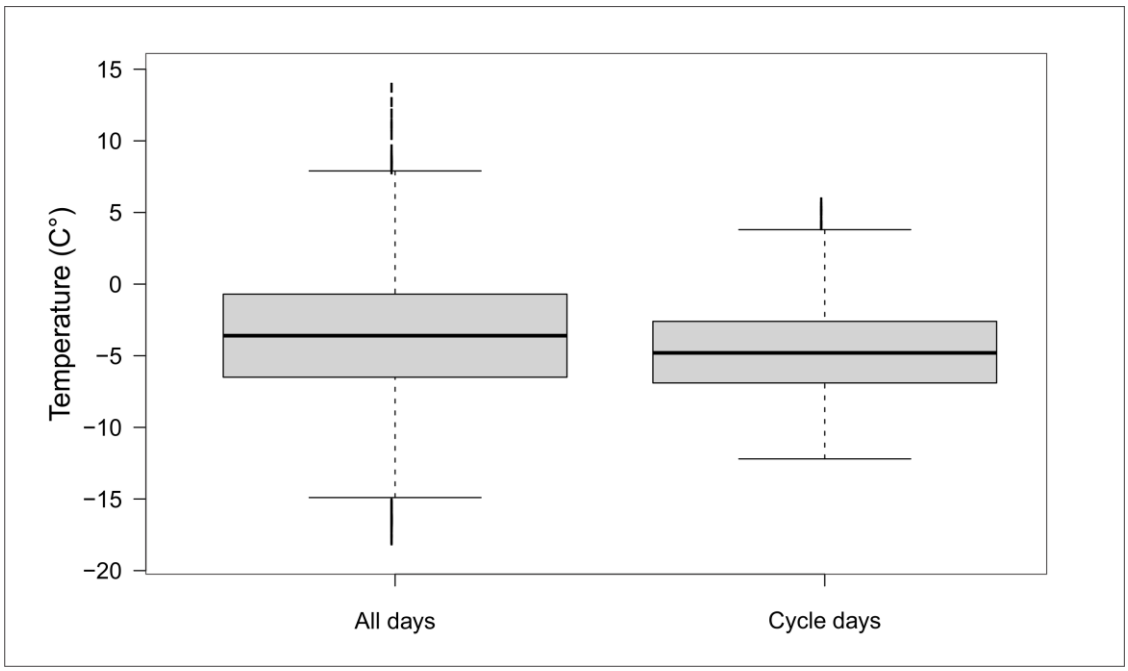

Figure 11. Box plot for air temperature from hourly measurements at Nordnesfjellet AWS for all winter days and cycle days.

4.3 Spatial analysis of avalanche activity

Nine avalanche cycles was defined for the avalanche activity dataset for the 16/17 winter using the criterions specified in section 2.1.2 with a duration between two and twelve days. Fifty-five out of the 189 days in the dataset was within the criterions for an avalanche cycle, which is 28.5% of all the days. In this chapter, these cycles will be studied with respect to spatial occurrence of avalanche activity. In order to precisely describe the spatial avalanche activity, the study area was divided into 9 sections as seen in Figure 12 where sections are Kvaløya North, Kvaløya South, Ringvassøya, Tromsø mainland North, Tromsø mainland South, Lyngen North, Lyngen South, Kåfjord North and Kåfjord South. Figure 13 and Figure 14 displays the spatial occurrence of avalanche activity for the different cycles, and is described in the section below.

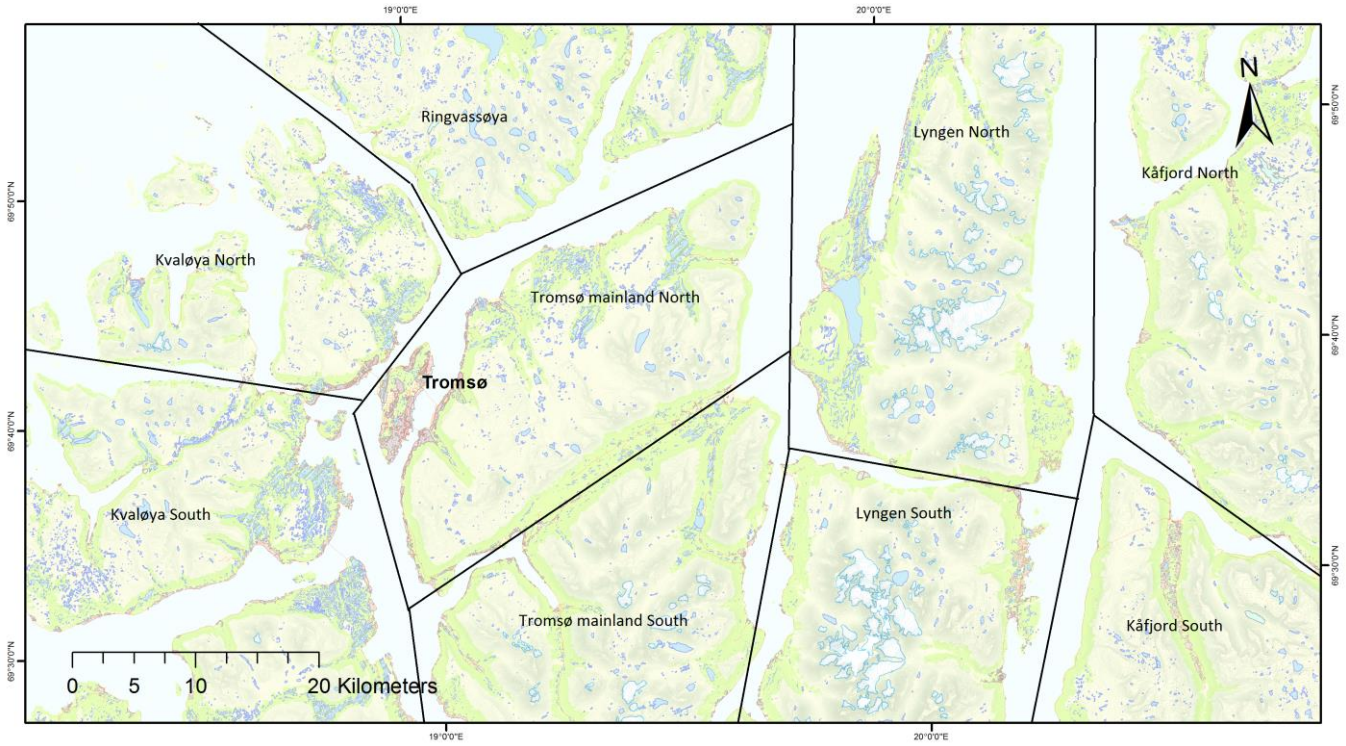

Figure 12. Sections of the study area for description of spatial avalanche activity.

Cycle 1, 2, 5 and 9 had prominent activity in in the Lyngen North and South, section as well as Tromsø mainland south and Kåfjord North, although sparse activity is also seen in all of the other sections. Cycle 7 and 8 had widespread activity throughout the region, and no clear trends in spatial occurrence can be seen. Cycle 4 had avalanche activity throughout the region exception from Kvaløya North and Ringvassøya where there were notably fewer avalanches. The activity in cycle 3 was concentrated in central parts of Lyngen North and southwestern part of Lyngen South areas. For cycle 6, the avalanche activity occurred with highest intensity in Kvaløya South, southern part of Tromsø Mainland North,

Tromsø Mainland South and Lyngen North. Little activity is seen in Kåfjord North and Kåfjord South. In the mentioned regions with high activity, avalanche occurrence had prominent trends where avalanches were stacked together along the sides of the large valleys and less in the high mountain areas.

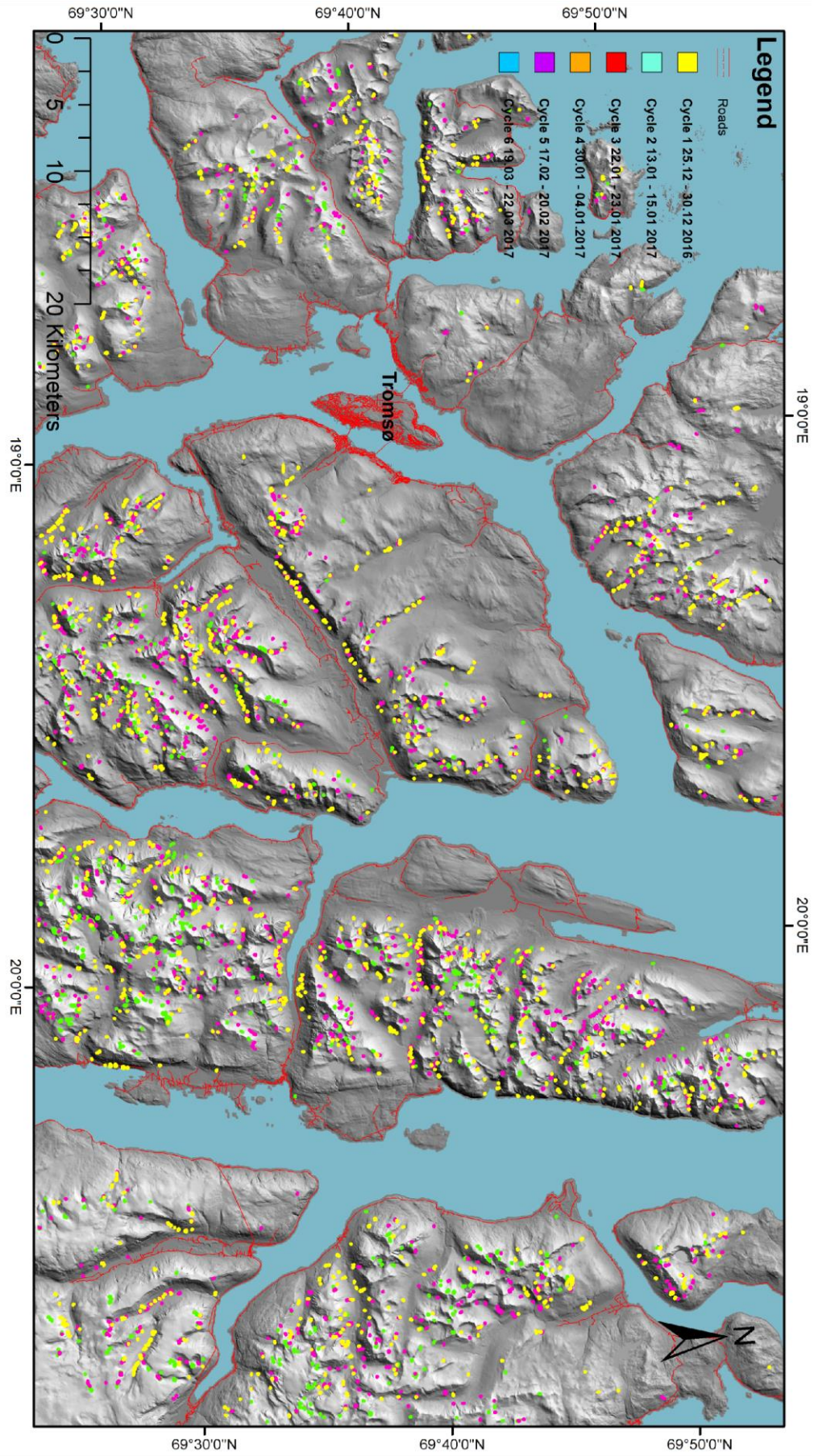

Figure 13. Spatial occurrence of avalanche cycles 1-6 in the study area.

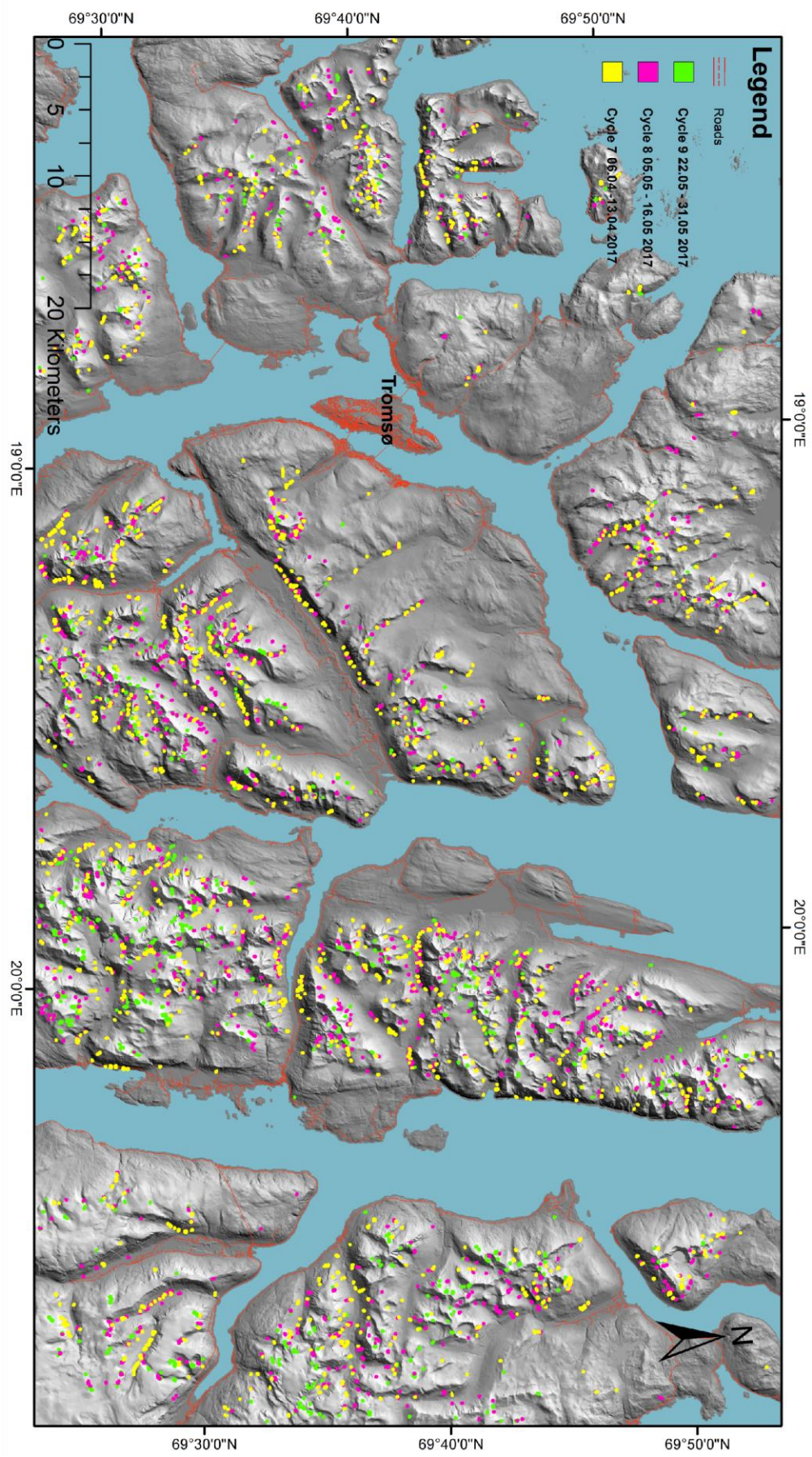

Figure 14 Spatial occurrence of avalanche cycles 7-9 in the study area.

4.4 Synoptic situations of avalanche cycles

The synoptic situation for the periods defined as avalanche cycles was described for 500mb geopotential height, 850mp geopotential height and mean sea level pressure with respect to the occurrence of high and low pressure systems, and their temporal and spatial development in the North Atlantic region. 500mb plot for each cycle is included in this section, while 850mb plots and MSLP plots are included in the appendix.

4.4.1 Cycle 1

In Figure 15 the 500mb geopotential height plots (Figure 15) and MSLP plots for the 25.12-30.12.2017 shows a low pressure-field situated over the Svalbard region with a trough extending southwestward into northern Scandinavia during the 25th and 26th. Then the low-pressure field moved eastward on the 27th and 28th and a high-pressure field extended from the British Isles towards southern parts of Scandinavia, and a ridge developed from this, reaching up to Svalbard. During the 29th and 30th this high-pressure field was stationary, and the ridge was gone.

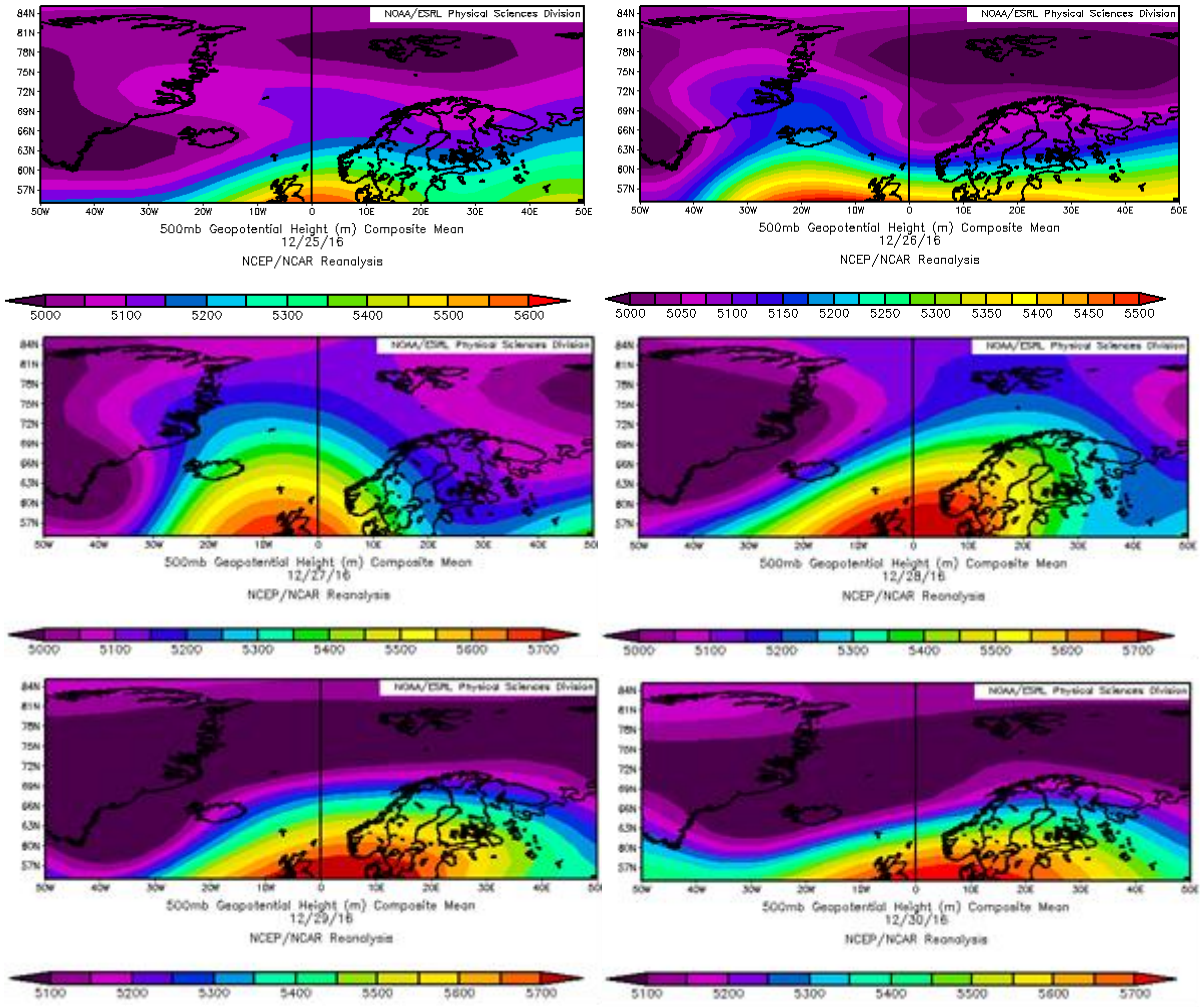

Figure 15. 500mb geopotential height plot for the North Atlantic region during 25.12-30.12.2016.

4.4.2 Cycle 2

In Figure 16 the 500mb height plots for the 13th-15th of January shows a high-pressure field situated west of The British isles, this was stationary during this period. In the 850 mb plot the high-pressure field extended north to Greenland during the 13th and 14th, and up through the Norwegian sea on the 15th, reaching Svalbard. 500mb plot show a large low-pressure area that extended progressively from Svalbard and The Fram Strait eastward to cover Greenland from the 13th-15th. During the 13th and 14th, this low-pressure area had troughs reaching southward to Scandinavia. In MSLP and 850mp a low pressure covered Scandinavia and the Barents Sea on the 13th and diminished progressively during the 14th and 15th.

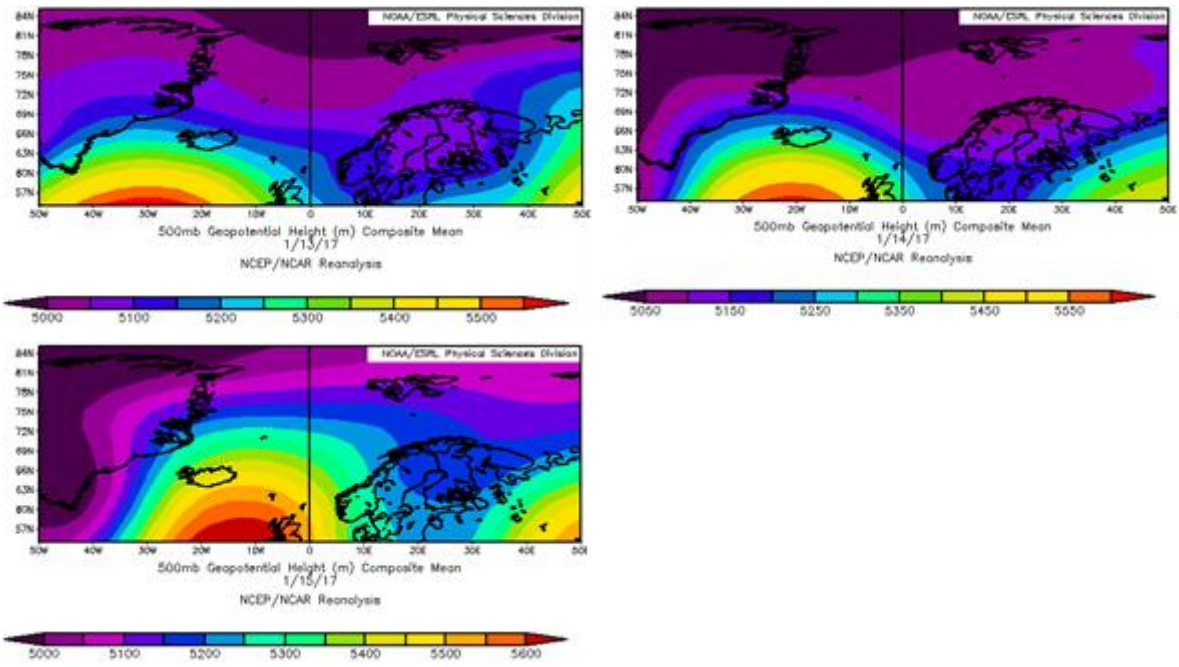

Figure 16. 500mb geopotential height plot for the North Atlantic region during 13.01-15.1.2017.

4.4.3 Cycle 3

The 500mb geopotential height plots (Figure 17) for the 22nd shows a high-pressure field situated over Denmark and southern Norway, that extended towards northwest, and in 850mb plot, this reached Greenland and Svalbard. On the 23rd, this high-pressure had moved westwards to the British Isles, and was less extensive towards Greenland. In 850mb, the north-extending ridge had strengthened, reaching past Svalbard. The MSLP shows a high-pressure over Denmark and the British Isles that developed a ridge during the 22nd and 23rd that extended over and east of Svalbard.

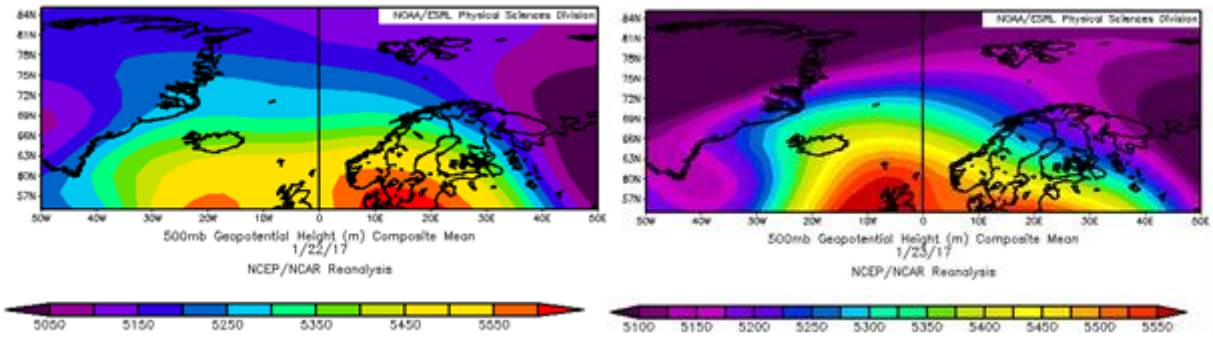

Figure 17. 500mb geopotential height plot for the North Atlantic region during 22.01-23.1.2017.

4.4.4 Cycle 4

The 500mb geopotential height plots (Figure 18) for the 29th shows a high pressure situated over eastern central Europe, which reached over Scandinavia and Iceland with a ridge that extended towards Greenland in 850mb. On the first to second of March, the situation was stable and on the third and fourth, the center of the high-pressure moved northward over Scandinavia in 500mb. A low pressure was situated in the Barents Sea on the 30th in 850mb and on the 30th of January and first of February, the high pressure and ridge remained stable, and the low pressure has moved east of Svalbard. On the 2nd, 3rd and 4th of March, the high pressure progressively expanded and moved its center over Scandinavia, and covered to the entire northern extent of the plot, also strengthening the ridge that reached Greenland.

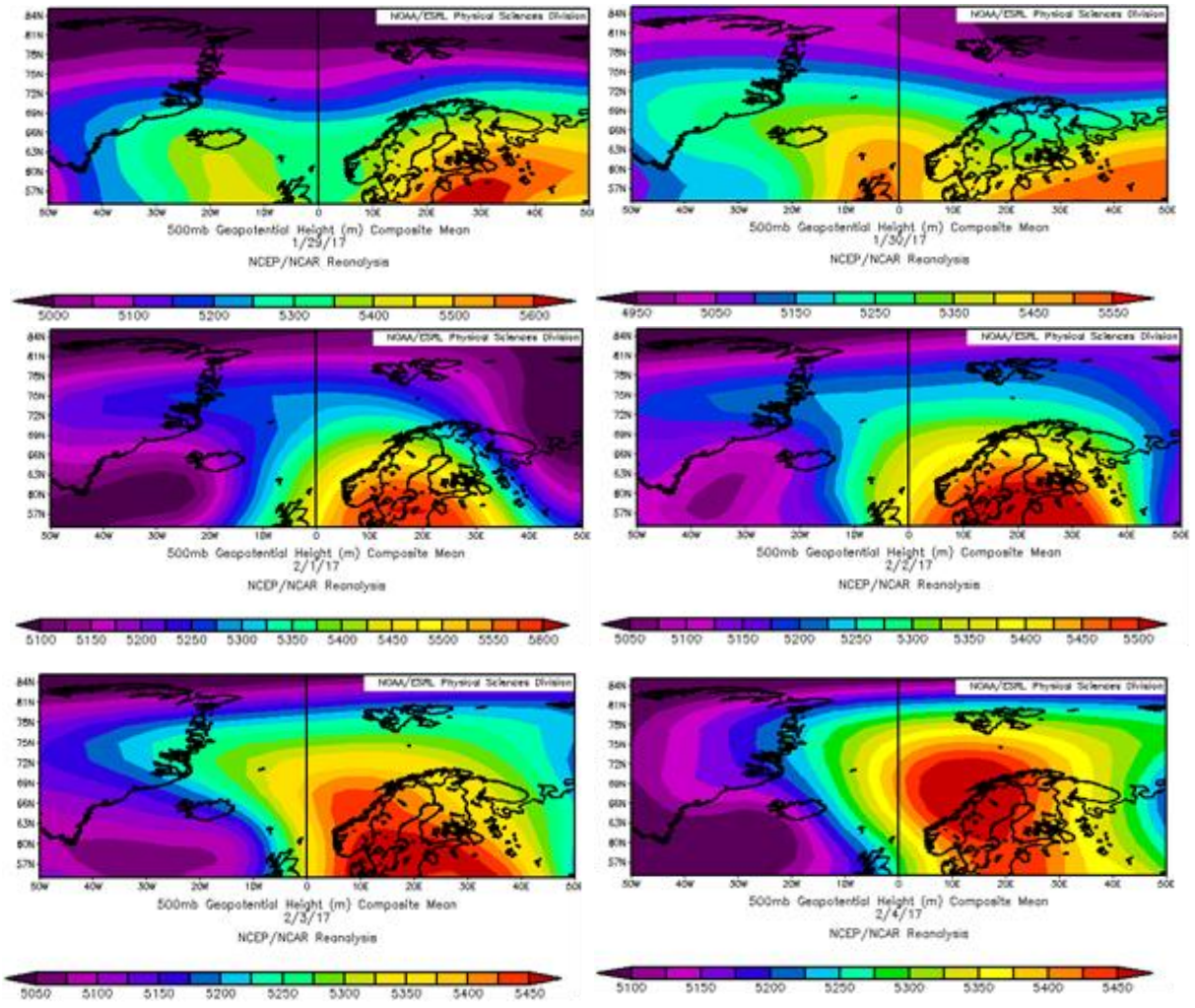

Figure 18. 500mb geopotential height plot for the North Atlantic region during 30.01-02.2.2017.

The mean sea level pressure plot for the 30th of January shows a high pressure that was situated over eastern central Europe, and another high-pressure field in northeastern part of Greenland. Two low-pressures was also occurring, one in the eastern Barents Sea and on southeast of Greenland. On the 31st of January and 1st of February both of the high-pressures extended toward Svalbard, and the low-pressure system that was here on the 30th is progressively moving eastward. On the 1st, 2nd and 3rd, a through progressively developed, that extended from the low pressure over Iceland toward the Barents Sea, reaching western parts of Svalbard on the 3rd. During these days, the high pressures remained stable and on the 4th, the through diminishes.

4.4.5 Cycle 5

In Figure 19 the 500mb geopotential height plots for 17th of February shows a high-pressure that was centered over the British Isles and extended to east over Iceland and Greenland and west over southern Scandinavia and Denmark. A large area of low pressure covered the entire northern extent of the plot. During the next three days, the high pressure was stable, and the low-pressure field progressively extended southward, covering central Scandinavia, Iceland and Greenland. The mean sea level pressure plots for the 17th shows two high-pressure fields, one over Greenland an one over the British Isles. Two low pressures were also present, one southwest of Iceland, and one over northern Scandinavia and the Barents Sea. A through extended between the two low-pressure fields, crossing over Iceland. From the 18th to the 20th, the through deepened and the pressure system in northeast progressively moves its center westward, covering the Barents Sea, Svalbard and Scandinavia.

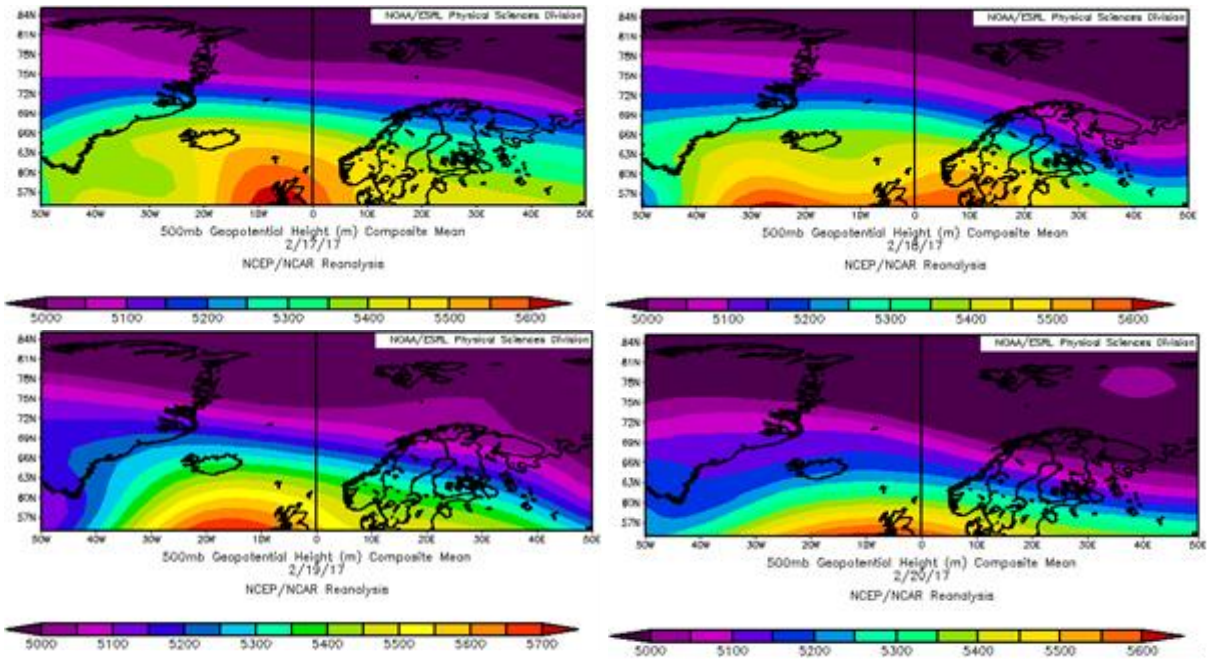

Figure 19. 500mb geopotential height plot for the North Atlantic region during 17.02-20.2.2017.

4.4.6 Cycle 6

In Figure 20 the 500mb geopotential height plots for the 19th to the 22nd of March shows a large area of low pressure in the entire northern part of the plot that developed a trough from the western Barents sea toward the coast of Norway. In addition, a high-pressure field can be seen south of Greenland at the 20th, and this came closer to Iceland during the 21st and 22nd.

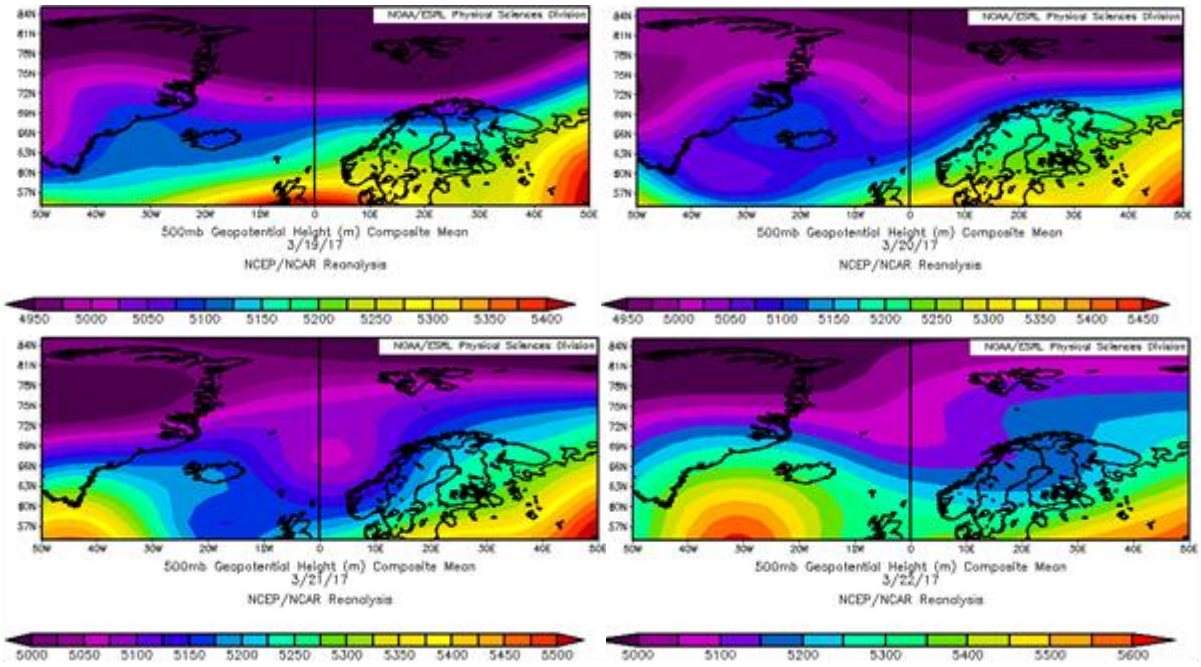

Figure 20. 500mb geopotential height plot for the North Atlantic region during 19.3-22.3.2017.

In the mean sea level pressure plots, a prominent low was present in between Iceland and Norway at the 19th, and this moved towards the Barents Sea and northern Norway during this period. A big low situated over Svalbard at the 19th moved eastward and disappeared from the extent of the plot during the 20th and 21st. A high pressure situated over Greenland at the 19th developed and became higher during the 20th and 21st and a ridge developed from a high-pressure situated south of Greenland, reaching into the Greenland high-pressure during the 21st and 22nd.

.

4.4.7 Cycle 7

In Figure 21 the 500mb geopotential height plots and MSLP plots for the 6th of April shows a high pressure center situated over the British isles, reaching into southern Scandinavia and Iceland. This high-pressure remained stationary until the 9th when it extended towards east and west, and was stationary for the rest of the cycle. A low pressure covered northern Greenland, the Fram Strait, Svalbard, the Barents Sea and northern Scandinavia during the 6th and 7th. On the 8th to 10th, the low pressure diminished, but a trough was extended from north of Svalbard towards northern Scandinavia. From 11th to 13th a low pressure was progressively developing, starting east of Scandinavia, eventually spread across the Atlantic Sea, and reached Greenland. In the MSLP plot, a high-pressure entered the region from northeast during on the 11th and progressively extended over the northern Barents Sea and Svalbard, and eventually reached across the Fram Strait and into Greenland on the 13th. Two low pressure systems is seen on sixth, one in south of Iceland and one covering northern Scandinavia and the Barents Sea. From the seventh to the 10th, the southern low pressure moved northeastward across the Norwegian Sea and eventually merged with the northern low pressure, and remained stationary over Scandinavia for the rest of the cycle.

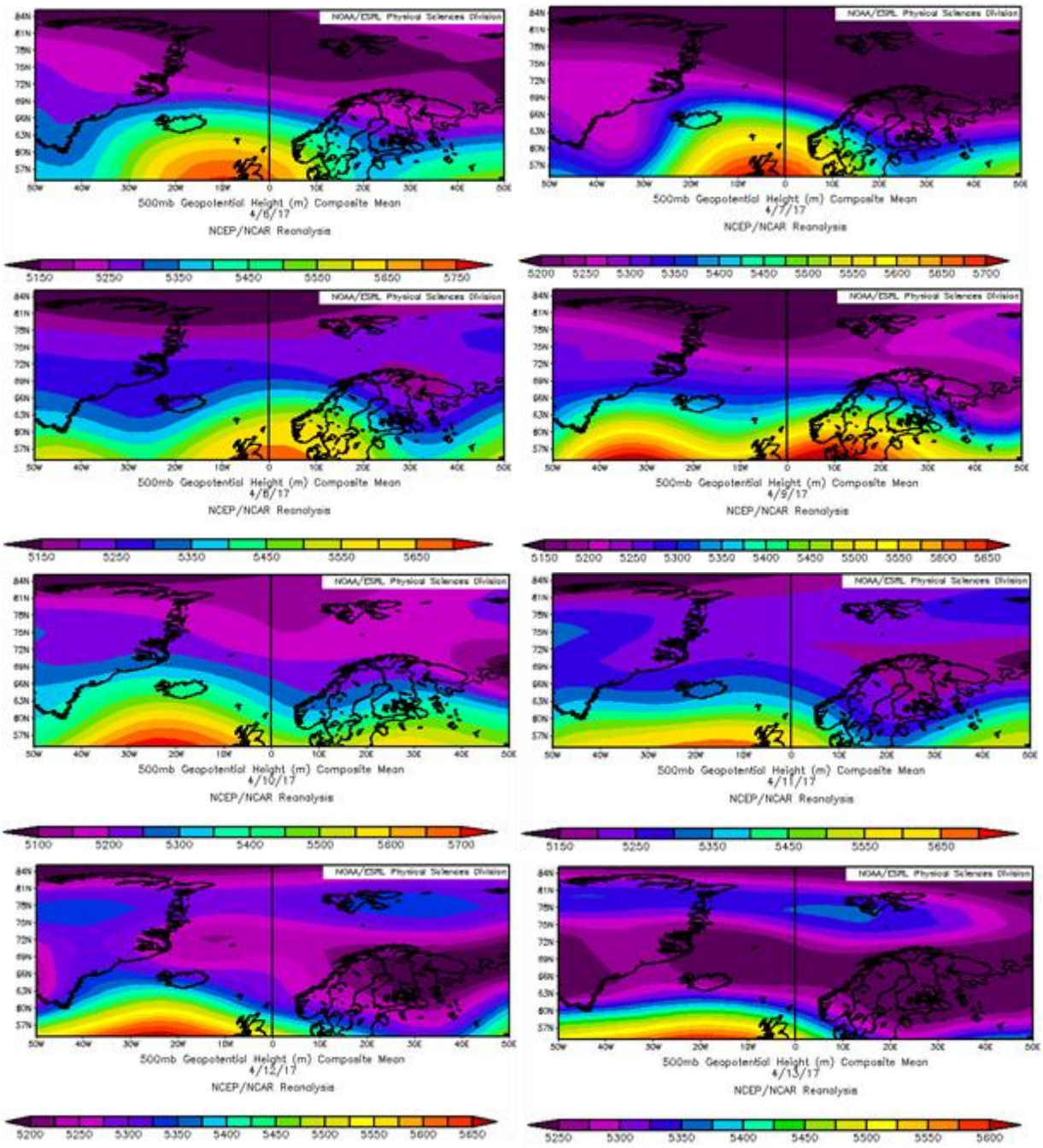

Figure 21. 500mb geopotential height plot for the North Atlantic region during 6.4-13.4.2017.

4.4.8 Cycle 8

In Figure 22, the 500mb geopotential height plots for the 5th of May to the 10th of May shows a high pressure system that was situated over Iceland, and extended over southern Scandinavia and southern Greenland. It progressively moved southwestward as a low pressure moved southwest from east of Svalbard and eventually covered Svalbard, the Barents Sea and Scandinavia, and remained here until the 13th. On the 10th, a trough extended from the low-pressure system and covered Iceland. During the 11th, a low pressure developed from the trough and deepened during the 12th and 13th and remained stationary for the rest of the period. On the 13th to 16th, a high-pressure ridge extended from central Europe toward Iceland and the Norwegian Sea, and eventually covered Scandinavia as well. During the same period, a low pressure was situated east of Scandinavia and covered Svalbard, the Barents Sea and Scandinavia. The mean sea level pressure plot shows that from the 5th to the 9th, a high pressure was situated over Greenland, The North Atlantic and Svalbard, while a low pressure covered the eastern part of Scandinavia. From the 9th to the 11th, a trough extended westward from eastern central Europe to south of Greenland, and a low pressure remained stationary here for the rest of the period. The high pressure remained over Greenland, the Fram Strait and Svalbard throughout the period. On the 11th, a ridge extended from the high pressure over Svalbard towards Scandinavia and from the 12th to the 16th, the high pressure over Svalbard progressively moved to the south of Scandinavia.

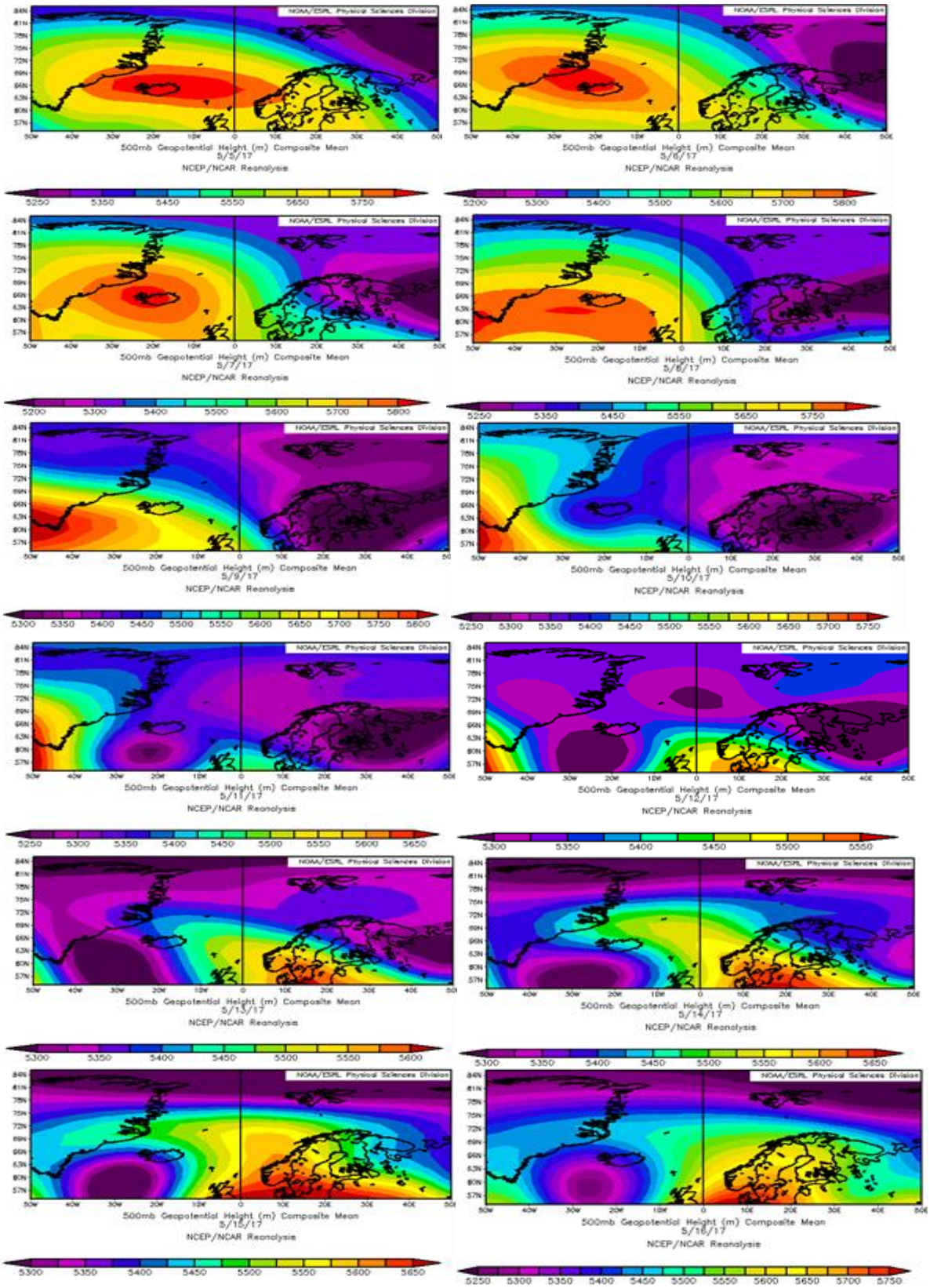

Figure 22. 500mb geopotential height plot for the North Atlantic region during 5.5-16.5.2017.

4.4.9 Cycle 9

In Figure 23 the 500mb geopotential height plots for the 22nd of May displays a high pressure was located over Denmark with a ridge extending north and westward, covering southern Scandinavia, Iceland and southern Greenland. A low pressure covered the northern extent of the plot. This situation lasted from the 22nd to the 29th when the ridge extended further north, and reached northern Greenland. From the 29th to the 31st a high pressure gradually developed over the Fram Strait. The mean sea level pressure plot for the 22nd and 23rd of May shows a similar synoptic situation as the 500mb plots, with two low-pressure fields, one east of Svalbard and one south of Iceland and a high-pressure ridge that extended from Scandinavia, through the Norwegian sea and into northern Greenland. On the 24th and 25th a through extended between the two low-pressure fields, while the northernmost low pressure moved south, and eventually eastward during the 26th and 27th. On the 26th to the 28th a ridge extended from northern Greenland over the Norwegian Sea. A trough moved progressively from a low pressure over Iceland into Scandinavia during the 27th to the 31st.

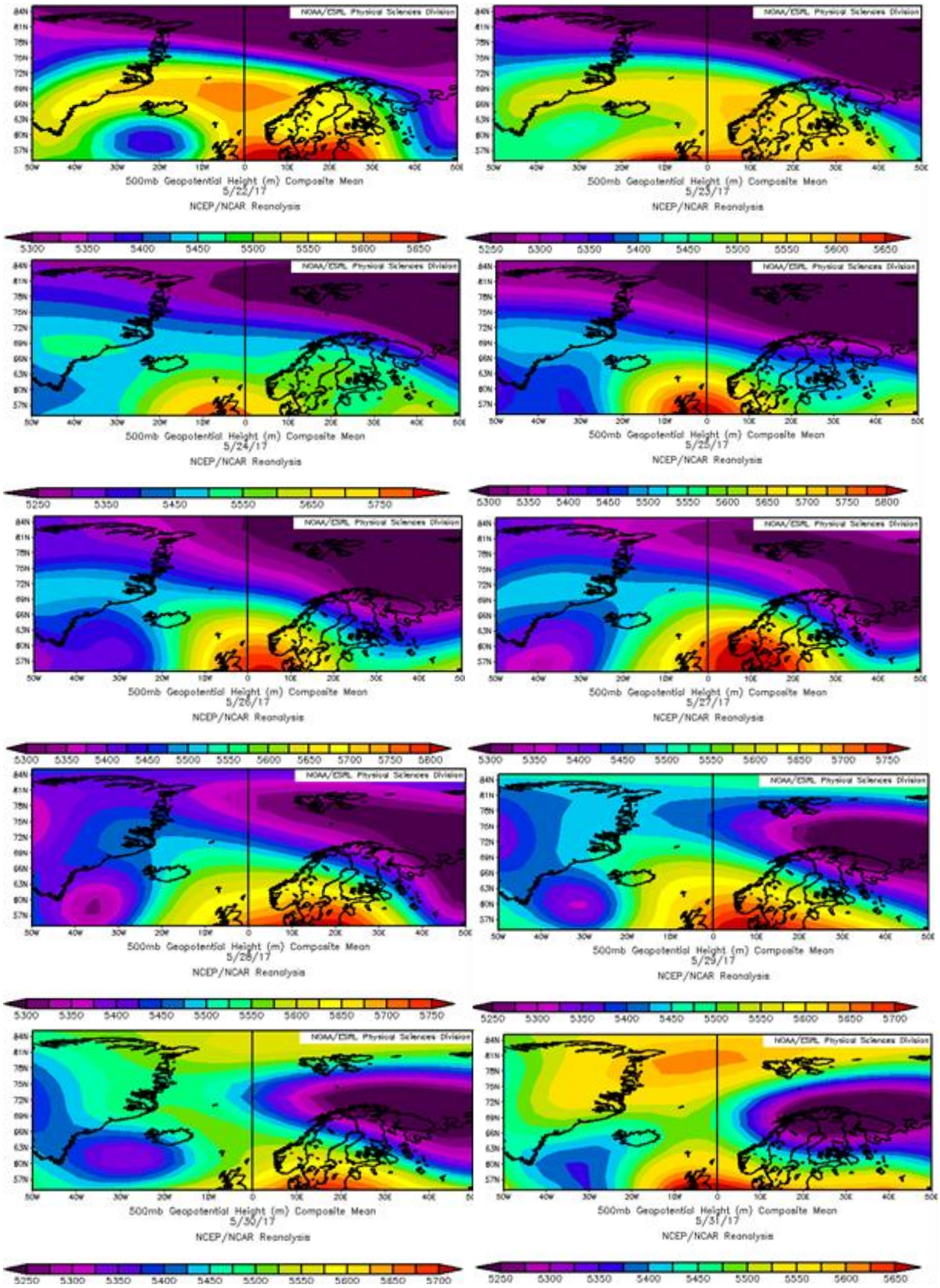

Figure 23. 500mb geopotential height plot for the North Atlantic region during 22.5-31.5.2017.

4.5 Categorization of synoptic types

The synoptic situation for each day in an avalanche cycle was categorized and displayed in Table 8 according to similarities of high and low pressure system occurrences in the North Atlantic region based on daily 500mb, 850mb and mean sea level pressure composite plots. Synoptic types, 1 and 4, occurred with the highest frequency, each with 18 avalanche cycle days. Type 1 and 3 has cycle days spread evenly throughout the winter, while Type 4 has the majority of days in May. Type 5 only occurred in April and May, while type 2, the synoptic type with fewest avalanche cycle days, only occurred December and March. The proportion of synoptic type days are displayed in Figure 24.

Table 8. Synoptic situation categorized by days. Numbers in brackets indicate number of consecutive days of one synoptic type.

Cycle	***Synoptic type 1: High over British Isles***	***Synoptic type 2: Low over North***	***Synoptic type 3: High to Southwest***	***Synoptic type 4: High over Central Europe***	***Synoptic type 5: Low over Scandinavia***
25.12-30.12	25.12-28.12 (4)	29.12-30.12 (2)			
13.01-15.01	15.01		13.01-14.01 (2)		
22.01-23.01	23.01			22.01	
30.01-04.02				30.01-04.02 (6)	
17.02-20.02	17.02-20.02 (4)				
19.03-22.03		19.03	21.03-22.03 (2)	20.03	
06.04-13.04	06.04-08.04 (3)		09.04-10.04 (2)		11.04-13.04(3)
05.05-16.05			05.05-08.05 (4)	12.05-16.05 (5)	09.05-11.05 (3)
22.05-31.05	22.05-26.05 (5)			27.05-31.05(5)	
Total amount of days	18	3	10	18	6

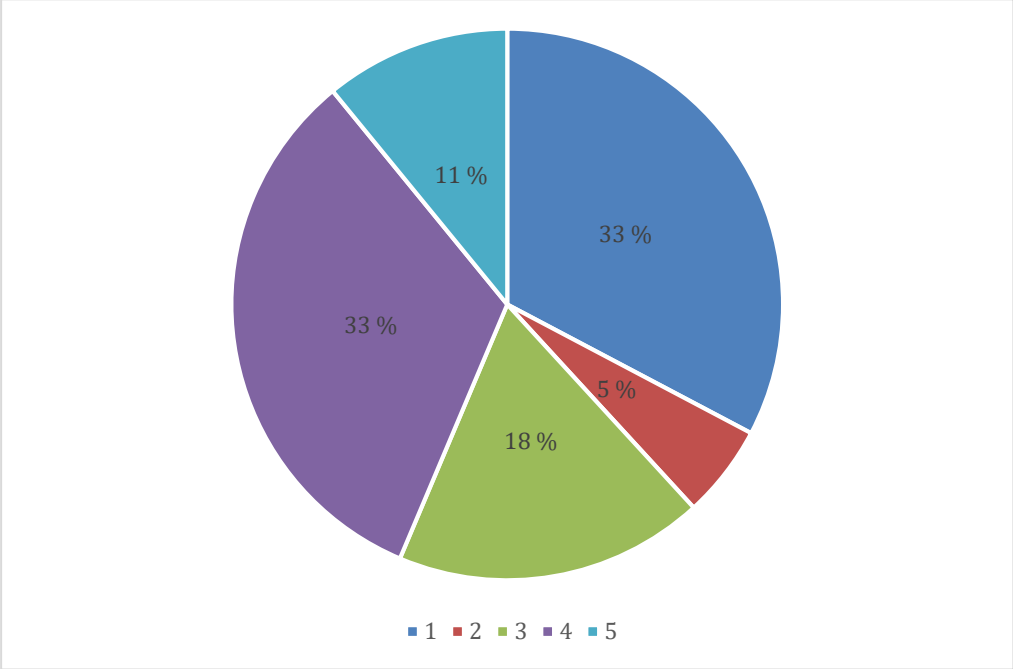

Figure 24. Pie chart displaying proportion of synoptic types as percentage of total number of days within an avalanche cycle.

4.6 Meteorological conditions for synoptic types

Meteorological data for the different synoptic types will be presented in this section. In Table 9, mean values for key meteorological values for the different synoptic types are displayed. Wind speed for the synoptic types ranges evenly in between 3.5 and 5.3 m/s. Synoptic type 1-4 has average wind direction in the southeastern sector, while type 5 has its average in the southwestern sector. Air temperatures for cycle 1-3 are relatively similar. Cycle 5 has the lowest air temperature (-6.2°C) and cycle 4 the highest (-3.5°C). Cycle 1 and 2 has about twice as much precipitation as the latter cycles.

Table 9. Key meteorological data for synoptic types. Hourly (wind speed, wind direction and air temperature) and daily (precipitation) for Nordnesfjellet AWS (Data source: eklima.no)

Synoptic type	***Hourly average wind speed (m/s scalar)***	***Hourly average wind direction (degrees)***	***Hourly average air temperature (°C)***	***Daily average precipitation (mm)***
1	3.5	162.5	-4.8	0.84
2	5	154	-4.8	0.73
3	5.3	172	-5	0.24
4	4.4	132	-3.5	0.34
5	3.8	249	-6.2	0.38

Hourly mean wind direction and speed for the synoptic types are displayed in wind rose diagrams in Figure 25. Synoptic type 1 has wind directions in all sectors, but most measurements occur in the southeastern sector. Wind speeds above 11 m/s are measured from southwest. Some wind measurements occur from the north and east. Synoptic type 2 has the main component of wind direction from southeast with wind speed up to 11 m/s. Type 3 has its main component of wind directions from southwest with wind speed up to more than 11 m/s. Winds up to 11 m/s and above 11 m/s are also measured in the northern sector, and a small component of measurements are from east. Type 4 has its main component in southwestern sector with wind speeds up to 11 m/s, and type 5 in western sector with wind speeds reaching above 11 m/s.

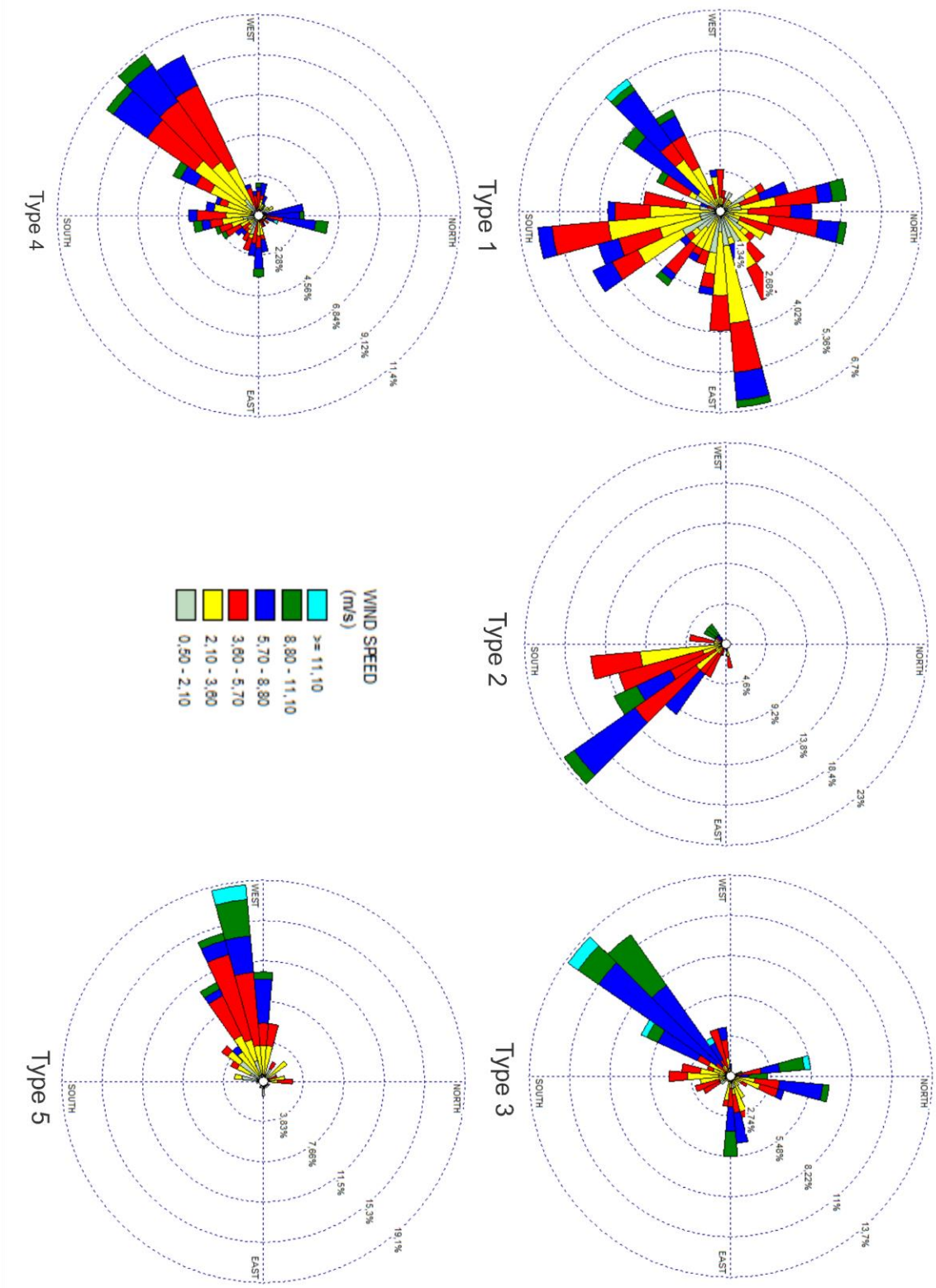

Figure 25. Wind rose for synoptic types 1-5 with hourly wind speed and direction from Nordnesfjellet AWS. Data source: NVE (2018a)

Box plots of hourly mean wind speed measurements showing the distribution of wind speed for each of the different synoptic types are displayed in Figure 26. Wind speed box plots for all synoptic types except type 3 shows a large span of wind speeds, with the majority of measurements in the third quartile and whiskers. Type 1 and 5 has the lowest first quartile, median and third quartile measurements, but has higher values in the whiskers than type 2. Type 3 has the largest range of measurements, the highest median values and the highest whisker values. Type 4 has higher values in the upper whisker than type 2, but relatively equal median and third quartile values.

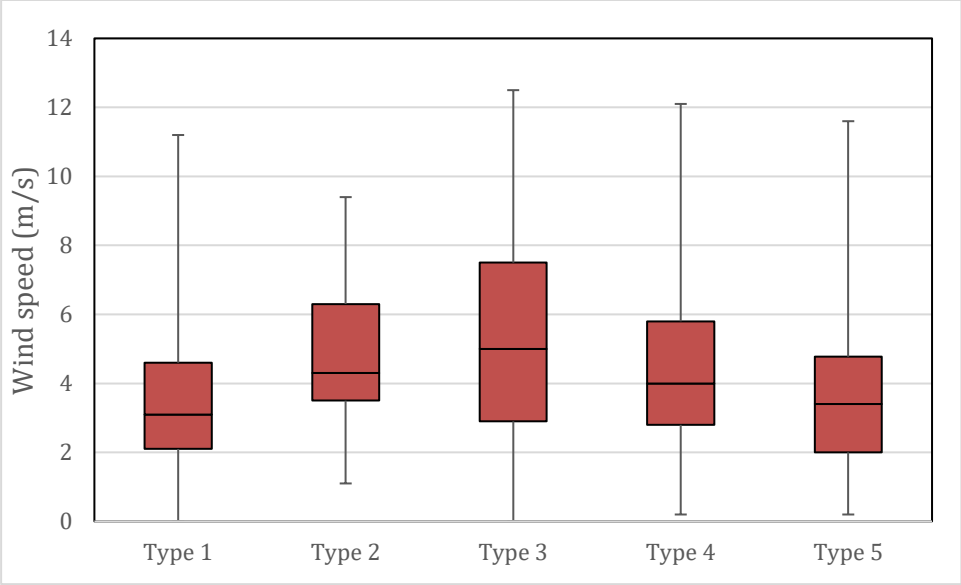

Figure 26. Box plot for synoptic types using hourly wind speed measurements from Nordnesfjellet AWS. Data source: NVE (2018a)

Figure 27 shows box plots displaying mean hourly air temperature measurements for the different synoptic types. Synoptic types 1 and 4 has the highest third quartile and whisker values and are the only synoptic types with air temperature exceeding 0° C while excluding outliers. They also have the lowest whisker values indicating a high range of air temperature measurements. The majority of the air temperature measurements for type 2 was in the first quartile, between -2.5 and -6°C. Type 3 and 5 have the lowest air temperature ranges, though type 3 has the most outliers, some reaching almost 5°C. All synoptic types have median values ranging between -2 and -5°C.

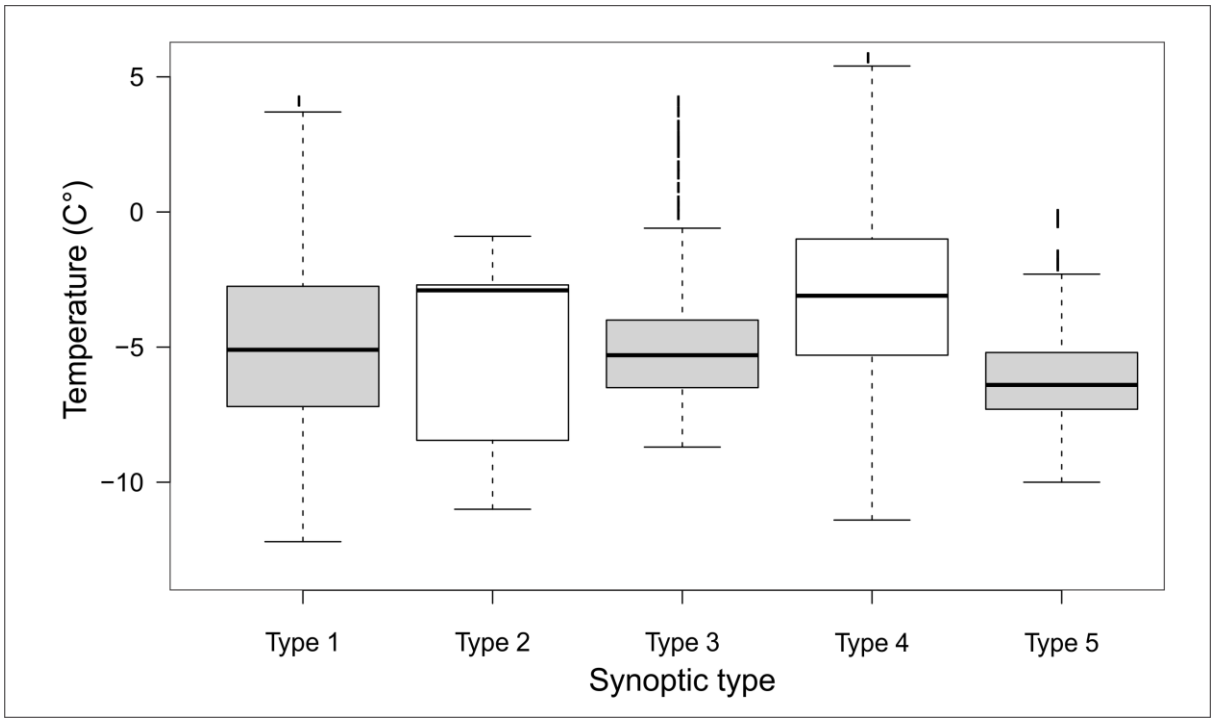

Figure 27. Box plot for synoptic types using hourly air temperature measurements from Nordnesfjellet AWS. Data source: NVE (2018a)

In Figure 28 the synoptic conditions for avalanche cycle days for each synoptic type has been compiled and displayed in 500mb geopotential height and MSLP. Synoptic type 1 was recognized by a high pressure centered over the British Isles and a low pressure covering the northern extent of the plot in 500mb. In MSLP, a low pressure was situated over northern Scandinavia and Russia. Type 2 exhibited a large low-pressure system in the northern extent of the 500mb plots and MSLP plot and high pressure over Central Europe in both. Type 3 exhibited a high pressure west of the British Isles in 500mb that extended a ridge towards Greenland in the MSLP plot. Northern Scandinavia was covered by a low-pressure system in both plots. In the plots for synoptic type 4, a high pressure was situated over Central Europe in 500mb, and in MSLP, which extended over Scandinavia, the Barents Sea and Svalbard. A low pressure was situated southwest of Iceland in both plots. Synoptic type 5 was recognized by a low pressure centered over eastern Scandinavia in both 500mb plot and MSLP, with a trough that extended westward over Iceland in MSLP.

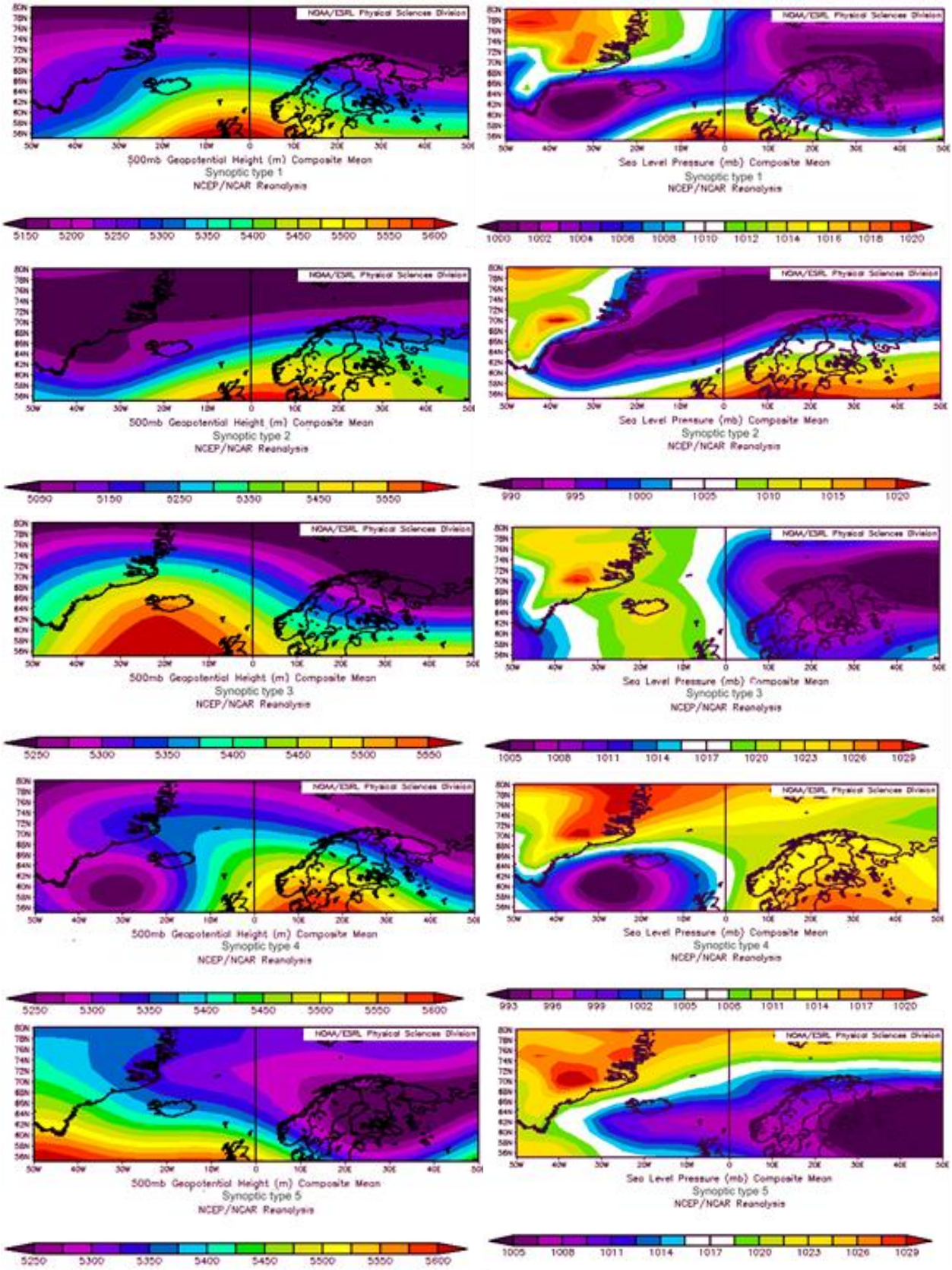

Figure 28. Synoptic conditions for synoptic types 1-5 using the categorized cycle days in 500mb geopotential height and mean sea level pressure.

5 Discussion

5.1 Local and synoptic conditions during avalanche cycles

In this section, the results concerning local meteorological conditions and synoptic conditions will be discussed in terms of their relation to generating the snowpack conditions leading to avalanche cycles. Data from Nordnesfjellet AWS (from heron referred to as NF) and Tromsø Vervarslinga weather station (from heron referred to as TV) were used.

Periods with avalanche cycle activity were distinguishable from non-cycle winter days by lower air temperatures (Figure 11), lower precipitation and higher average wind speed (Table 7). They also exhibited values well above the threshold for transportation of snow (Figure 10) as described by Li and Pomeroy (1997), where 9.9 m/s and 7.7 m/s was found to be the average wind speeds necessary for the transportation of wet and dry snow, respectively. Wind direction for non-cycle winter days had a main component in the southwestern sector and a minor component from south-southwest, likewise as cycle days. Cycle days did however have a distinguishable northern component with strong winds (Figure 9). Lower air temperatures and less precipitation during cycle days is not in accordance with findings by Birkeland and Mock (1996), who related atmospheric conditions that produced storm events with heavy snowfall to the occurrence of avalanches. Also, Hansen and Underwood (2012) found that a slight increase in air temperatures and conditions favorable for transportation of moist air were induced by certain atmospheric patterns, which allowed for heavy snow precipitation which overloaded the snowpack and caused size 5-avlanches. It may be explained by that low air temperatures slows down the stabilization process in the snow cover, and higher wind speeds may lead to snow transportation and subsequent avalanche activity (McClung, 2006). The low temperatures can also contribute to avalanche activity by the process of widespread constructive metamorphism in the snow pack, that acts as weak layers and cause formation of avalanches (Schweizer et al., 2003) . This is consistent with the findings by Velsand (2017), who discovered that the climatic conditions in the study area were favorable for the creation of these layers.

5.1.1 Avalanche cycle properties and triggering mechanisms

Avalanche cycles in this dataset occurred throughout the winter season in a variety of conditions. Six cycles (cycle 1, 3, 4, 5, 6, 7) occurred within 72 hours after periods of precipitation, either as rain at sea level, or as snow, with air temperatures close to 0 °C. Among these, cycles 4 and 7 had air temperatures

reaching over zero degrees at NF. It is, however, likely that precipitation occurred as snow in higher altitudes. Wind directions during precipitation before these cycles was from western to northern sector, and above the threshold for wind transportation of snow, found by Li and Pomeroy (1997). Periods after precipitation were characterized by wind directions changing to east or southerly. Precipitation as snow and wind speed above the threshold for snow transportation leads to loading of mountain slopes and creation of dry slab avalanches (Schweizer, 2016). These will typically occur during or in the first days following a wind and snow event, before the snow pack has been able to stabilize. Further wind events leading to transport of snow will prolong the cycles. According to the avalanche forecast at varsom.no for Lyngen and Tromsø forecasting region, winds slabs or storm slab was the main avalanche problem during all these cycles. Both avalanche problems are related to the induction of new or old snow added to the snowpack during precipitation under wind events or redeposited from wind transport (NVE, 2018b).

Cycle 2 occurred without precipitation and with southerly winds in advance of the cycle, and also too early in the winter for the sun to be a factor for avalanche release, which makes it difficult to assess the triggering factor for the cycle. The avalanche problem during this cycle were wind slab at the 13th and storm slab during the 14th and 15th of January for Tromsø and Lyngen forecasting region (Appendix figure 14, Appendix figure 15). Small amounts of precipitation (< 1mm) were measured during the avalanche cycle days, however, the spatial occurrence of precipitation may differ throughout the region, making storm slab a likely problem in areas where snowfall may have occurred.

Cycle 7, 8 and 9 occurred late in the season. All three avalanche cycles followed after a warm period with southeasterly winds, and all cycles had precipitation as snow at high mountain altitude during the duration of the cycle. The length of the cycles did however allow for different triggering mechanism for the avalanches during their extent. Cycle 8 had winds above the threshold for wind transportation which was described by Li and Pomeroy (1997) during the 4th and 5th, and also during the 7th of May, combined with snowfall and winds from northwest, making transportation of loose snow in the terrain a possible cause for avalanching. Another factor for avalanching in the late season were wet loose snow avalanches triggered by high air temperatures or from sun radiation (Schweizer et al., 2003). This assumption is in favor with the avalanche forecast where wet loose avalanches were the primary or secondary avalanche problem for the last three days of cycle 7, the eight last days of cycle 8 and the seven first days of cycle 9 for Lyngen and Tromsø forecasting region (Appendix figure 14, Appendix figure 15).

Wind direction from the western sector, air temperature increase and precipitation in the beginning of the cycles were in a majority of the situations occurring simultaneously, which is in agreement with how the governing climatic conditions in the region for wintertime are described in literature by Parding (2016). The synoptic conditions governing the initiation of avalanche cycles initiated by westerly flow and precipitation were recognized with low-pressure activity originating from east or north in 500mb geopotential height, with troughs that extended over northern Norway and the Norwegian Sea in 850mb

geopotential height and at ground level. An example for this situation is shown in Figure 29, displaying 500mb geopotential height, 850mb geopotential height and mean sea level pressure for the 19.03.2017.

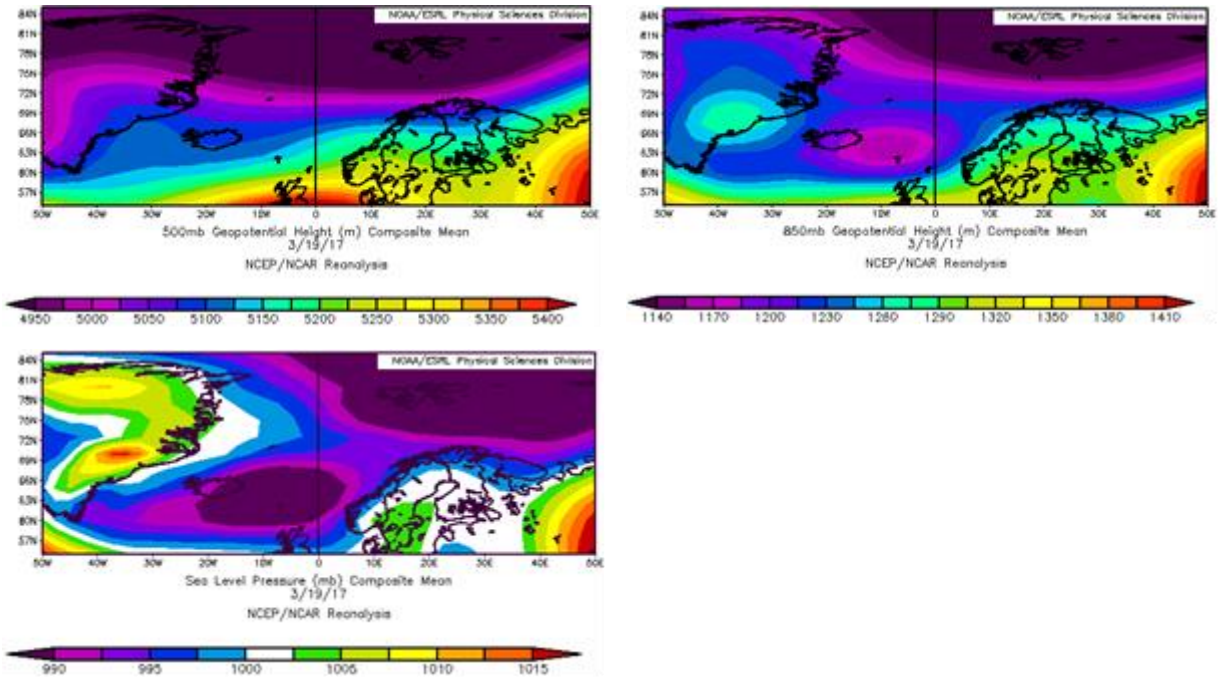

Figure 29. 500mb geopotential height, 850mb geopotential height and mean sea level pressure for the 19.3.2017.

Periods with little precipitation often occurred in combination with easterly or southerly flow. Varying synoptic situations were associated with these conditions, e.g. cycle 2, which occurred while a high pressure were over southern Scandinavia, and the study area was placed in the northern extent of this in 500mb geopotential height, and under a ridge in MSLP. Another e.g. were during the latter half of cycle 8, and from the 26th to 29th of May during cycle 9, where negligible amounts of precipitation was measured, and wind speeds were low and originating from the eastern sector. Synoptic conditions for these periods were recognized with a high pressure over central Europe in 500mb geopotential height, and ridges that extended northwards over northern Norway and the Barents Sea from this in 850mb geopotential height and mean sea level pressure as in e.g. Figure 30, displaying 500mb geopotential height, 850mb geopotential height and sea level pressure for the 26.05.2017.

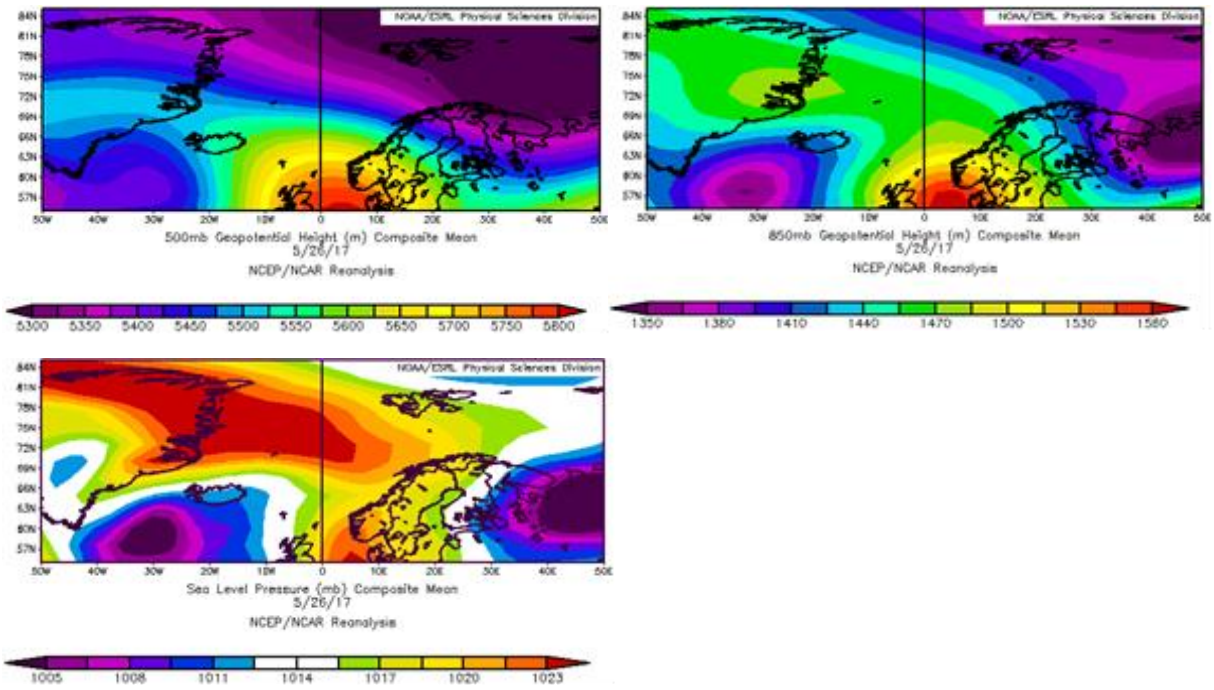

Figure 30. 500mb geopotential height, 850mb geopotential height and mean sea level pressure for the 26.05.2017

Differences in the spatial occurrence of avalanche activity in the study area were in most cases related to the intensity and magnitude of the respective avalanche cycle since more widespread spatial activity was occurring during cycles with more intense or prolonged avalanching. In the opposite case, avalanche cycles with less intensity or a shorter time span had a spatial distribution restricted the high mountain areas. E.g. are cycle 5, which was the most intense avalanche cycle with highest number of avalanches per day of all the avalanche cycles, and had widespread activity throughout the study area. An example for the opposite case was avalanche cycle 3, which was the shortest cycle and the avalanche activity was constrained to Lyngen north and south sector. Avalanche cycle 6 displayed a significant pattern in distribution of avalanche activity (Figure 31), where avalanche debris occurred in all aspects, but particularly in the southwest, south and southeast facing hillsides of valleys, where the avalanche debris was occurring in close proximity to each other along the hillsides. The cause for this spatial pattern may be correlated to the specific meteorological conditions during the cycle. 10 cm of new snow was recorded at TV within 72 hours prior to the cycle while north to northwesterly winds prevailed until the 19th when the wind direction changed to southwesterly - southerly. According to varsom.no, the avalanche problem for the Tromsø and Lyngen forecasting region (Appendix figure 14, Appendix figure 15) were wind slabs and persistent weak layers. The spatial pattern of avalanche activity may therefore be a result of snow transportation during the north – northwesterly wind event into southwest, south and southeast facing hillsides, where dry slab avalanches were triggered due to loading on an already unstable snowpack. The southwestern and southern winds later in the cycle may have been responsible for snow transportation into north and northeast facing hillsides, causing further avalanche activity here.

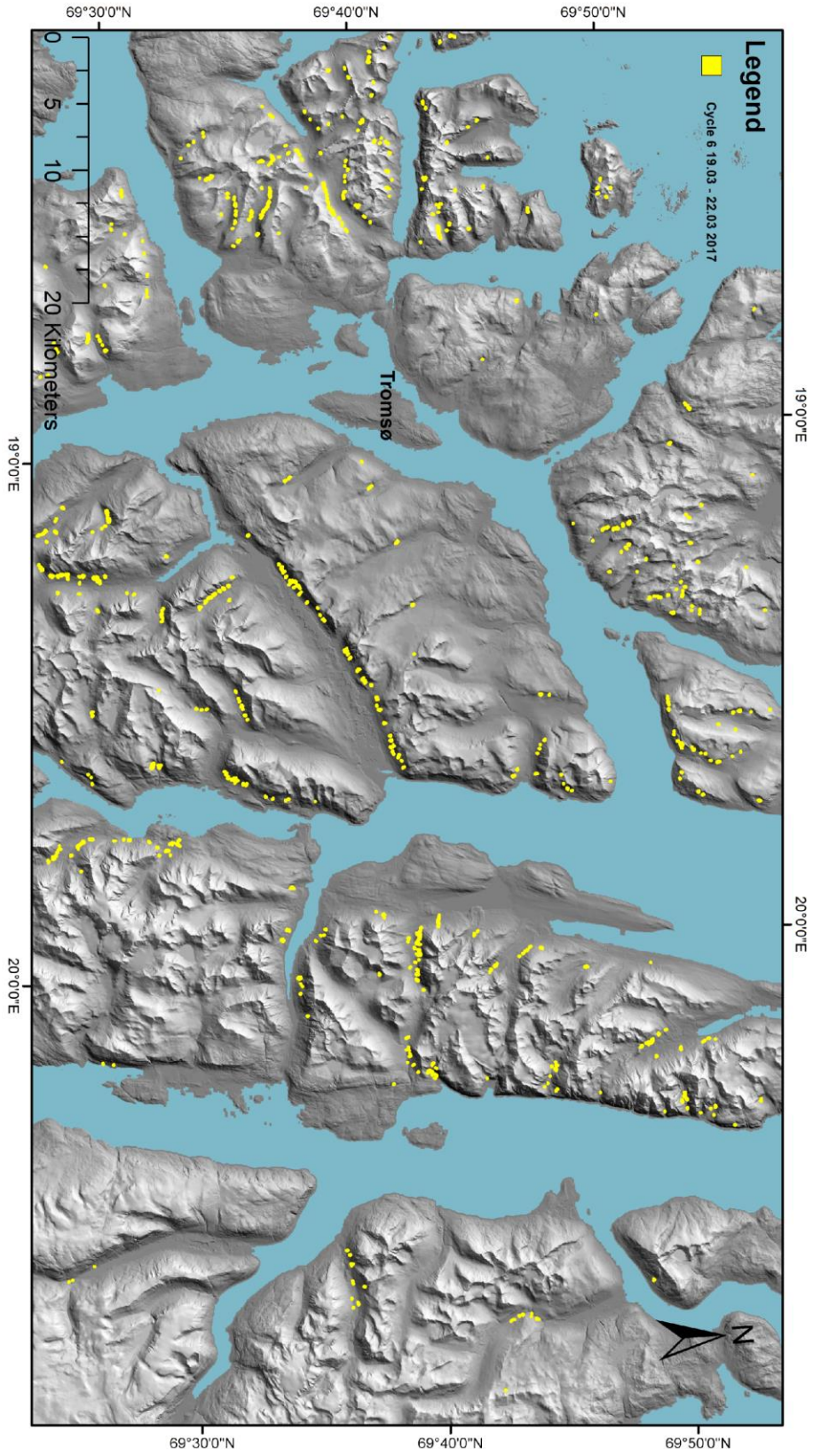

Figure 31. Spatial occurrence of avalanche activity for cycle with avalanche debris in blue.

5.2 Temporal occurrence of avalanche cycles

The avalanche cycles in the 16/17 winter season occurred from the end of December to the end of May. The constraining factor for this period were the satellite detections that were done during the avalanche forecasting season, lasting between December and May. The spatial occurrence of avalanche cycles was characterized by short avalanche cycles with a maximum duration of 6 days during the first four months and avalanche cycles with up to 12 days of duration during the latter two months. Fifty four percent of all avalanche cycle days occurred in April and May. This may be linked to the growing complexity of the snowpack during the winter. This is indicated by the fact that seventy percent of avalanche cycle days during the three last cycles had more than one avalanche problems and only twenty-four percent of the avalanche cycle days during the first six cycles had more than one avalanche problem in both Tromsø and Lyngen forecasting regions, whilst the remaining had only one. Growing snow pack complexity is also indicated by the occurrence of persistent weak layers, which was occurring during cycle 6-8 in the Tromsø forecasting region (Appendix figure 14) and during cycle 5-8 in the Lyngen forecasting region (Appendix figure 15). Moreover, increasing air temperatures and rain during the spring may have caused destabilization of the snowpack and the occurrence of wet snow avalanching (McClung, 2006). The shorter spatial extent of the first six avalanche cycles may be related to that the main avalanche problem in the forecasting regions considered was either storm slab or wind slab, which are characterized by stabilization within a few days after wind or snow events if the conditions are favorable (NVE, 2018b), leading to a decrease in avalanche activity.

5.3 Synoptic types

500mb geopotential height plots and mean sea level pressure plots were used to distinguish and categorize individual cycle days into five different synoptic types, displayed in Figure 28. The five synoptic types show different atmospheric circulation patterns over Scandinavia and the North Atlantic region during days of avalanche activity. In this section, the meteorological conditions occurring during the respective cycles will be discussed.

One of the two most frequent synoptic types for this dataset was type 1 (Figure 28), which was recognized during eighteen avalanche cycle days occurring evenly throughout the season. It was characterized by high pressure situated over the British Isles, and low pressure were covering Greenland, the Fram Strait, the Barents Sea and northern Scandinavia at 500mb geopotential height. At sea level, the low pressure was limited to cover the Barents Sea and northern Scandinavia. The wind directions for synoptic type 1 exhibits wind from all sectors (Figure 25), with a slight majority of wind directions were occurring in the southeastern and eastern sector. The range of wind speeds (Figure 20) and air temperatures (Figure 27) were among the highest for the synoptic types, and the daily average precipitation was higher than for all other types. A type with a similar synoptic situation, but less common was type 2, which differed in mean sea level pressure where a low pressure extended from eastern Barents Sea, across Scandinavia and to Greenland (Figure 28). These two types also differed in wind directions, since type 2 had a clear trend of southeastern winds, with wind speeds up to 11 m/s. Type 2 was also occurring during days with lower air temperatures than type 1, alongside higher median wind speeds. Synoptic type 1 and 2 exhibited the highest average for precipitation among the synoptic types, combined with easterly winds. This is inconsistent with current literature, were precipitation is assigned to originate from northerly or westerly flow (Klimaservicesenter, 2016; Rabbe, 1975). The synoptic situation of type 1 and 2 does however show similarities with findings from Pohjola and Rogers (1997), where low pressures in the vicinity of Iceland and in the Barents Sea at sea level pressure and high pressure over central Europe in 500mb geopotential height are related to precipitation in northern Scandinavia during wintertime.

Synoptic type 3 (Figure 28) was the third most common synoptic type associated with avalanche activity with 10 days during the 16/17 winter season. It was characterized with air temperatures below the average for cycle days. It had the highest wind speed of the synoptic types (Figure 27) and a significant occurrence of wind originating from southwest with wind speed that exceeded 11 m/s, and a minor portion of wind measurements occurring from the northern sector with wind speed exceeding 11 m/s (Figure 25). It did, however exhibit the lowest values for precipitation among the types. These conditions were induced by a low pressure situated over northwestern Scandinavia at 500mb geopotential height and at sea level, while a large high pressure is situated south of Iceland in 500mb geopotential height, and a ridge extending from this high pressure over Greenland at sea level (Figure 28). Synoptic type 3

is somewhat similar to the conditions that favor the northerly flow from the Barents Sea and Fram Strait and sometimes the occurrence of polar low outbreaks that reach the mainland, described by Wilhelmsen (1985), which are associated with local precipitation and wind events (Kolstad et al., 2009).

The other most frequently occurring type was type 4, which was recognized in 18 cycle days during the winter. It was the synoptic type with highest air temperatures, reaching up to 5 °C. This may be related to the fact that majority of the days occurred in May. The remaining days occurred from late January to the middle of March. Wind directions were almost exclusively from the southwestern sector, with wind speeds up to 11 m /s. Precipitation for this type was the second lowest among the types. For this type, a high pressure was situated over central Europe in 500mb geopotential height, and extended northward ridge, covering Scandinavia and the Barents Sea at sea level pressure. A low pressure was situated south of Iceland in 500mb geopotential height and at sea level. This synoptic set up allows for warm, moist laden southwestern airflow in a pattern similar to those described by Serreze et al. (1993) for winter cyclone paths into the North Atlantic.

Synoptic type 5 was recognized for six avalanche cycle days, three in April and three in May. It exhibited the lowest air temperatures of the synoptic types. Wind speeds had the second lowest median, but the highest measurements were at over 11 m/s. A significant trend was seen in the wind direction for this cycle, as close to all measurements originated from west. Precipitation for this type was the highest for synoptic types with westerly flow. The synoptic situation for type 5 was a low pressure covering Scandinavia with a trough that extended towards northern Greenland in 500mb geopotential height and a low pressure over the same area at sea level pressure.

The synoptic types 3, 4 and 5 that occurred with significant signals in wind direction from the western sector were also the ones with the lowest average measures for precipitation. This may be related to the placement of Nordnesfjellet AWS in relation to the coast where westerly precipitation originated from, as topography and distance from the coast affects the temporal distribution of precipitation (Klimaservicesenter, 2016; Uvo, 2003).

5.4 Study limitations

The limitations in this study are related to the reliability of the datasets applied in the analyses, their temporal resolution and coverage as well as the uncertainties related to measurements of the meteorological parameters. These limitations will be discussed in the sections below.

5.4.1 Avalanche activity dataset

The avalanche activity dataset used in this thesis was acquired using Sentinel 1 satellites with daily orbit over the study area. Gaps occur in the dataset for every fifth day. This creates an uncertainty regarding temporal precision when applying the definitions for avalanche cycles given in the 2.1.2 Avalanche cycles section. However, the definition (used in this thesis) of an avalanche cycle includes the day prior to the day when the threshold for avalanche activity is reached. The application of SA1 satellite images combined with an avalanche detection algorithm allows for a precision of up to 72% of correctly detecting avalanche debris when compared to manual detection. Also, slopes with lower angle than 35° has been masked out from the algorithm, which may exclude debris from small avalanches deposited in steep slopes from being detected (Eckerstorfer et al., 2016). Thus, some avalanche activity of certain size and spatial distribution may not have been detected.

5.4.2 Meteorological data

In this study, meteorological data from the weather station at Nordnesfjellet complemented with data from Tromsø Vervarslinga formed the basis for description of meteorological conditions for situations of interest for the winter season 2016/2017. Nordnesfjellet weather station was chosen because of availability of types of recorded parameters, the temporal availability and its mountainous location. However, gaps in the dataset occur. Tromsø weather station was chosen for its coast-near location and continuous data coverage. Nordnesfjellet AWS constitutes a suitable source of meteorological data for this study because of its mountainous location. The use of two weather stations for the whole study area introduces uncertainty regarding how representative the meteorological data is for the spatial extend of the avalanche activity dataset they are correlated to, as topography and distance affects the temporal distribution of meteorological patterns.

5.4.3 Synoptic categorization

For the categorization of the different synoptic types over the North Atlantic region in section 4.4, 500mb geopotential height plots, 850mb geopotential height plots and mean sea level pressure plots for avalanche cycle days was used to discriminate five different synoptic situations. Such a method for classification of synoptic types are known as subjective or manual classifications (Huth et al., 2008). This method has been applied by e.g. Hess and Brezowsky (1969) over Europe and Fitzharris and Bakkehoi (1986) for Norway. Other methods for categorizing synoptic situations includes application of objective, statistical differentiation e.g. García et al. (2009) who applied a principal-component analysis procedure to distinguish 6 atmospheric circulation patterns related to avalanching in the Pyrenees. However, such techniques for classification of synoptic types acquires statistical methods beyond the scope of this thesis.

6 Conclusion

6.1 Main findings

The objective of this thesis was to discover the causal relation between present meteorological conditions induced by synoptic weather patterns and the occurrence of high avalanche activity in Troms. Nine periods comprised of a total of 55 days of high avalanche activity were defined as avalanche cycles using an avalanche activity dataset from the 2016/2017 winter season. Representative meteorological parameters from the study area has been described for each respective avalanche cycle and for comparison of avalanche cycle days with non-cycle days. The synoptic situation occurring during periods of high avalanche activity was also described and categorized into five synoptic types, using 500mb geopotential height plots, 850mb geopotential height plots and mean sea level pressure plots for the North Atlantic region. The meteorological conditions for the synoptic types have also been described. Avalanche cycle days are characterized by lower air temperatures and higher wind speeds, which facilitates wind transportation of snow and delayed stabilization of the snow pack. The main differences between the five synoptic types were related to the placement of low-pressure systems over the Barents Sea and northern Scandinavia for four out of five situations, whilst a high-pressure ridge stretching from Central Europe towards northern Scandinavia in the last. These situations allowed for the manifestation of different meteorological conditions on the ground causing an unstable snowpack and subsequent avalanching.

Synoptic type 1 and 2 occurred while a low pressure covered the Barents Sea, producing easterly airflow in the study area, and avalanche problems were mainly related to dry slab avalanching. Type 3 displayed a synoptic situation where a low pressure were situated over northeastern Scandinavia, allowing for winds from the southwest and north generating avalanche activity related to dry slab avalanches. An opposite synoptic situation occurred during cycle 4, where a high pressure situated over Central Europe extended a ridge over Scandinavia, allowing for warm, southwesterly airflow with high wind speeds, causing dry slab avalanching in the winter months and warming events leading to wet snow avalanching in the spring. Synoptic type 5 occurred only during April and May, and was characterized by a low pressure that covered all of Scandinavia generating westerly airflow. Under these conditions, avalanching were mainly related to wet snow avalanches.

This work is the first study on synoptic conditions causing widespread, high avalanche activity in Northern Norway. It is an important step in forecasting avalanche cycles by closely investigating synoptic conditions in the North Atlantic sector, following the evolution of low-pressure systems and their paths towards Northern Norway.

Avalanche climatology assesses the occurrence of avalanche in relation to governing climatic conditions on a temporal scale of daily to decadal. Since no winters are like each other, and the climate is in an ever state of change, an analysis of the governing climatic conditions for the study area using a dataset spanning for one winter season will not be sufficient to address the long-term trends for governing atmospheric circulation patterns. Future analysis of the avalanche climatology for the region should include avalanche activity data with longer temporal span and more extensive statistical methods for differentiating these data and the related meteorological data.

Works cited

Andersen, B.G., 2000. Ice Age Norway: Landscapes Formed by Ice Age Glaciers. Universitetsforlaget.

Armstrong, R.L. and Armstrong, B.R., 1987. Snow and avalanche climates of the western United States: a comparison of maritime, intermountain and continental conditions. IAHS Publ, 162: 281-294.

Aronsen, I.B., 2016. Vinterturismen har skutt i været, iTromsløø.

Barfod, E., Müller, K., Saloranta, T., Andersen, J., Orthe, N.K., Wartianien, A., Humstad, T., Myrabø, S. and Engeset, R., 2013. The expert tool XGEO and its applications in the Norwegian Avalanche Forecasting Service', International Snow Science Workshop Grenoble—Chamonix Mont-–Blanc, pp. 7-11.

Bellaire, S., Jamieson, J.B. and Fierz, C., 2011. Forcing the snow-cover model SNOWPACK with forecasted weather data. Cryosphere, 5(4): 1115-1125.

Birkeland, K.W. and Mock, C.J., 1996. Atmospheric circulation patterns associated with heavy snowfall events, Bridger Bowl, Montana, USA. Mountain Research and Development, 16(3): 281-286.

Birkeland, K.W. and Mock, C.J., 2001. The major snow avalanche cycle of February 1986 in the western United States. Natural Hazards, 24(1): 75-95.

Birkeland, K.W., Mock, C.J. and Shinker, J.J., 2001. Avalanche extremes and atmospheric circulation patterns. Annals of Glaciology, Vol 32, 2001, 32: 135-140.

Bjornsson, H., 1980. Avalanche Activity in Iceland, Climatic Conditions, and Terrain Features. Journal of Glaciology, 26(94): 13-23.

Brattlien, K., 2012. Skredulykke Sorbmegaisa, Troms mandag 19.03.2012.

Dannevig, P., 2009. Troms - klima. Store Norske Leksikon.

Eckerstorfer, M., 2017. Skredaktivitet fra radarsatellitt i Tromsø og Lyngen varslingsområde 2016-2017.

Eckerstorfer, M., Buhler, Y., Frauenfelder, R. and Malnes, E., 2016. Remote sensing of snow avalanches: Recent advances, potential, and limitations. Cold Regions Science and Technology, 121: 126-140.

Eckerstorfer, M. and Christiansen, H.H., 2011. The “high Arctic maritime snow climate” in central Svalbard. Arctic, Antarctic, and Alpine Research, 43(1): 11-21.

Eckerstorfer, M. and Malnes, E., 2015. Manual detection of snow avalanche debris using high-resolution Radarsat-2 SAR images. Cold Regions Science and Technology, 120(Supplement C): 205-218.

Eckerstorfer, M., Malnes, E., Frauenfelder, R., Domaas, U. and Brattlien, K., 2014. Avalanche debris detection using satellite-borne radar and optical remote sensing, Proceedings of the Inter-15 national Snow Science Workshop, pp. 122-128.

Esteban, P., Jones, P.D., Martin-Vide, J. and Mases, M., 2005. Atmospheric circulation patterns related to heavy snowfall days in Andorra, Pyrenees. International Journal of Climatology, 25(3): 319-329.

Farukh, M.A. and Yamada, T.J., 2014. Synoptic climatology associated with extreme snowfall events in Sapporo city of northern Japan. Atmospheric Science Letters, 15(4): 259-265.

Fitzharris, B., 1987. A climatology of major avalanche winters in western Canada. Atmosphere-Ocean, 25(2): 115-136.

Fitzharris, B.B. and Bakkehoi, S., 1986. A Synoptic Climatology of Major Avalanche Winters in Norway. Journal of Climatology, 6(4): 431-446.

Föhn, P., Good, W., Bois, P. and Obled, C., 1977. Evaluation and comparison of statistical and conventional methods of forecasting avalanche hazard. Journal of Glaciology, 19(81): 375-387.

García, C., Martí, G., Oller, P., Moner, I., Gavaldà, J., Martínez, P. and Peña, J.C., 2009. Major avalanches occurrence at regional scale and related atmospheric circulation patterns in the Eastern Pyrenees. Cold Regions Science and Technology, 59(2-3): 106-118.
Greene, E., Atkins, D., Birkeland, K., Elder, K., Landry, C., Lazar, B., McCammon, I., Moore, M., Sharaf, D., Sternenz, C., Tremper, B. and Williams, K., 2010. Snow, weather, and avalanches : observation guidelines for avalanche programs in the United States. American Avalanche Association, Pagosa Springs, CO, vii, 152 pages pp.
Greene, E., D. Atkins, K. Birkeland, K. Elder, C. Landry, B. Lazar, I. McCammon, M. Moore, D. Sharaf, C. Sternenz, B. Tremper, and K. Williams, 2010. Snow, Weather, and Avalanches: Observation Guidelines for Avalanche Programs in the United States. Pagosa Springs, CO, American Avalanche Association.
Haegeli, P. and McClung, D.M., 2007. Expanding the snow-climate classification with avalanche-relevant information: initial description of avalanche winter regimes for southwestern Canada. Journal of Glaciology, 53(181): 266-276.
Hageli, P. and McClung, D.M., 2003. Avalanche characteristics of a transitional snow climate - Columbia Mountains, British Columbia, Canada. Cold Regions Science and Technology, 37(3): 255-276.
Hancock, H., Hendrikx, J., Birkeland, K.W., Eckerstorfer, M. and Christiansen, H.H., 2016. Synoptic Meteorological Conditions Associated With Snow Drift And Avalanche Activity in a High Arctic Maritime Snow Climate, nternational Snow Science Workshop 2016, Breckenridge, Colorado.
Hansen, C. and Underwood, S.J., 2012. Synoptic Scale Weather Patterns and Size-5 Avalanches on Mt. Shasta, California. Northwest Science, 86(4): 329-341.
Hansen, J.A., 2015. Tar hånd om skiturismen i nord, Framtid i Nord.
Helgaas, O.-A., Hellum, Ø.S. and Andreassen, D.T., 2012. Avalanche Protection on Highway E8 to The City of Tromsø, Northern Norway, International Snow Science Workshop. Norwegian Public Roads Administration,, Anchorage, Alaska.
Hendrikx, J., Owens, I., Carran, W. and Carran, A., 2005. Avalanche activity in an extreme maritime climate: The application of classification trees for forecasting. Cold Regions Science and Technology, 43(1-2): 104-116.
Hess, P. and Brezowsky, H., 1969. Katalog der grosswetterlagen Europas.
Holler, P., 2009. Avalanche cycles in Austria: an analysis of the major events in the last 50 years. Natural Hazards, 48(3): 399-424.
Huth, R., Beck, C., Philipp, A., Demuzere, M., Ustrnul, Z., Cahynova, M., Kysely, J. and Tveito, O.E., 2008. Classifications of Atmospheric Circulation Patterns Recent Advances and Applications. Trends and Directions in Climate Research, 1146: 105-152.
Hächler, P., 1987. Analysis of the weather situations leading to severe and extraordinary avalanche situations. Int. Assoc. of Hydrological Sci. Publ, 162: 295-304.
Hägeli, P. and McClung, D.M., 2000. A new perspective on computer-aided avalanche forecasting: scale and scale issues. Montana, 1: 8.
I. Hanssen-Bauer, E.J.F., I. Haddeland, H. Hisdal, S. Mayer, A. Nesje, J.E.Ø. Nilsen, S. Sandven, A.B. Sandø, A. Sorteberg, B. Ådlandsvik, 2015. Klima i Norge 2100.
Ikeda, S., Wakabayashi, R., Izumi, K. and Kawashima, K., 2009. Study of snow climate in the Japanese Alps: Comparison to snow climate in North America. Cold Regions Science and Technology, 59(2): 119-125.
Kalnay, E., Kanamitsu, M., Kistler, R., Collins, W., Deaven, D., Gandin, L., Iredell, M., Saha, S., White, G., Woollen, J., Zhu, Y., Chelliah, M., Ebisuzaki, W., Higgins, W., Janowiak, J., Mo, K.C., Ropelewski, C., Wang, J., Leetmaa, A., Reynolds, R., Jenne, R. and Joseph, D., 1996. The NCEP/NCAR 40-year reanalysis project. Bulletin of the American Meteorological Society, 77(3): 437-471.
Keylock, C.J., 2003. The North Atlantic Oscillation and snow avalanching in Iceland. Geophysical Research Letters, 30(5).
Klimaservicesenter, N., 2016. Klimaprofil Troms.

Kolstad, E.W., Bracegirdle, T.J. and Seierstad, I.A., 2009. Marine cold-air outbreaks in the North Atlantic: temporal distribution and associations with large-scale atmospheric circulation. Climate dynamics, 33(2-3): 187-197.
LaChapelle, E.R., 1966. Avalanche forecasting-a modern synthesis. US Department of Agriculture.
Lachapelle, E.R., 1980. The Fundamental Processes in Conventional Avalanche Forecasting. Journal of Glaciology, 26(94): 75-84.
Li, L. and Pomeroy, J.W., 1997. Estimates of threshold wind speeds for snow transport using meteorological data. Journal of Applied Meteorology, 36(3): 205-213.
Mallet, P.E., Claud, C., Cassou, C., Noer, G. and Kodera, K., 2013. Polar lows over the Nordic and Labrador Seas: Synoptic circulation patterns and associations with North Atlantic - Europe wintertime weather regimes. Journal of Geophysical Research: Atmospheres, 118(6): 2455-2472.
Malnes, E., Eckerstorfer, M., Larsen, Y., Frauenfelder, R., Jonsson, A., Jaedicke, C. and Solbø, S.A., 2013. Remote sensing of avalanches in northern Norway using Synthetic Aperture Radar, Proceedings of the International Snow Science Workshop, pp. 955-959.
Malnes, E., Eckerstorfer, M. and Vickers, H., 2015. First Sentinel-1 detections of avalanche debris. The Cryosphere Discussions, 9(2): 1943-1963.
McClung, D.M., 2002. The elements of applied avalanche forecasting - Part II: The physical issues and the rules of applied avalanche forecasting. Natural Hazards, 26(2): 131-146.
McClung, D.S., Peter, 2006. The Avalanche Handbook. The Mountaneers Books.
MET, 2018. eklima. Norwegian Meteorological Institute, eklima.no.
Mock, C.J. and Birkeland, K.W., 2000. Snow avalanche climatology of the western United States mountain ranges. Bulletin of the American Meteorological Society, 81(10): 2367-2392.
Mock, C.J., Carter, K.C. and Birkeland, K.W., 2017. Some Perspectives on Avalanche Climatology. Annals of the American Association of Geographers, 107(2): 299-308.
NGI, 2017. Ulykker med død, Norges Geotekniske Institutt.
NVE, 2017a. NVE Atlas.
NVE, 2017b. Om Xgeo.no.
NVE, 2017c. Snøskredulykker- og hendelser.
NVE, 2018a. xgeo.
NVE, S., Bane Nord, Met.no, 2018b. varsom.no, pp. Public avalanche bulletin service.
Nygaard, A.H.S., Ivar L. Berntsen, Paul. Tellefsen, Tryggve. Husby, Stein. Due, Jan. Lied, Karstein. Hansen, Geir., 1986. Skredulykken i Vassdalen 5. Mars 1986.
Parding, K.M.B., Rasmus, 2016. Storm activity and climate change in northern Europe, Norwegian Meteorological Institute.
Perla, R., 1970. On contributory factors in avalanche hazard evaluation. Canadian Geotechnical Journal, 7(4): 414-419.
Pohjola, V.A. and Rogers, J.C., 1997. Coupling between the atmospheric circulation and extremes of the mass balance of Storglaciaren, northern Scandinavia. Annals of Glaciology, Vol 24, 1997, 24: 229-233.
Rabbe, A.s., 1975. Arctic instability lows. Meteorologiske annaler v 6, no 11. H. Aschehoug, Oslo, p. 304-329 pp.
Ramberg, I.B., Bryhni, I., Nøttvedt, A. and Norsk geologisk forening., 2007. Landet blir til : Norges geologi. Norsk geologisk forening, Trondheim, 608 p. pp.
Roch, A., 1949. Report on snow avalanche conditions in the U.S.A. western ski resorts from the 26th of January to the 24th of April, 1949, Eidg. Institut für Schnee und Lawinenforschung Internal Rep.
Rogers, J.C., 1997. North Atlantic storm track variability and its association to the North Atlantic Oscillation and climate variability of northern Europe. Journal of Climate, 10(7): 1635-1647.
Schweizer, J., Bruce Jamieson, J. and Schneebeli, M., 2003. Snow avalanche formation. Reviews of Geophysics, 41(4).
Schweizer, J., Reiuter, B., Herwijnen, A. v. & Gaume, J., 2016. Avalanche release 101, International Snow Science Workshop 2016, Breckenridge, Colorado.

Scweizer. Jürg, J., Bruce J. Skjonsberg, David, 1998. Avalanche forecasting for transportation corridor and backcountry in Glacier National Park (BC, Canada). Hestnes E (ed) 25 years of snow avalanche research. Voss, Norway,.
Serreze, M., Box, J., Barry, R. and Walsh, J., 1993. Characteristics of Arctic synoptic activity, 1952–1989. Meteorology and Atmospheric Physics, 51(3-4): 147-164.
SSB, 2018. Kommunefakta - Tromsø. Statistisk Sentralbyrå, https://www.ssb.no/kommunefakta/tromso.
SVV, 2015. Skredsikringsbehov for riks og fylkesveg, Statens vegvesen, Region Nord, Plan og utredning.
Thompson, D.W. and Wallace, J.M., 1998. The Arctic Oscillation signature in the wintertime geopotential height and temperature fields. Geophysical research letters, 25(9): 1297-1300.
Thorsnæs, G., 2016. Troms. Troms. Store Norske Leksikon, https://snl.no/Troms.
Uvo, C.B., 2003. Analysis and regionalization of northern european winter precipitation based on its relationship with the North Atlantic oscillation. International Journal of Climatology, 23(10): 1185-1194.
Van Loon, H. and Rogers, J.C., 1978. The seesaw in winter temperatures between Greenland and northern Europe. Part I: General description. Monthly Weather Review, 106(3): 296-310.
varsom.no, 2017. Snøskredproblemer. NVE.
Velsand, p., 2017. Comparison and classification of an Arctic Transitional snow climate in Tromsø, Norway, Univeristy of Tromsø - The Norwegian Arctic University.
VG, 2000. - Bussen fullstendig knust, VG.
Vickers, H., Eckerstorfer, M., Malnes, E., Larsen, Y. and Hindberg, H., 2016. A method for automated snow avalanche debris detection through use of synthetic aperture radar (SAR) imaging. Earth and Space Science, 3(11): 446-462.
Wilhelmsen, K., 1985. Climatological Study of Gale-Producing Polar Lows near Norway. Tellus Series a-Dynamic Meteorology and Oceanography, 37(5): 451-459.

Appendix

Avalanche cycles

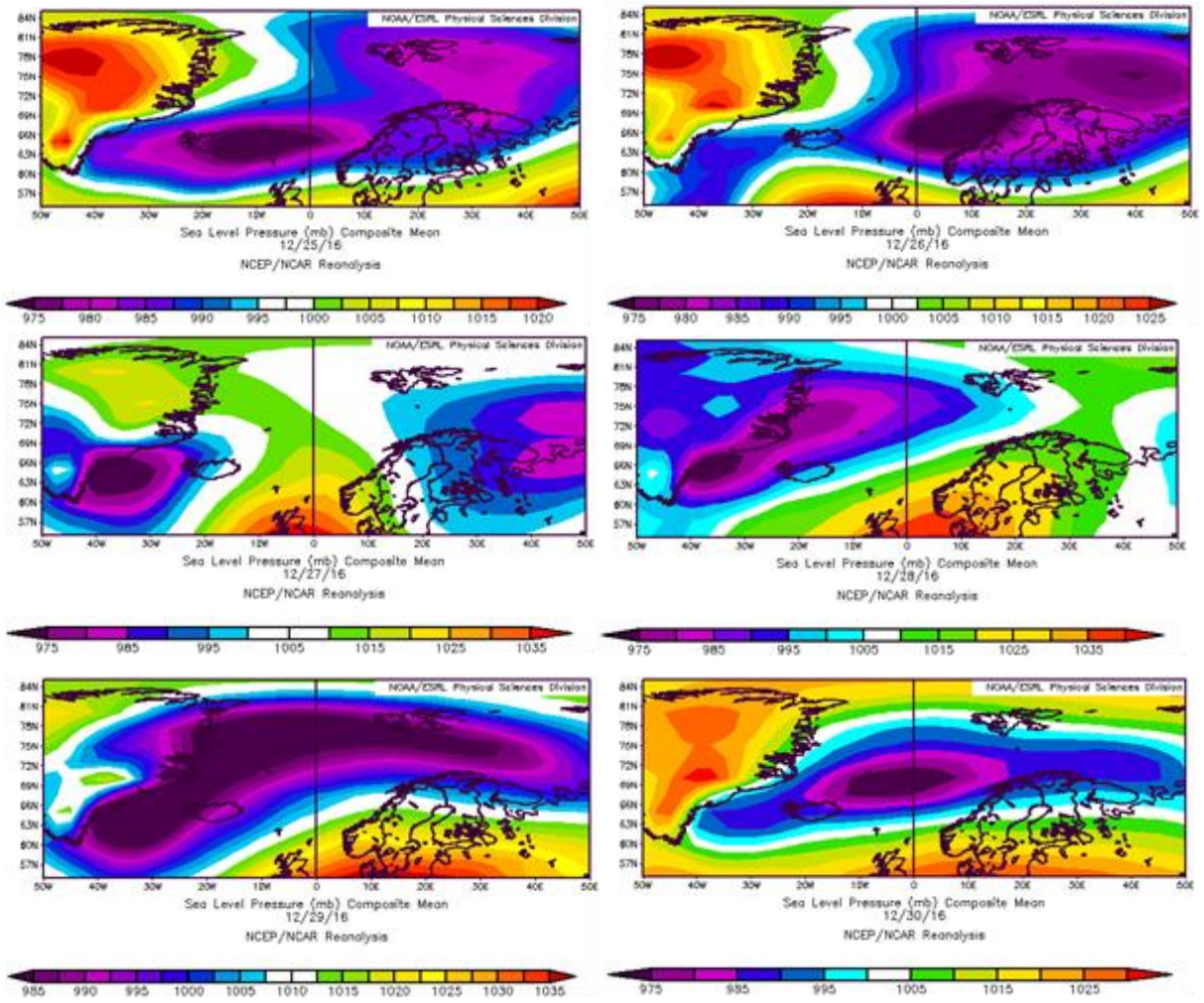

Appendix figure 1. Sea level pressure plot for the North Atlantic region during 25.12-30.12.2016.

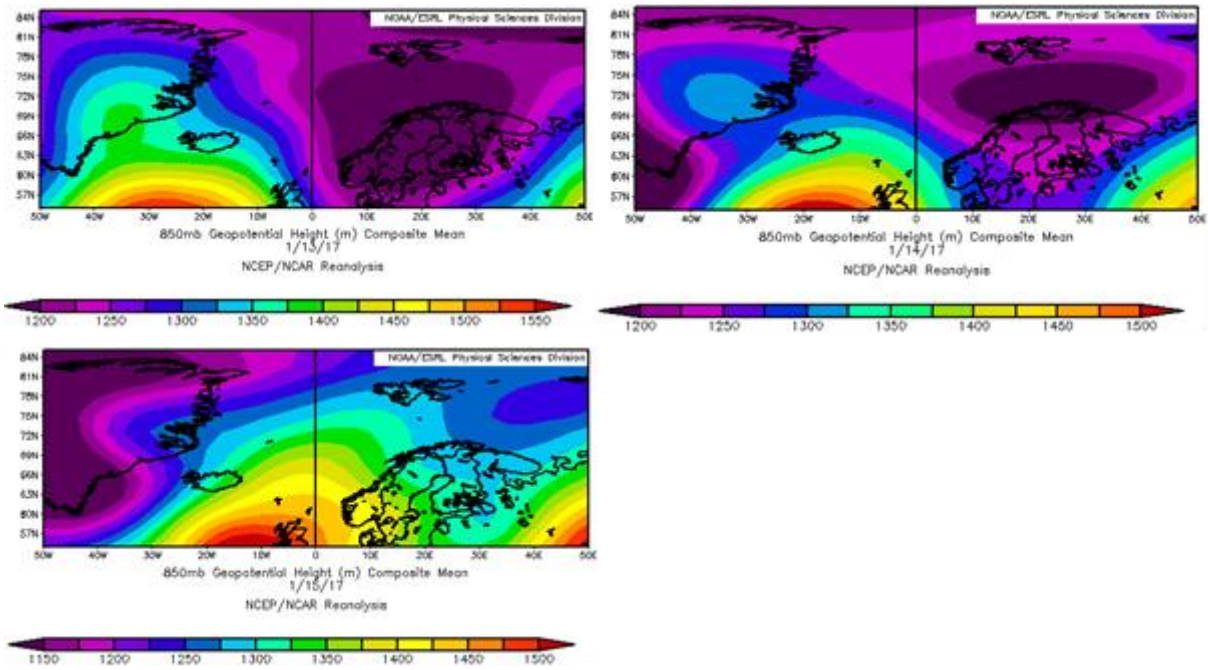

Appendix figure 2. 850mb geopotential height plot for the North Atlantic region during 13.01-15.01.2017.

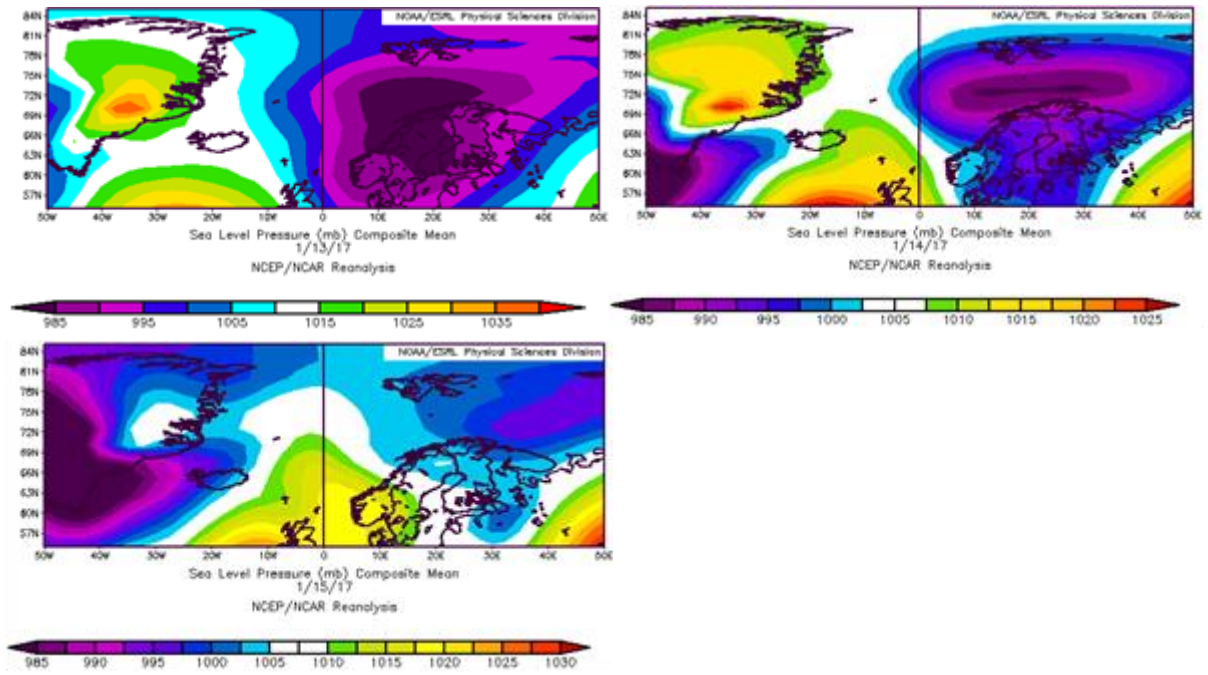

Appendix figure 3. Sea level plot for the North Atlantic region during 13.01-15.01.2017.

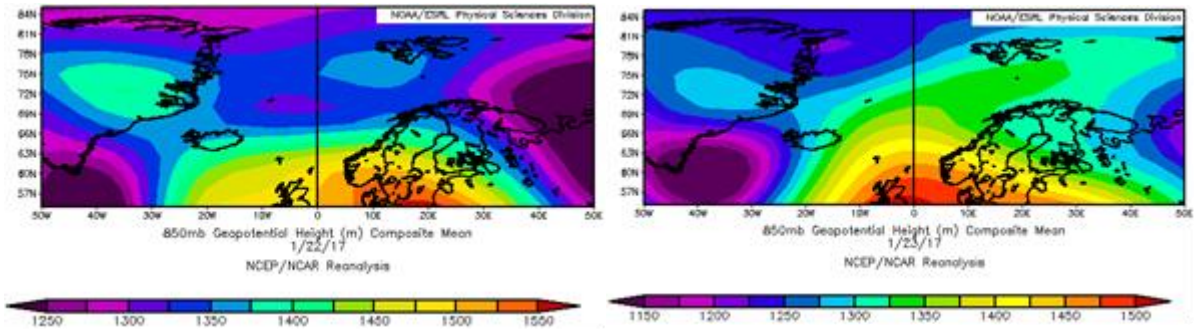

Appendix figure 4. 850mb geopotential height plot for the North Atlantic region during 22.01-23.01.2017.

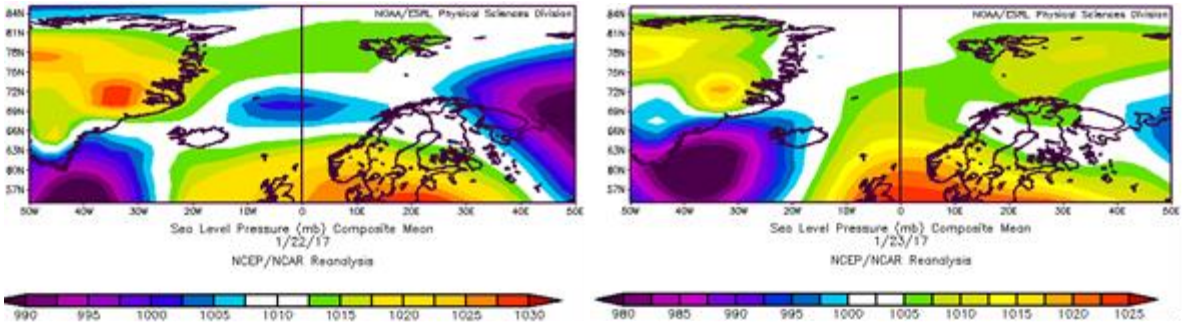

Appendix figure 5. Sea level plot for the North Atlantic region during 22.01-23.01.2017.

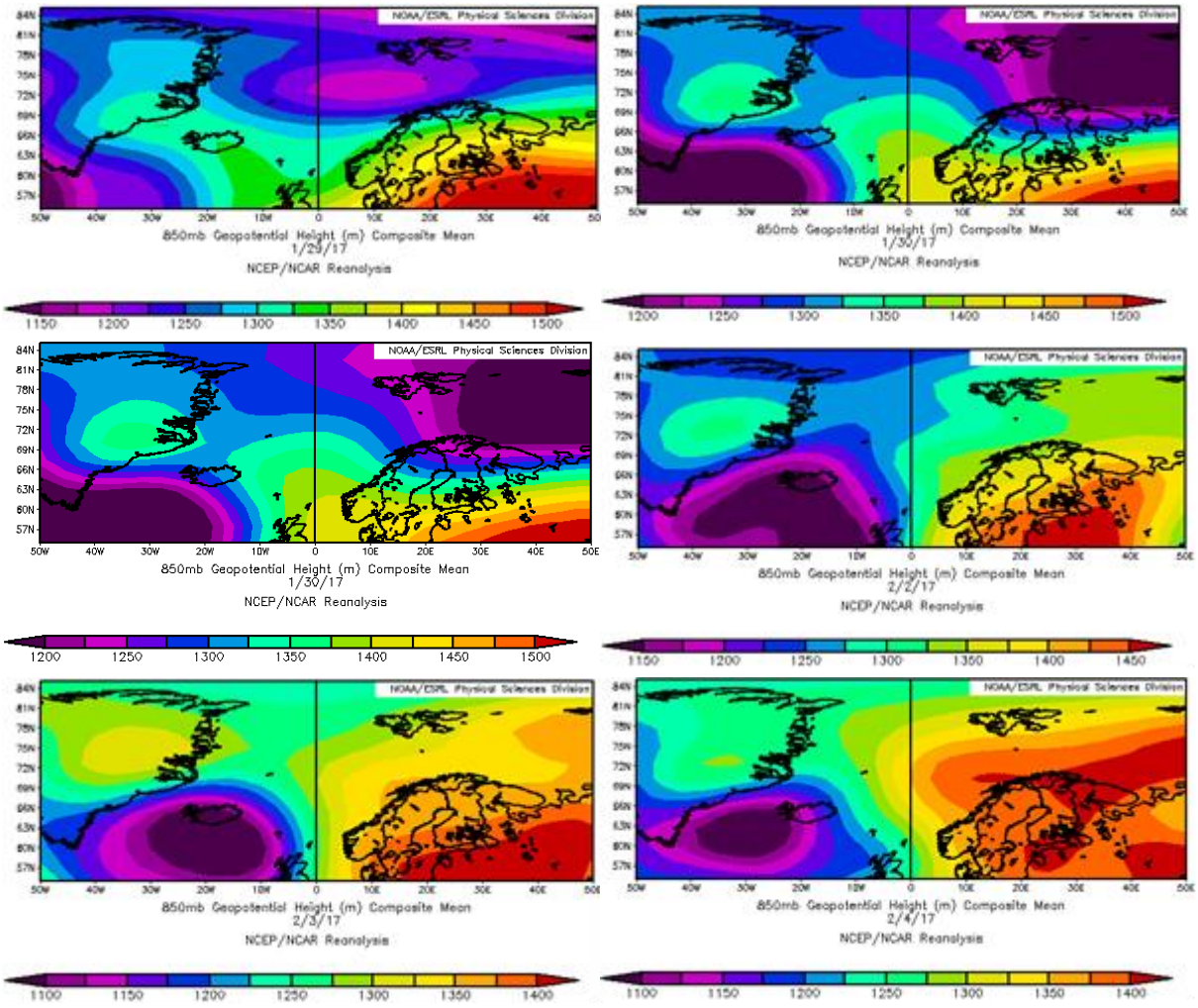

Appendix figure 6. 850mb geopotential height plot for the North Atlantic region during 29.01-04.02.2017.

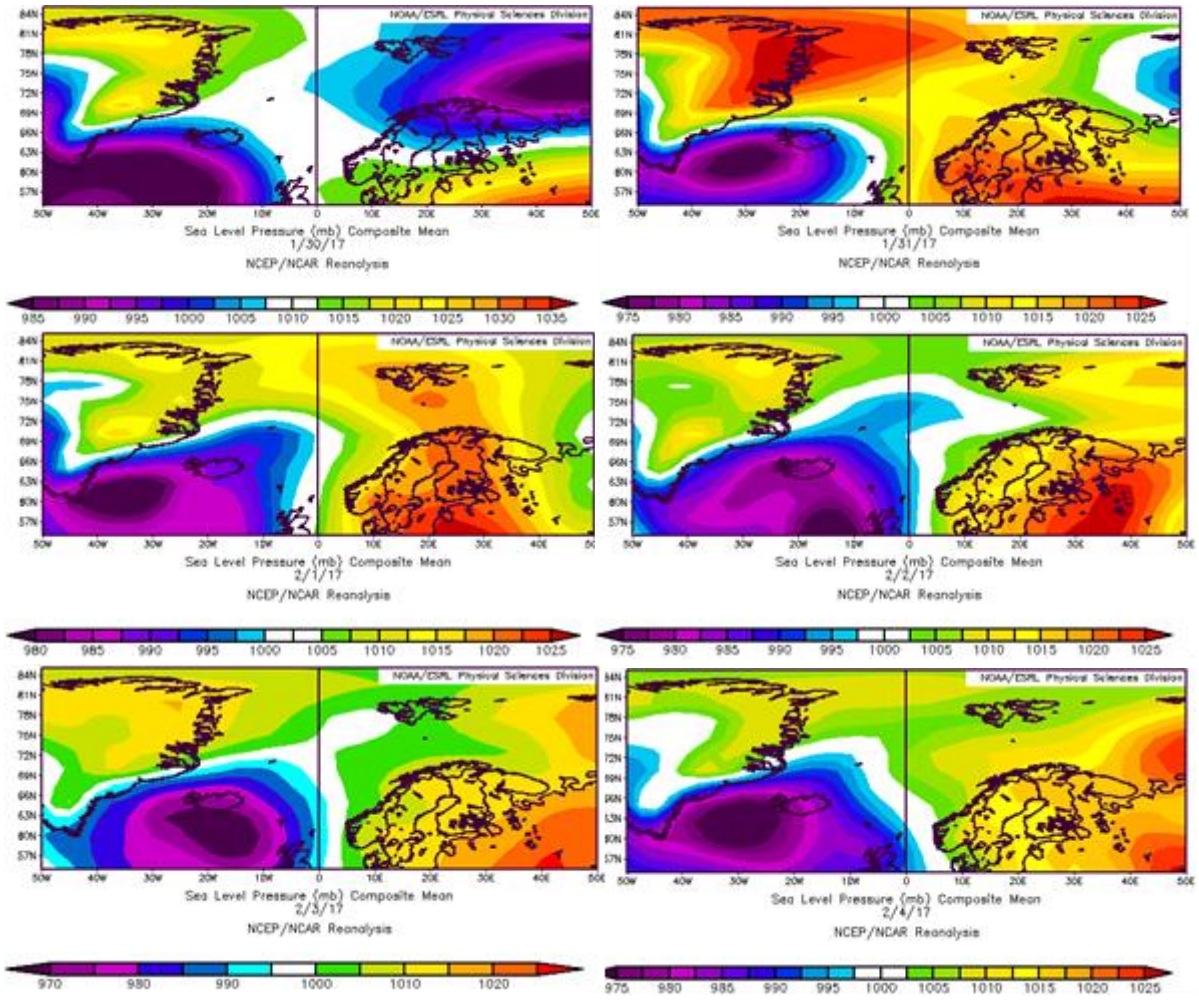

Appendix figure 7. Sea level plot for the North Atlantic region during 29.01-04.02.2017.

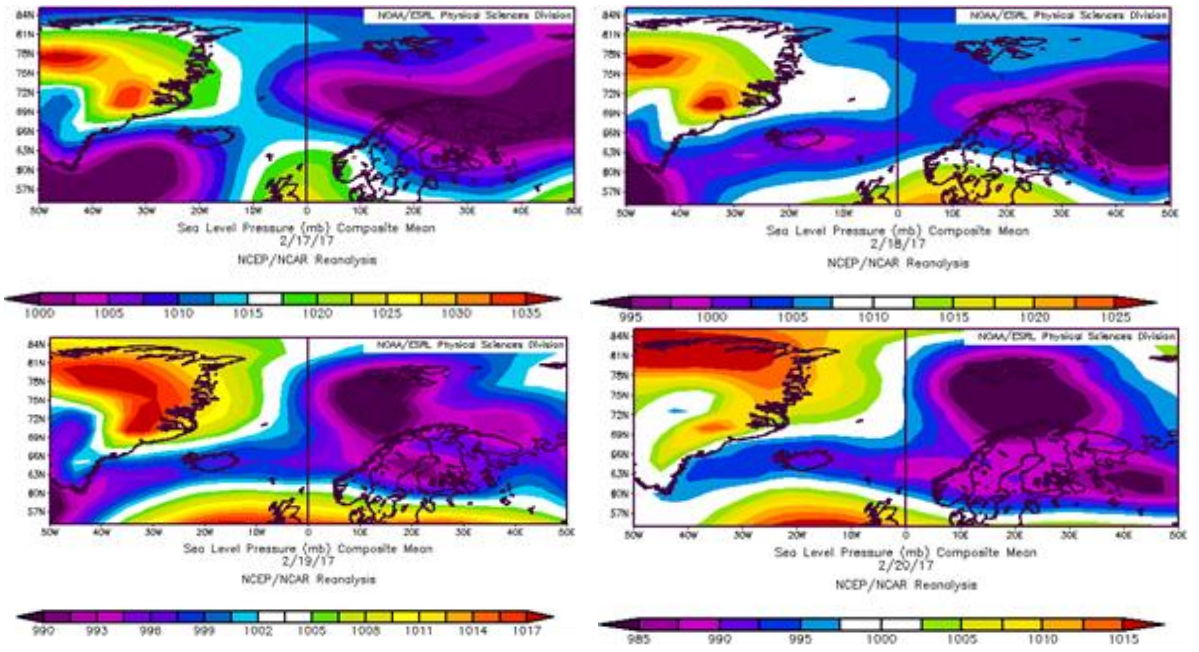

Appendix figure 8. Sea level plot for the North Atlantic region during 17.02-20.02.2017.

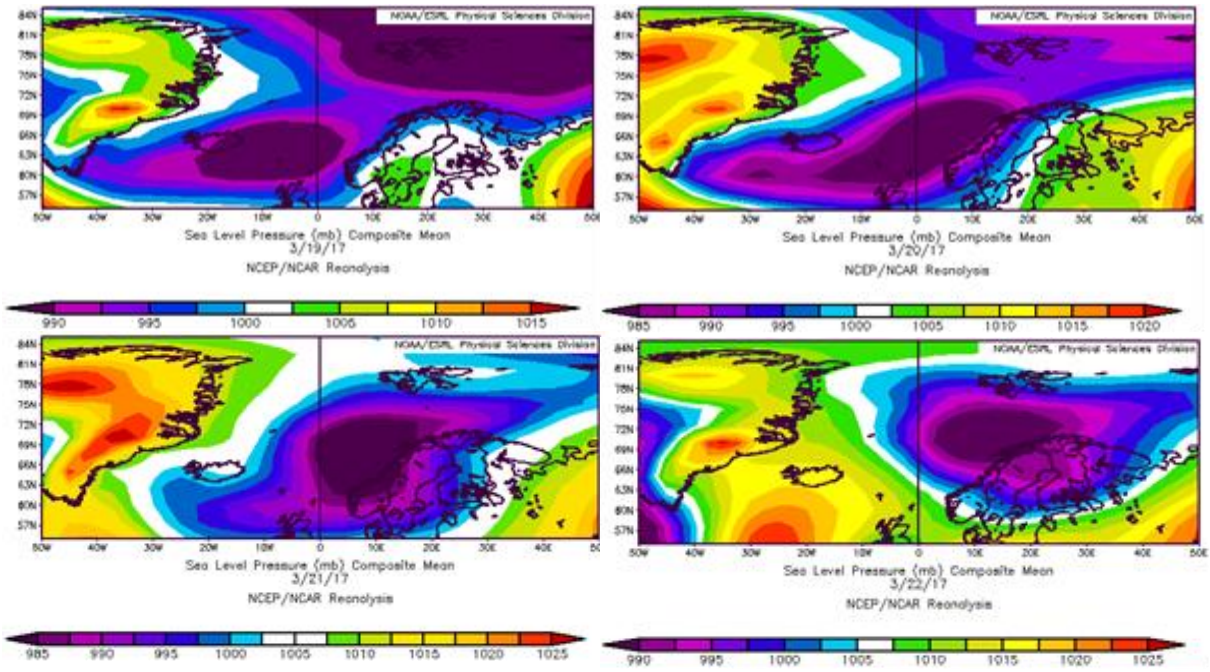

Appendix figure 9. Sea level plot for the North Atlantic region during 19.03-22.03.2017.

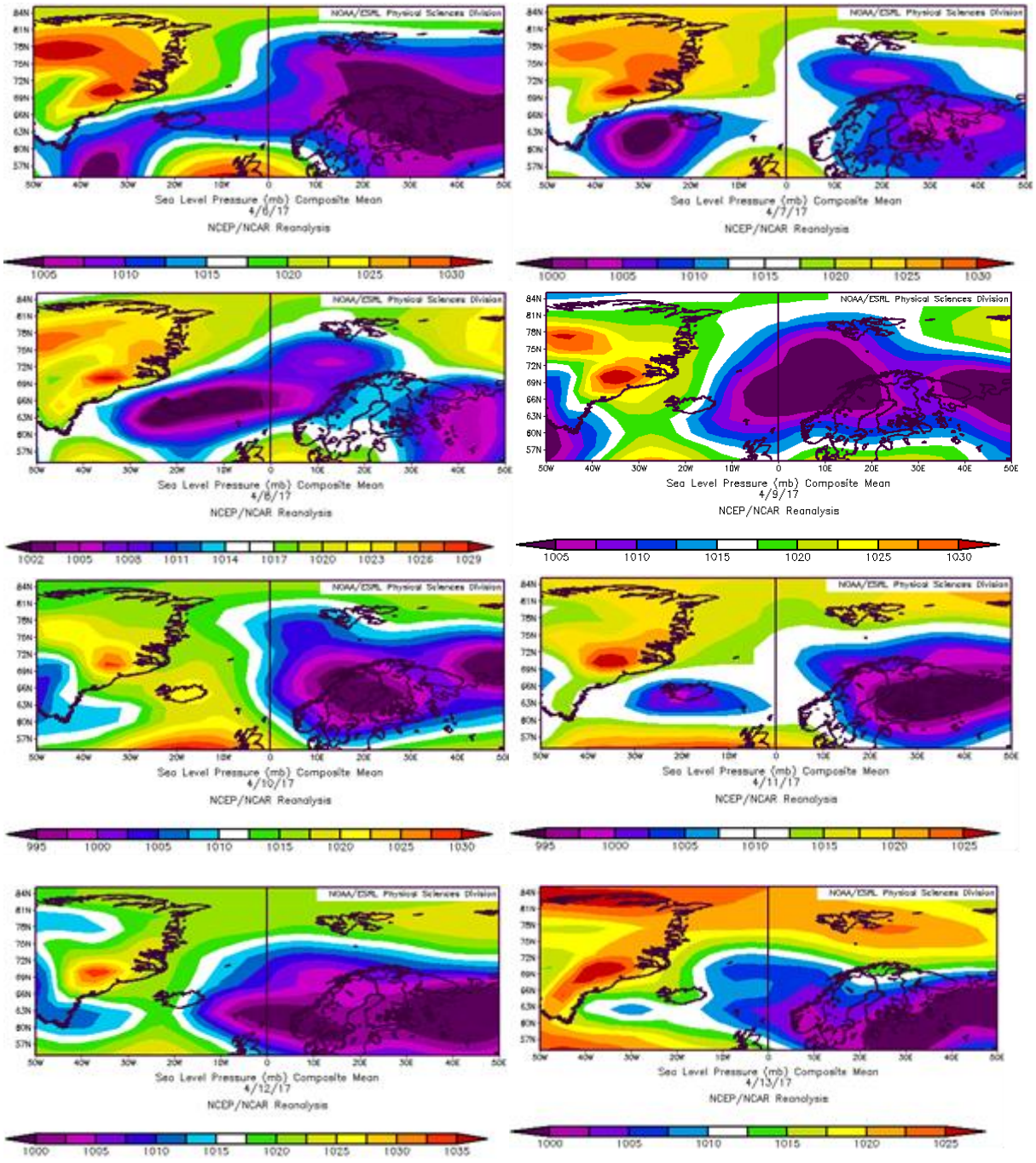

Appendix figure 10. Sea level plot for the North Atlantic region during 06.04-12.04.2017.

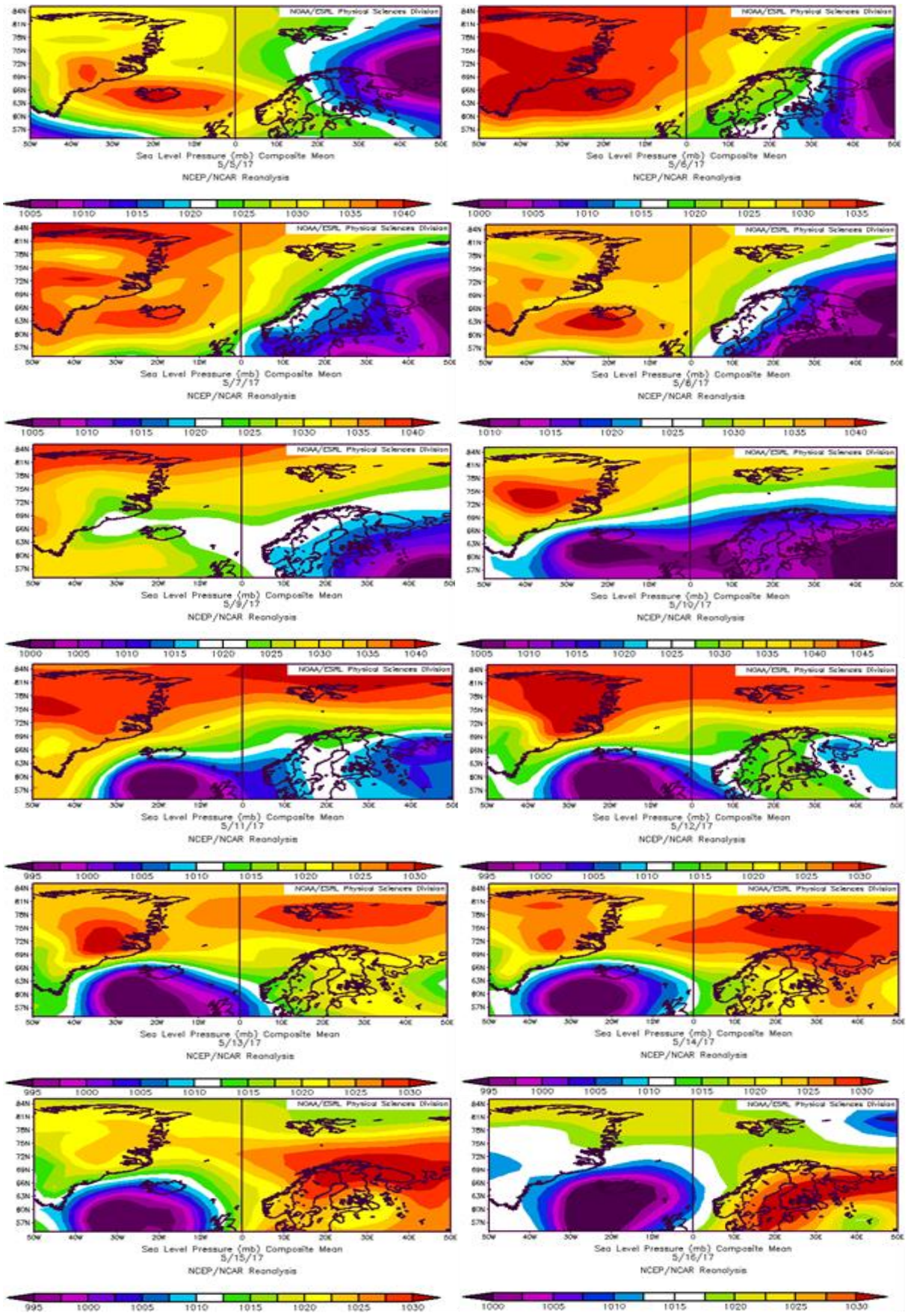

Appendix figure 11. Sea level plot for the North Atlantic region during 05.05-16.05.2017.

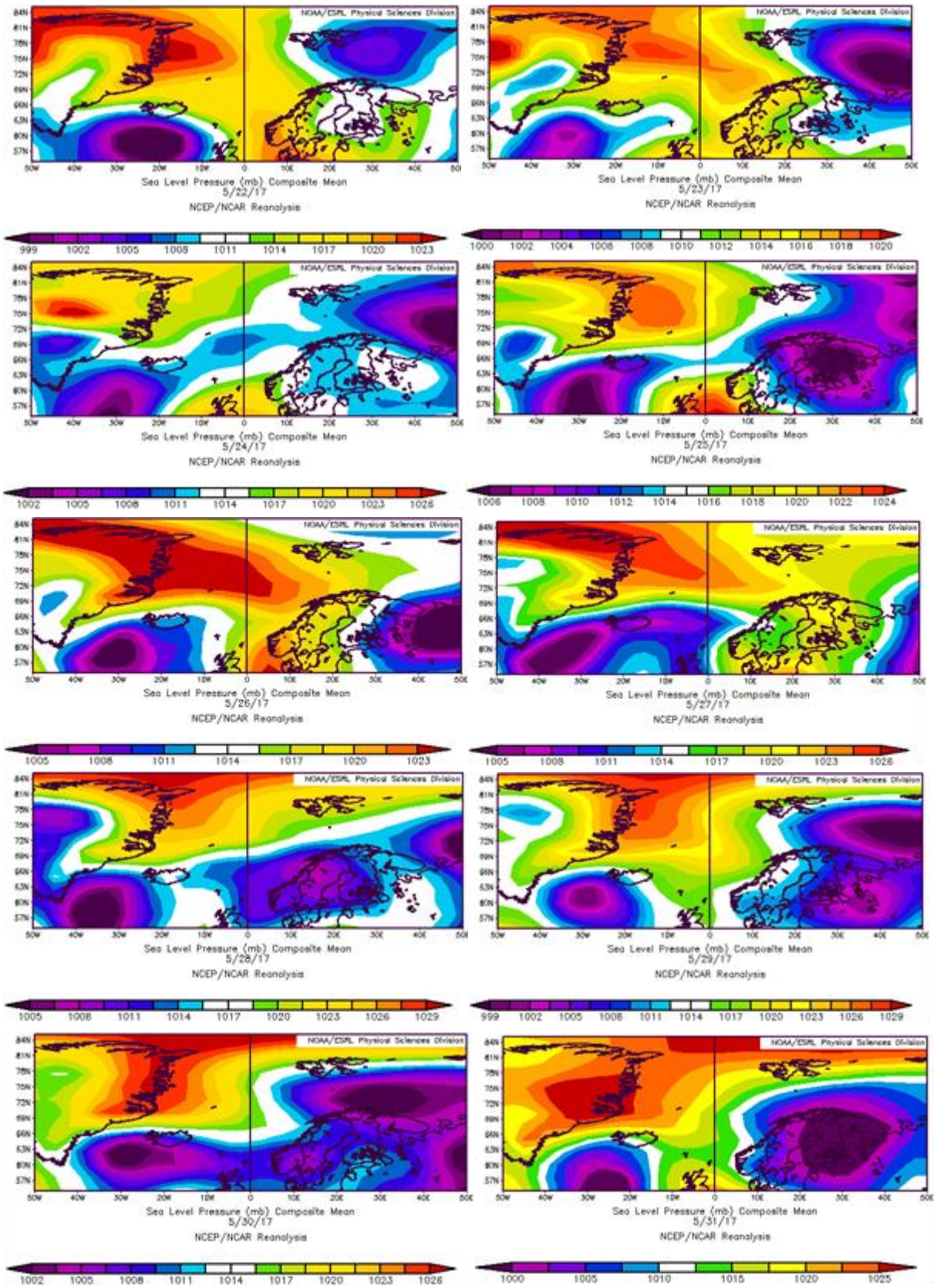

Appendix figure 12. Sea level plot for the North Atlantic region during22.05-31.05.2017.

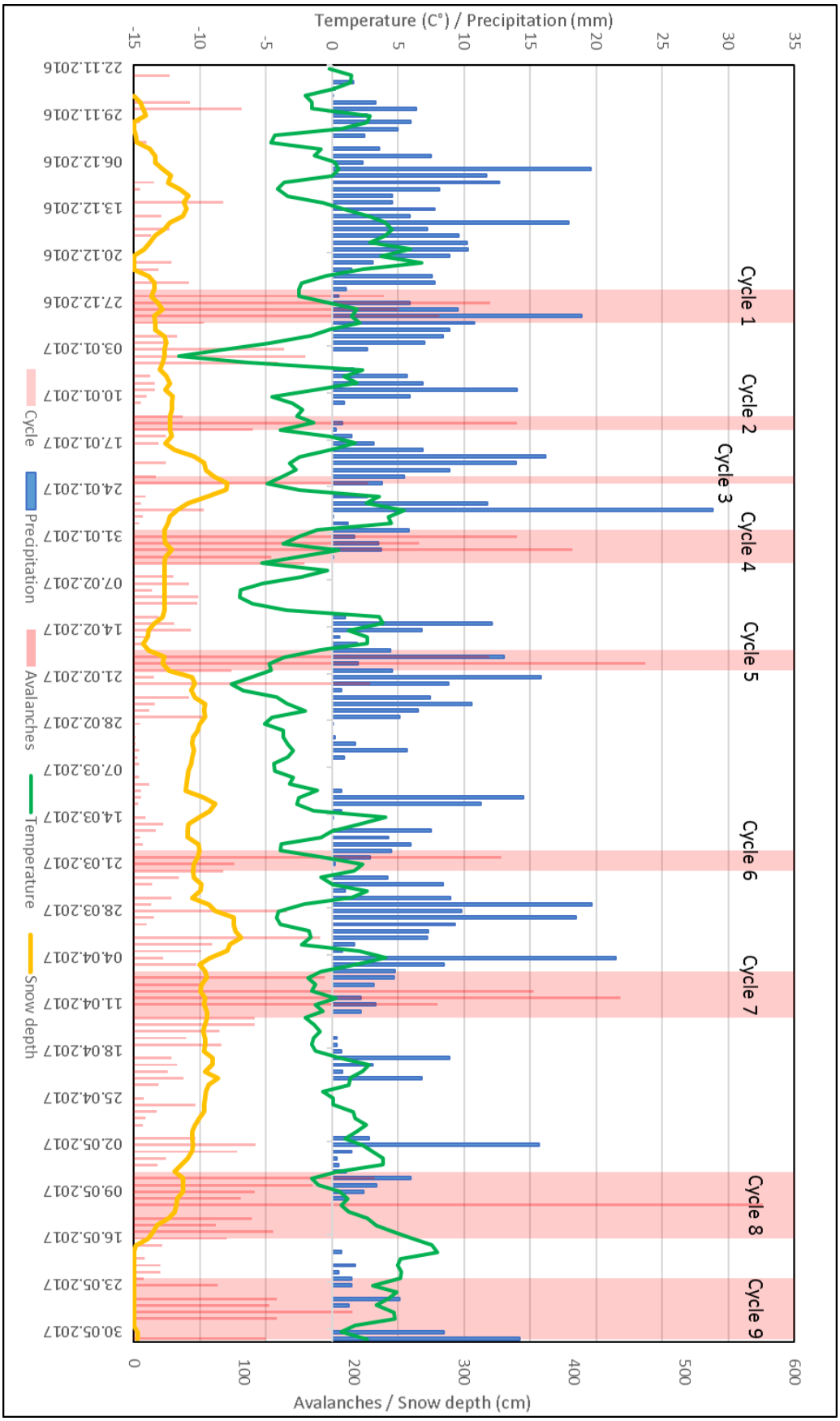

Appendix figure 13. Avalanche activity with meteorological data of daily averages from Tromsø vervarslinga (Data source: eklima.no)

Tromsø forecasting region												
Cyle	Date/avalanche problem									Legend:		
1	25.des	26.des	27.des	28.des	29.des	30.des				1 = Wind slab		
	1	1	2	1,6	2	2,6				2 = Storm slab		
2	13.jan	14.jan	15.jan							3 = Persistent weak layer		
	1	2	2							4 = Deep persistent weak layer		
3	22.jan	23.jan								5 = Wet loose snow avalanche		
	1	1								6 = Wet slab avalanche		
4	30.jan	31.jan	01.feb	02.feb	03.feb	04.feb				7 = Glide avalanche		
	1	1	1	1	1	1						
5	17.feb	18.feb	19.feb	20.feb								
	1	1	1	1								
6	19.mar	20.mar	21.mar	22.mar								
	1,3	1,3	1,3	1,3								
7	06.apr	07.apr	08.apr	09.apr	10.apr	11.apr	12.apr	13.apr				
	2,4	2,4	2,5	1	1	1,5	1,5	1,5				
8	05.mai	06.mai	07.mai	08.mai	09.mai	10.mai	11.mai	12.mai	13.mai	14.mai	15.mai	16.mai
	1,3	1,3	1,3	1,3	1,5,3	5	5	5	5,1	5,1	5,1	5,6
9	22.mai	23.mai	24.mai	25.mai	26.mai	27.mai	28.mai	29.mai	30.mai	31.mai		
	1,5	1,5	5,1	1,5	5	5,7	5,1	1	1	1		

Appendix figure 14. Forecasted avalanche problems for days in avalanche cycles with numeric identifiers in order as in forecast for Tromsø forecasting region. Data source: (NVE, 2018b)

Lyngen forecasting region												
Cyle	Day/problem											
1	25.des	26.des	27.des	28.des	29.des	30.des				Legend		
	1	1	2	2	2	2,6				1 = Wind slab		
2	13.jan	14.jan	15.jan							2 = Storm slab		
	1,3	1,3	1,3							3 = Persistent weak layer		
3	22.jan	23.jan								4 = Deep persistent weak layer		
	1,3	1,3								5 = Wet loose snow avalanche		
4	30.jan	31.jan	01.feb	02.feb	03.feb	04.feb				6 = Wet slab avalanche		
	2	1	1	1	1	1				7 = Glide avalanche		
5	17.feb	18.feb	19.feb	20.feb								
	1	1,3	1,3	1,3								
6	19.mar	20.mar	21.mar	22.mar								
	1,3	1,3	1,3	1,3								
7	06.apr	07.apr	08.apr	09.apr	10.apr	11.apr	12.apr	13.apr				
	2,3	2,3	2,3	1,3	1,3	1,5	1,5	1,5				
8	05.mai	06.mai	07.mai	08.mai	09.mai	10.mai	11.mai	12.mai	13.mai	14.mai	15.mai	16.mai
	1,3	1,3	1,3	2,4	2,5,3	5,1	5,1	5,1	5,1	5,6	5,6	5,6
9	22.mai	23.mai	24.mai	25.mai	26.mai	27.mai	28.mai	29.mai	30.mai	31.mai		
	1,5	1,5	5,1	1,5	5	5,7	5,1	1	1	1		

Appendix figure 15. Forecasted avalanche problems for days in avalanche cycles with numeric identifiers in order as in forecast for Lyngen forecasting region. Data source: (NVE, 2018b)